POLITECNICO DI TORINO

Master of Science in Energy and Nuclear Engineering

Master of Science Thesis

Floating photovoltaic systems: state of art, feasibility study in Florida and computational fluid dynamic analysis on hurricane resistance

Supervisor: **Candidate:**

Prof. Filippo Spertino   Giovanni Blengini

Co. Supervisor:

Prof. Antonio Buffo

Academic Year 2019/2020

Summary

1. Introduction

This thesis aims to analyze the floating photovoltaic systems and whether they can be an effective solution as renewable energy producer also in tropical areas under extreme weather conditions. The reason for the evaluation of this specific topic lay on the consideration that the Sun Belt (the most relevant area for the photovoltaic production) of the northern hemisphere offers a huge amount of water surface fitted for the installation of floating photovoltaic farms. Nowadays, floating PV installation in these areas are yet rare, so they constitute a huge potential for the future development of solar energy. The analysis ranges from different aspects of this innovative technology focusing on the engineering, energetic, environmental, and economic aspects, carrying out comparison with conventional ground mounted systems. The focus on the state of Florida leads to a comprehension on how the floating photovoltaic can be an opportunity that could deeply modify the energetic pattern of the region. In the peculiar zone of Florida what threatens photovoltaic systems are extreme environmental conditions such as hurricanes, which are involving the territory more and more often due to climate change. An investigation on the features of hurricanes, their probability, and the threat that they present has been carried out. For the sake of knowing whether these floating systems could resist to such extreme events, a Computational Fluid Dynamic (CFD) analysis has been performed following the state norms and the physical properties of wind gusts applied as inputs. The simulation is explained in detail from the 3D geometry creation to the final solutions, focusing on the physics of the model and on the most particular aspects. The CFD simulation has been applied on numerous system designs, with the wind coming from different directions and with different modules inclinations. The purpose is to find the optimal configuration and ideal tilt angle for such systems in order to resist to category five hurricanes producing emphasis on a specific patented floating system, *NRG Island*, produced by the Italian Company *NRG Energia*.

2. Solar resource assessment

The star known as Sun, at the center of our planetary system, is continuously hitting the earth with wave-corpuscle energy quanta called photons, which are born from the continuous nuclear fusion inside this massive star. The sun is shining approximately 3,400,000.00 exajoules (10^{18} J) of energy each year on the earth's surface [1], nearly 6000 times the world annual energy consumption of 2019 [1]. In order to harvest this amount of energy, photovoltaic solar systems and concentrated solar power systems have been adopted.

Solar energy is one of the most used renewable energy sources, and through photovoltaics systems, it is becoming more popular since the spread of this technologies is increasing at a very fast pace. The fame is due to the low price, simplicity and relatively high efficiency of this technology. From 1977 to 2020 the cost of production of solar panels has dropped of 600 times, passing from 77$/W to the 0.25$/W of today and it is still lowering, this drop has followed the Swanson law which states that for every doubling of a technology production its cost will decrease by 20% [2]. This technology has also been appreciated thanks to the straight conversion of energy from the sun light to one of the most refined energy vectors: electricity.

At the end of 2019 more than 629 GWp of solar panels were installed [3], most of this power amount came from ground mounted systems and from residential, commercial and industrial rooftops. These two design classifications are recognized the two pillars of PV (abbreviation of photovoltaic) systems, but from just more than a decade a third promising pillar has grown: the floating photovoltaic systems.

---

[1] Global Energy Statistical Yearbook 2020 (Enerdata).

3. Floating Photovoltaic Systems

The floating photovoltaic systems, also mentioned as *floatovoltaics,* are solar design engineering structures laid on water bodies. The solar panels are typically installed on pontoon fluctuating assemblies moored and anchored to steady locations. The most suitable water bodies for this type of installation are non-natural ones, such as industrial, mining, hydroelectric or waste water treatment basins, since they represent a non-utilized source often near populated areas. The very first FPV (abbreviation of floating photovoltaic) system was built in Japan in 2007, producing skepticism and uncertainty, but the success brought by the numerous advantages of this technology lead to the production of many more projects all over the world with China, Japan and Korea as major protagonists (see *Fig. 1, 2*).
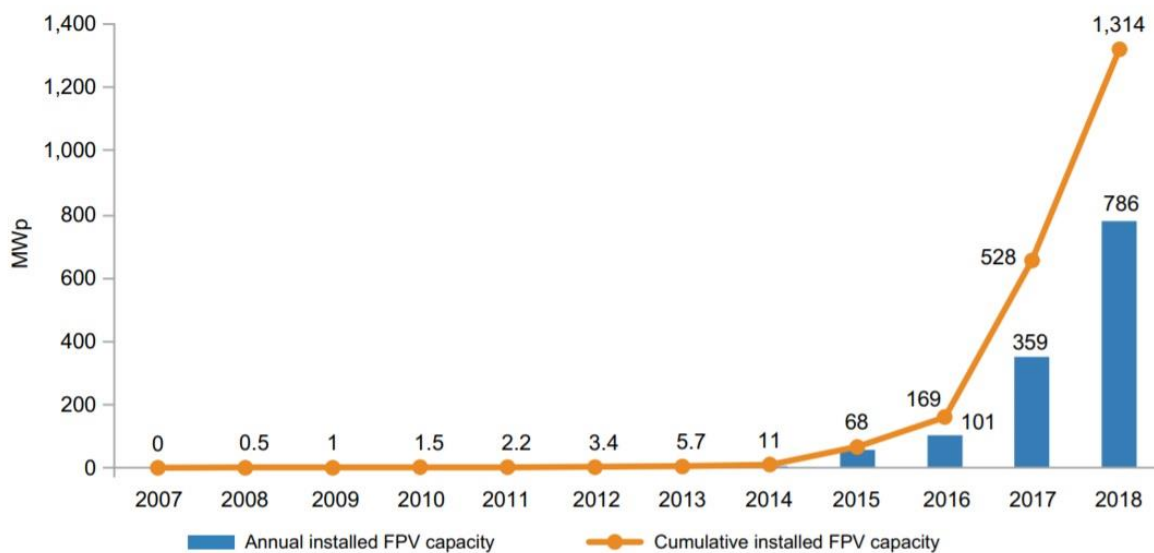
Figure 1: Annual and cumulative installed FPV capacity, World Bank Group, ESMAP, and SERIS 2019 [4].

Most of the systems have an installed power usually lower than 2 or 3 MWp, but in the last years wider structures have been mounted, similarly to what happened to conventional photovoltaic systems this technology is gaining confidence and interest over time and so bigger plants are becoming feasible. A growth rate of 20 % is expected in the coming 5 years since more than 60

countries in the world are pursuing this technology and 2/3 of them are in Asia, where the manufacturing cost is low [1], [4], [5].

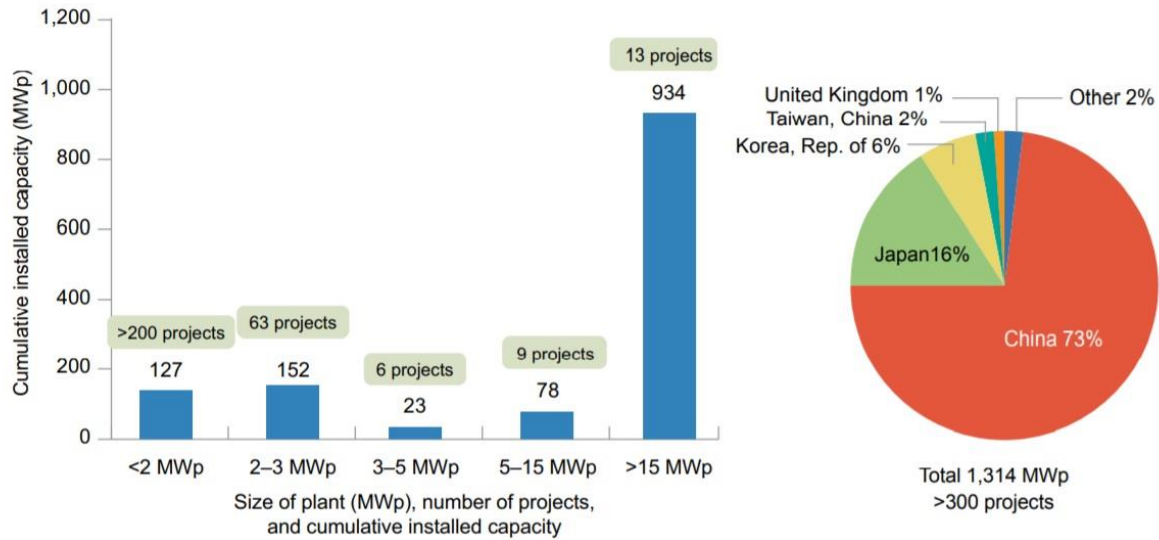*Figure 2: Cumulative installed FPV capacity world by size and by world share, World Bank Group, ESMAP, and SERIS 2019 [1].*

3.1. Floatovoltaics design engineering

The configuration of a FPV system does not differ much from a standard land-based system, the electrical configuration is similar with the exception to the inverter site that might be installed on a separate floating platform; moreover, instead of having metallic field structures this technology uses floating platform moored and anchored in different ways depending on the type of site they float on. Therefore, this technology is almost identical to the ground mounted one and differs only in the structural part. A schematic representation of this system is reported in *Figure 3*.
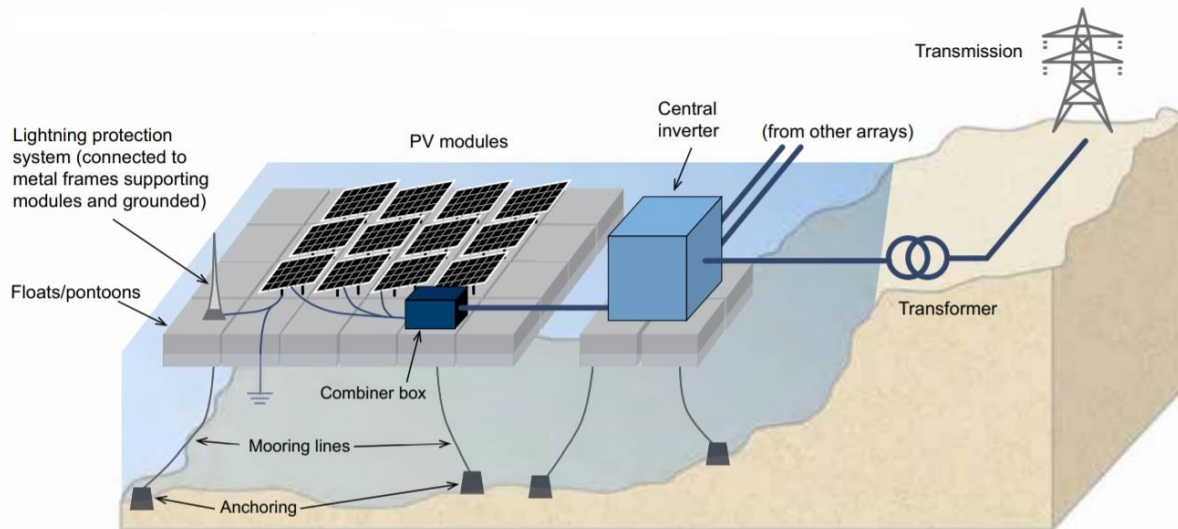
Figure 3: Floating photovoltaic system design, World Bank Group, ESMAP, and SERIS 2019 [4].

3.1.1. Suitable applications

FPV can have several different applications, from the typical manmade water bodies and industrial ponds to agriculture ponds and offshore sites. The man-made locations are often reservoirs for flood control, water catchment areas, hydropower areas or residential water ponds, while the industrial applications could vary from exhausted mines to wastewater treatment ponds and cooling ponds such those used for nuclear power applications. These platforms are also suitable for aquaculture and for offshore-nearshore environments, where different approaches need to be taken into account since a higher resistance to waves is required.

3.1.2. Main components

The components of the system are not so different from the classical land-based ones (modules, combiner box, inverters, transformer, lightning protection system, etc.) the only difference is the need of floats and fastening systems, which will be analyzed in the following paragraphs.

3.1.2.1. Floats

Floats must guarantee a homogeneous baseline structure in order to maintain a stable position even when extreme events occur. The material used is high density polyethylene (HDPE) corrosion and UV resistant. There are three major types of floating platform designs.

The *pure float design* uses two float types, one is in charge of supporting the PV modules and provide the desired tilt angle, and the other ensures the connection to the main floats, guaranteeing a walkway path used for maintenance. The *pontoon and metal frame system* is often used as well, it utilizes a metallic structure made mostly of aluminum, stainless or galvanized steel, to support PV panels similar to the land based systems, the floats do not need a special design, block or pipe shapes are commonly used. This second type of floats has the advantage to be simple to create and so to source locally, also the wave movement between panels is less variable so the connections and wirings will suffer less wear and tear but anyway the more rigid structure can cause localized stresses. The third type of floats used are the *membrane* ones which cover the whole surface and prevent much more evaporation losses, these are mainly used in water reservoirs but are more difficult to be scaled [4].

3.1.2.2. Anchoring & mooring

Appropriate mooring and anchoring system are essential to guarantee resistance to dangerous external events such as waves, winds, loads, water currents etc., the three main ways to anchor a system are the *bottom anchoring*, the *bank anchoring* and the *piles (see Fig. 4)*. They can be used considering the bathymetry, the water level variations, the substrate soil and the surrounding environment.

Bottom anchoring is the most used method since it is more versatile and guarantees a great resistance for more than 25 years at least, consistently with the solar panel's lifetime. A heavy concrete block is laid on the bottom of the soil and will act as a death weight resisting to movements. The size and weight of the blocks are determined in order to resist to strong wind and

wave induced forces that might move the block leading to uneven resistive forces that can damage the system. The bank anchoring system can be used for small ponds where the plant is close to the shore and when other options cannot be applied. This is the most cost-effective solution but not the most resistant one. Piles are used in very shallow waters where drilling is possible and would not harm the ecosystems.
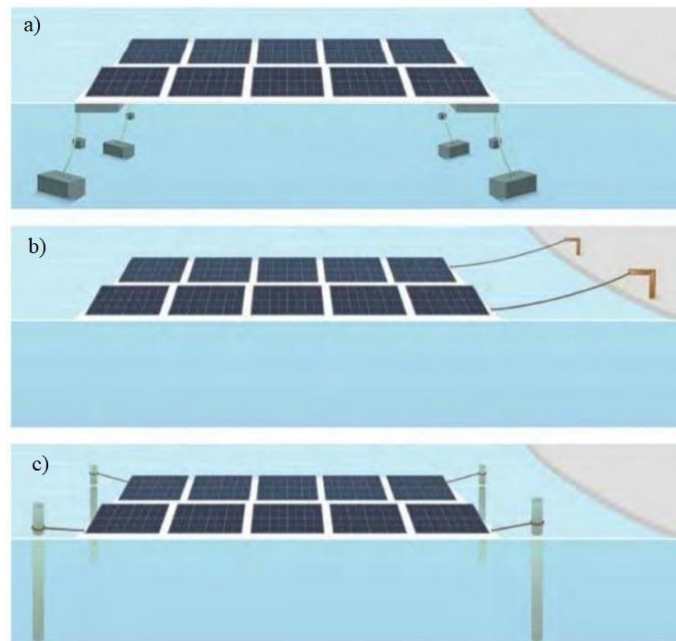

Figure 4: Anchoring and mooring techniques for FPV systems, from the top it is shown the bottom anchoring (a), the bank anchoring (b) and at the bottom the pile anchoring (c), World Bank Group, ESMAP, and SERIS 2019 [1].

To guarantee tension in the mooring lines a preliminary study on how the water level of the pond changes due to seasonality and exceptional events is carried out, consecutively the length of the mooring line can be calculated. In order to guarantee a constant strain two methods can be used. The first method is to create a mooring triangle from the anchors to the floating platform, the two catheti are linked from a buoy or a weight and the hypotenuse links the anchor to the platform guaranteeing a constant over time tension on the hypotenuse, the other way is not to create a triangle but just two segments linked by a buoy as shown in the following *Figure 5*.
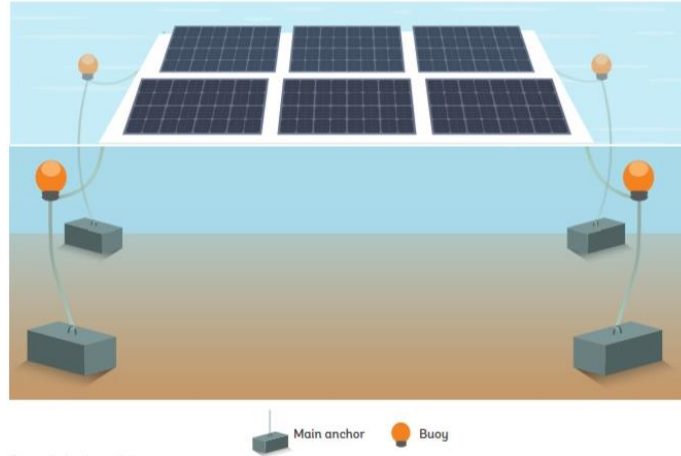
Figure 5: Anchoring using the buoy method, World Bank Group, ESMAP, and SERIS 2019 [1].

Innovative elastic mooring lines can also be adopted, the adjustable length permit them to be used for different bathymetry [1].

3.2. The key advantages

This technology entails numerous advantages, some of them are game changers while others could be defined marginals, these benefits are moreover related to numerous factors such as weather, aquatic and surrounded land environment and technology advancement of the state. The major ones are explained hereafter.

3.2.1. Land saving

Floating systems are majorly installed on man-made water bodies such as coal mining subsidence areas, industrial lakes, dams, desalination plants, fish farms and water ponds, these areas are mostly unused and some of them could not be used because of the pollution they contain. A great number of man-made lakes are near housing regions or near industries where electric transmission lines already exist, so there is no need to pay to build an energy transport infrastructure including

expensive transformers and safety precautions related.

So, thanks to this synergy with electrical infrastructure and cheap water body loan, the price related to the leasing land lowers a lot if compared to ground mounted systems where huge areas might be stolen to agriculture urbanization or any other needs that will produce benefits and revenues and, because of this, will have a higher price.

It is also easier to find sites for floating PV near densely populated zones and so less transmission losses will take place. FPV could also be used in aquaculture spots and hydropower generating dams where they not only employ unutilized lands, but also provide wide gains for the utilities increasing the wellness of fish and decreasing the evaporation of water which for the dam is a double energy profit [4], [6].

3.2.2. Reduction of water evaporation

The evaporation of water can be brought by different factors, the more important are the solar radiation, the heat exchange with air, the vaporization due to latent heat, the air pressure, the area exposed, the subsoil heat exchange, and the convection due to wind. The energy balance equation that describes the evaporation rate il shown below.

$$m_w c_p \frac{dT_w}{dt} = A_w q''_{soil} + A_w q''_{air} + A_w q''_{rad} + A_w q''_{wind} - A_w m''_{ev} L_{ev} \quad [\frac{J}{s}]$$

Where m_w is the water mass flowrate, c_p is the water heat capacity, dT_w is the infinitesimal delta of temperature of water over time, A_w is the area of the water basin, q''_{soil} is the heat flux exchanged through soil conduction and it is greater in porous subsoils, q''_{air} is the conductive heat flux correlated to the Fourier law due to the difference between air temperature and water temperature, q''_{wind} is the convective heat flux exchanged through wind and depends on the wind velocity and on air properties, m''_{ev} is the evaporated flowrate and L_{ev} is the latent heat of water which is 2.46 MJ/kg in standard conditions [7].

The major evaporative contribution of a large water pond or a reservoir are due to sun radiation and forced wind convection. And these two influences are reduced thanks to the floating platform. Indeed, the panels cover the water and so act as a shield of external energy income in the body, floating structure also reduce the wind affecting the surface of water lowering the convection induced. This benefit is critical in places where water is scarce but also in reservoirs and hydropower dams where every liter of water saved is an economic and environmental gain. It has been estimated that the area covered by floating PV will reduce its evaporation from 10 % to 80 % depending on the type of solar platform and on the weather conditions [8].

3.2.3. Implemented water quality

Floatovoltaics are considered environmental benign since they do not harm the environment and they might increase its wellness. The polymer the floats use is high density polyethylene HDPE, the same plastic used for foods packaging since it does not release toxic substances; it is a thermoplastic polymer that if drugged will not degrade to ultra violet light and to environment weather. In most of the artificial lakes algae growth can be a harm since they might create a marshy environment letting the place ideal for dangerous bacteria harming the aquatic life and creating unpleasant smells. In order to decrease the algae growth covering technologies are used. The FPV can be useful in this case because it will create shading that will discourage algae prosperity, and produces clean electricity that might be used to pump air in the water oxygenating it and creating a better environment for the fauna [4].

3.2.4. Increased energy yield

A higher energy yield of FPV is associated to the cooling effect which decreases the temperature of the cell, increasing the efficiency from 5% in colder regions to over 10 % in warmer ones. The module temperature is related to different causes and can be calculated with the following equation

$$T_m = T_a + G * \left(\frac{\tau * \alpha}{U}\right) * \left(1 - \frac{\eta(T)}{\tau * \alpha}\right)$$

T_m is the module temperature, it is dependent on the temperature of surrounding air T_a, the irradiance G, the transmittance of glazing τ, fraction of solar spectrum which is absorbed α, U is the heat loss coefficient measured in $W/m^2/K$ and $\eta(T)$ is the efficiency which is also correlated to the temperature [1].

The cell losses related to temperature are a well-known threat since they are one of the major energy losses, the increasing temperature lowers the power producible from about 0.35%/°C to over 0.5%/C° depending on the photovoltaic cell type (see *Fig. 6*) [9] [10]. This is a great problem in places with warmer seasons where at noon the temperature of the cell could reach temperatures over 80°C and these periods match the times where most radiation hits the panels and so when the producibility could be at the maximum value. To reduce this problem different cooling techniques have been adopted, from pumping and spraying water on the back sheet of the panel to create a water film on top of the panel's glass, but since these approaches consumed energy, they were not always energetically and economically feasible. Floating photovoltaic is instead a solution to this problem since no external energy is needed to cool the panels. And the intrinsic natural effects lower the temperature of the panels. There are three main factors which reduce the module temperature, the first one is the lower temperature under the modules, the air between the panels and the water has from 1°C to 3°C lower temperature compared to ground mounted applications [1]. The wind effect is more persistent and effective on floating panels so a higher convective effect cools the surfaces. Being on a water body increases the moisture around the system, also wind could splash water on the back sheet of the panels, this has a heavy effect because water has

a higher conductive coefficient compared to air (k_{water}=0.6 W/m/k, k_{air}= 0.026 W/m/K at T=25°C)[2] and thus the heat exchange will speed. Moreover, water settled on the modules could evaporate, which means that such high latent heat as the water one (2.46 MJ/kg$_w$) will be able to lower the module temperature from 5°C to over 15°C, increasing, as a consequence, the overall yield and thus the energy production of the system.

The cooling effect is considered to have also a long-term beneficial effect since the cells will degrade less and few maintenances are required relatively to this problem.
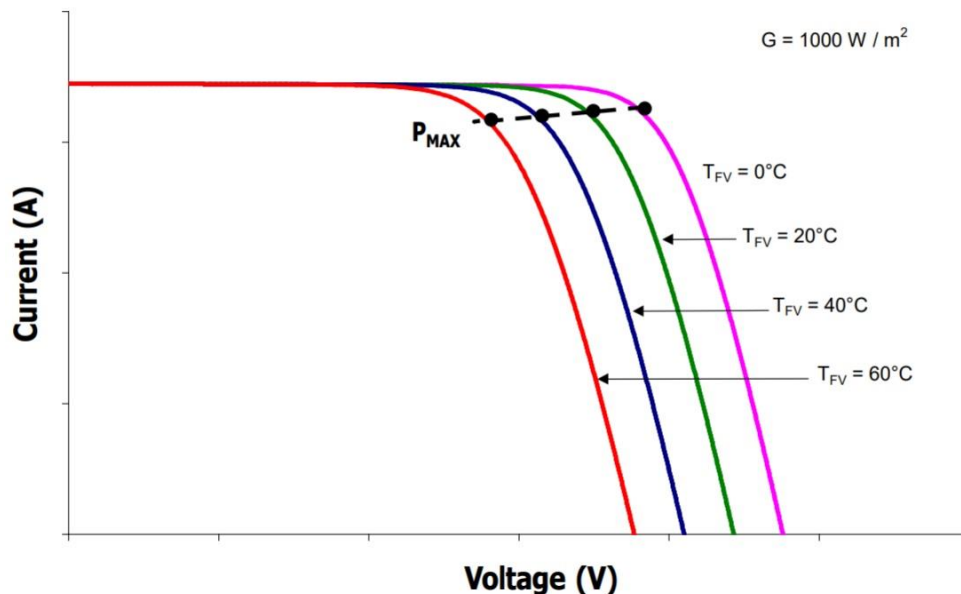
Figure 6: Current-Voltage diagram showing the effects of temperature on the solar panel power production, Spertino F., slides of the course "solar photovoltaic systems" [9].

The yield is also usually higher because of the less shades, in fact floating plants are rarely shaded, also due to the low tilt angles. The dust covering the modules is another common loss factor which could lower to more than 3% the efficiency. Usually FPV platforms are located in less dusty areas compared to arid and desert places where solar farms are commonly located and where soil could easily deposit on the panels.

---

[2] Torchio M F Tabelle di Termodinamica e Trasmissione del Calore - Proprietà delle sostanze di uso frequente. CLUT Ed., Torino 2012

3.2.5. Simple installation and deployment

With exception to anchoring and mooring, no other civil work is required, the platform is easily assembled on site with short deployment times. The avoidance of time and work for the site preparation translates in less installation costs. Furthermore, these systems can be modulated over time and easily removed making them more versatile.

3.3. Floating PV compared to Ground mounted PV

Further advantages can be related to the floating photovoltaic technologies but also some disadvantages need to be taken into consideration, a comparison between FPV and GMPV is synthetized in the *Table 1*.

Parameter	Floating PV	Land mounted PV
Yield	✓ Lower cell temperature ✓ Low soil debris and dust deposition ✓ Long term degradation ✓ Almost no shading	✓ Suitable with tracking, bifacial panels ✓ It is possible to reach a high tilt angle X More temperature losses, especially in warm climates
Design	✓ Possible to rearrange over time in a modular way X Limited tilt angle and design due to wind resistance prerequisites X Anchoring and mooring adequate design	✓ Yield prediction is easier to establish X Terrain constrains

Parameter	Floating PV	Land mounted PV
Land use	✓ Lower leasing costs ✓ Reducing water evaporation ✓ Possible integration with aquaculture and dams ✓ Easy to find sites closed to densely populated areas ✓ Does not consume useful land	X Affordable and suitable lands may be far from the transmission lines and from the load centers X Higher land cost X Competes with industrial, agriculture and city dwellings purposes
Environment	✓ Reduction of algae flowering ✓ Reduction of water evaporation X Potentially impact on ecosystems X Long term effects are not yet known	X Possible impacts during construction like deforestation.
Power system relation	✓ Possibility to match hybrid operations with hydropower plants ✓ Synergy with electrical transmission infrastructures	X High grid interconnection cost if far from the infrastructures
Installation and deployment	✓ Easy to assembly X Difficulty in floats transportation since they have a great volume so a local production would be needed X Need suitable deployment area X Wind resistance	X Heavy equipment is used X Soil quality dependance
Investment	✓ Slightly higher costs compared to ground mounted ✓ Costs may drop faster over time due to higher requests X Risk is highly perceived	✓ Established investments knowledge ✓ Continue cost drop

Parameter	Floating PV	Land mounted PV
Operation and maintenance	✓ Lower risk of vandalism X Higher O&M costs especially if the use of boats is needed, more frequent inspections, might need divers and replacing some parts is complex, X Attraction to bird drops	✓ Easy access and clean X Affected by growth of vegetation
Leasing possibility	✓ Easy to lease since it can be removed and reused in different settings and with less civil works, installations and excavations	X Hard to lease since it cannot be removed for a long time period
Safety	✓ Lower insulation resistance to the ground X Risk of staff falling into water	✓ Safe and easy to test
Durability	X More than 10 years of usual warranty	✓ More than 20 years warranty
Maturity	• Capacity at the end of 2018 was 1.3 GWp X A bit more than 10 years of experience but only 5 years of experience with large scale projects	• Capacity at the end of 2018 was more than 500 GWp ✓ More than 30 years of experience
Regulation and permits	X Difficulty for natural lakes applications X Lack of well-established regulations in some places	✓ Permitting processes are more established ✓ Clear regulations

Table 1: Comparison different aspects of the Floating photovoltaic systems to the conventional ground mounted systems.

The production of the FPV is different than the one of a ground mounted system, a comparison has been developed by NRG Energia measuring two systems located in Bubano (Bologna, Italy). The water body is a flooded ex-cave and on it a 500kWp floating system was built by the company in 2010 covering 5000 m², in 2010 such a plant was possible tanks to feed-in tariff incentives. Just 1.7 km away from the aforementioned platform, a ground mounted system was installed, and this allowed a comparison since both systems would have similar weather conditions. The two systems used the same PV panels and same inverters, the parameter that differentiated them was the inclination since a 35° tilt angle was applied on the ground mounted system while the floating system had a 5° module angle, and both the systems were facing true south. The measured FPV energy production exceeded the forecasted by 8% and was just 2% lower than the one of the ground mounted system still having a very diverse tilt angle. The global yearly production spread was different though. As shown in *Figure 7,* a more flatten production curve was measured on the ground mounted system while a sharper shape was associated to the floating production, the FPV production shape was due to the low tilt of the panels, which increases the production in summer and lowers it in the winter periods but the shape is also related to the cooling effect which produces more energy than the forecasted and this overproduced amount is majorly distributed in the warmer periods [8] 12] [16].
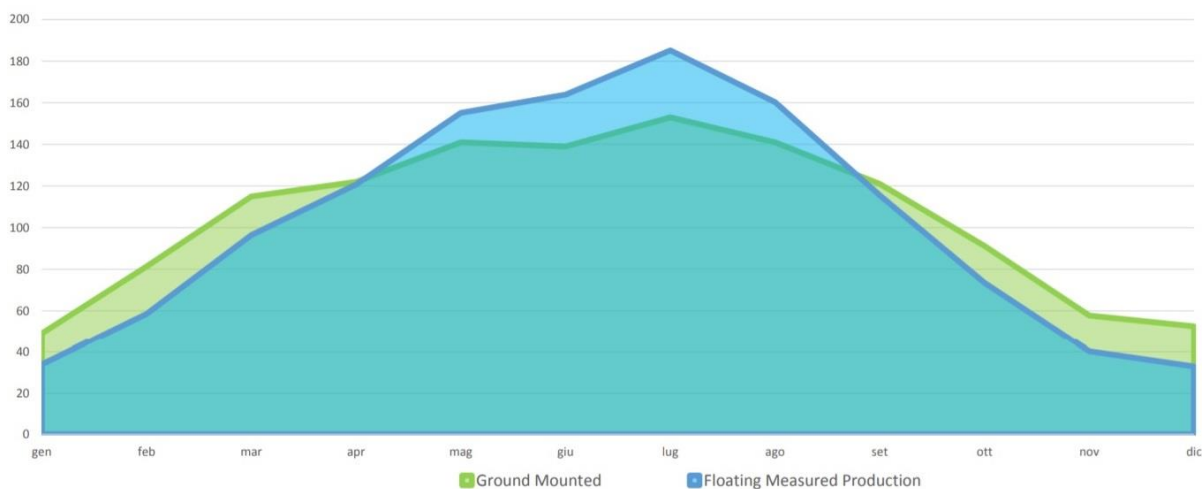
Figure 7: Energy production of a ground mounted system and a floating mounted system over the year, test carried out by NRG Energia [8].
Note: the y axis represents kWh/kWp

It is possible to see how the two production shares differ. On cold months the floating PV production is lower since the water-cooling benefit is not affecting much the system due to the already cold weather, and so the tilt angle effect weights on the floating system resulting in a minor production. On the other hand, on warm periods so from April to the end of August a higher production is achieved since the cooling effect makes a great difference (see *Fig. 8*). In most countries, sufficiently near the tropics, the warmer periods are correlated to a higher electricity consumption, majorly used to cool residential and industrial buildings, so the FPV system can match this consumption in best way.
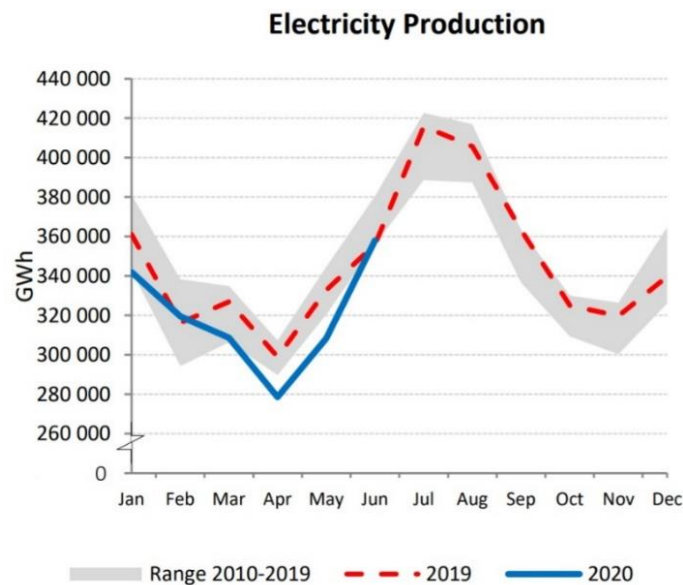

Figure 8: Electricity production in USA, data from IEA monthly energy statistics [11].

The whole comparison is also just focused on the energy production, but further advantages such as an avoidance use of useful land and a lower water evaporation are what also distinguish this two electricity generating systems [11].

3.4. The market potential

The photovoltaic global market potential is immense, its main potential is in zones near the tropics where the weather is mostly arid, but those places are also the less inhabited.
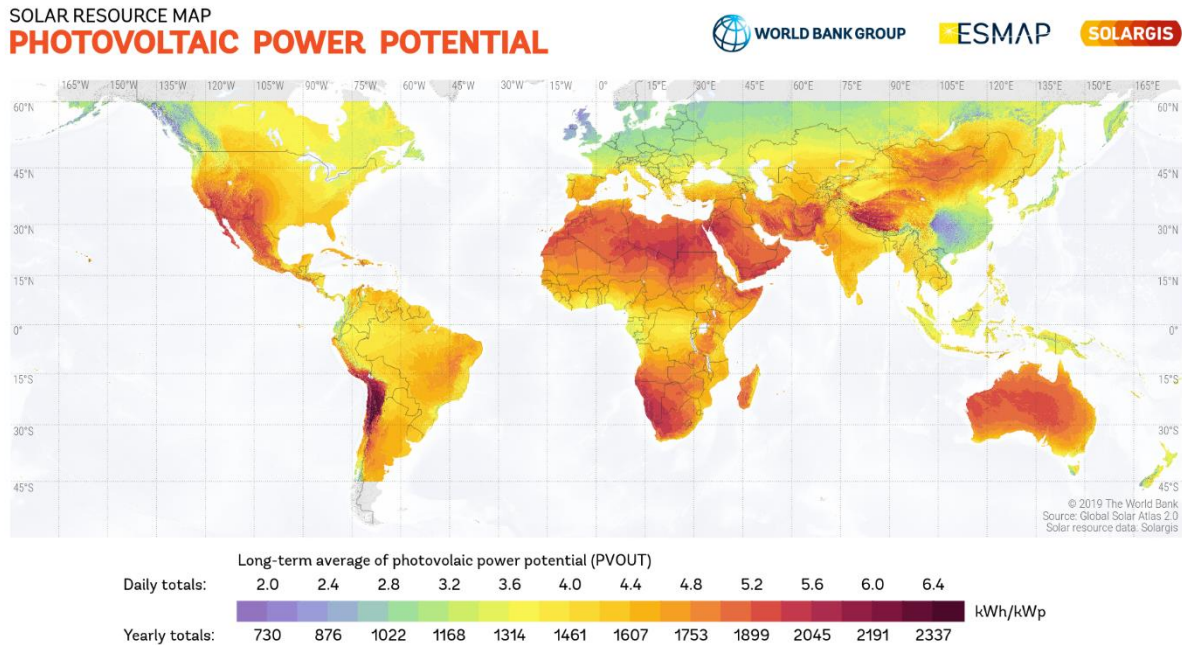

Figure 9: Photovoltaic global power potential, Global Solar Atlas (https://globalsolaratlas.info).

Solar on water has also a great potential, the water bodies of its applications can be natural or man-made, since a deep study on the effects of this technology on natural environments is not well established the focus will be on man-made water bodies. Using data from the Global Reservoir and Dam Database it is possible to estimate the potential of floating solar power installed. Considering a conservative 100 Wp/m^2 installability, the potential installed capacity would be 400 GWp if only 1% of the manmade water bodies surfaces were used, this capacity turns to more than 4000 GWp if the used surfaces becomes 10%. This percentages were chosen in order to not achieve environmental impacts but higher values can be accomplished as well, guaranteeing environmental safety. The 10% scenario shows a capacity of over 1000 times the cumulative installed capacity so far and this is without tapping the potential natural resources and the oceans. Which have the

majority of solar irradiation income. As shown in *Figure 10*, the main continents rich of available floating areas are north America, Asia and Europe. Which are also the most developed, populated and energy-intensive countries. It is possible to see from the table that in the 10% scenario more than 5000 TWh annual electricity can be produced, that equals 22.55% of 2019 electric energy domestically consumed (23,105 TWh [3]). It also means that **44.34%** of worldwide manmade water bodies covered by floating solar systems can produce the amount of energy sufficient to cover 100% of 2019 electric global domestic energy consumption. It needs to be stated that this is only possible with proper storage units in order to be able to temporally link production and consumption.

Continent	Total surface area available [km²]	No. of water bodies assessed	Total FPV capacity potential [GWp] (% of water surface used for PV installation)			Total annual FPV energy output potential [GWh/y] (% of water surface used for PV installation)		
			1%	5%	10%	1%	5%	10%
Africa	101,130	724	101	506	1,011	167,165	835,824	1,671,648
Asia*	115,621	2,041	116	578	1,156	128,691	643,456	1,286,911
Europe	20,424	1,082	20	102	204	19,574	97,868	195,736
N. America	126,017	2,248	126	630	1,260	140,815	704,076	1,408,153
Oceania	4,991	254	5	25	50	6,713	33,565	67,131
S. America	36,271	299	36	181	363	58,151	290,753	581,507
Total	**404,454**	**6,648**	**404**	**2,022**	**4,044**	**521,109**	**2,605,542**	**5,211,086**

Figure 10: Floating photovoltaic potential, capacity and energy generation by continent for man made reservoirs and dams only, World Bank Group, ESMAP, and SERIS 2019 [4].
*Notes: *middle east is included in Asia*

---

[3] Global Energy Statistical Yearbook 2020 (Enerdata) Electricity domestic consumption
https://yearbook.enerdata.net/electricity/electricity-domestic-consumption-data.html

3.5. Economic considerations

Floating installations have different purposes and serve different needs, so an exact economic comparison is hard to produce. These systems can work in tandem in hybrid hydropower plants helping reduce seasonal erraticism of hydropower generation, besides producing energy with a higher efficiency they produce different additional benefits that ground mounted systems cannot archive. For floating systems, a total project cost can change due to the environmental and legislative constrains, some projects will add grid connection costs (which can greatly fluctuate if the connection is in low or medium voltage), the lease of water ponds and some projects could be easier to implement than others. As capital expenditure the main differences between ground mounted and floating systems are the floats, the mooring and anchoring parts which are also highly site specific and can change their cost by different reasons. The PV panels are usually the same, a glass-glass poly or monocrystalline 60 or 72 cells module is often used in FPV which guarantees a good resistance to moisture. The inverters are the same as well as the connections to the grid.

The capex of a large scale unsophisticated FPV system was at the end of 2018 about 0.7$/Wp to 0.8$/Wp (see *Fig. 11)*.

CAPEX component	FPV 50 MWp ($/Wp)	Ground-mounted PV 50 MWp ($/Wp)
Modules	0.25	0.25
Inverters	0.06	0.06
Mounting system (racking)*	0.15	0.10
BOS**	0.13	0.08
Design, construction, T&C	0.14	0.13
Total CAPEX	0.73	0.62

Figure 11: Comparison of capital investments: FPV vs ground-mounted systems, World Bank Group, ESMAP, SERIS 2019, data from 2018 [4].
Note: BOS= balance of system; T&C= testing and commissioning
*Includes the floating structure and anchoring systems; **includes the monitoring system.

These values do not take into account the engineering, procurement and construction costs and the margin, the overall price is usually 1.25 times the total CAPEX, so for the FPV it is 0.91 $/Wp and for the ground mounted it is 0.78 $/Wp (*Table 2*).

CAPEX component	FPV 50 MWp [%]	Ground mounted PV 50 MWp [%]
Modules	27.47%	32.05%
Inverters	6.59%	7.69%
Mounting system	16.48%	12.82%
Balance of systems	14.29%	10.26%
Design , construction	15.39%	16.67%
Engineering and procurement	19.78%	20.51%

Table 2: Comparison of capital investments percentage: FPV vs ground-mounted systems

The difference in cost between FPV and GM is related to the mounting and racking system, the balance of system and slightly correlated to the design and construction, these higher costs have a margin of reduction by increasing the maturity of the technology.

FPV has then an overall higher capex cost. Furthermore, the levelized cost of electricity considering 20 years lifetime for both the technologies is just slightly higher due to the higher efficiency of this systems (see *Fig. 12*).

LCOE ($cents/kWh)			Ground-mounted PV 50 MWp	Floating PV 50 MWp	
				Conservative (+5% PR)	Optimistic (+10% PR)
Tropical	WACC	6%	6.25	6.77	6.47
		8%	6.85	7.45	7.11 base case
		10%	7.59	8.28	7.91
Arid/desert	WACC	6%	4.52	4.90	4.68
		8%	4.96	5.39	5.15
		10%	5.51	6.01	5.74
Temperate	WACC	6%	6.95	7.53	7.19
		8%	7.64	8.30	7.93
		10%	8.49	9.26	8.85

Figure 12: Levelized cost of electricity produced by FPV and ground mounted, comparison with conservative and optimistic performance ratio, World Bank Group, ESMAP, and SERIS 2019 [4].

Note: The LCOE is higher than the one that can be expected because the WACC is high, today lower Weighted Average Cost of Capital are applied (3%)

It is important to state that while standard PV systems is a mature technology, the FPV is not established yet since it is on its early stage and not on a large-scale manufacturing processes, so it is expected a higher margin of cost reduction [1], [4].

4. NRG Island

NRG Energia is a world leader supplier and installer of modular systems for the realization of floating solar PV plants on calm water bodies.

Their patented floating system "NRG Island" is one of its kind and represents a simple and modular solution for FPV applications, the sun light shielding and the specific geometry aim to reduce by 80% the evaporation rate and enhances the circulation of air under the modules providing a cooling effect that increases the PV efficiencies especially during warm weathers. The NRG Island unit system includes one metal frame made of aluminum or steel and four floating units made of high-density polyethylene (HDPE) enriched with UV and freeze resistance additives, this material is nontoxic and not harmful to aquatic ecosystems and has a useful life of over 25 years. Each "NRG unit" can support 4 PV modules of any brand, kind and dimension usually in portrait mode. The floating units can connect to each other and so different assemblies can be made to satisfy different needs.

Since 2010 with multiple experiences all over the world the plant has been implemented gaining the acknowledgement as the largest FPV plant installed in the world in 2010.

This system is easy to assemble and can be directly installed on the shore of the basins, the floating units can be pre-assembled on land and further joined to form columns or rows of the floating plant. The assembled parts can be pushed on the water surface, they are very easy to handle since they are extremely light and resistant, the connections are easy and do not need any divers or under water work because the floats can be linked to each other's from above, using specific HDPE bolts and screws. The floats in addition to being used to sustain the modules are also operated to provide a walkway to let men to assemble, provide maintenance and are also used to place and fix electric cables. After the connection of floats and metal frames the solar panels installment can already take place, and in a small amount of time the system is completed.

The platform can be adapted to satisfy each kind of need taking into consideration the variation of water's level. The anchors used can be of two types, the first type is a deadweight and chains underwater installed, the second type is a concrete weight placed or buried on shore connected to the FPV system through resistant chains or tenacious ropes. The electric cables and the string boxes can be installed on apposite additional floats.

The system was conceived to resist on any kind of water, from fresh still to salty, it is very resistant and comes with a 10 years warranty against any factory defect.
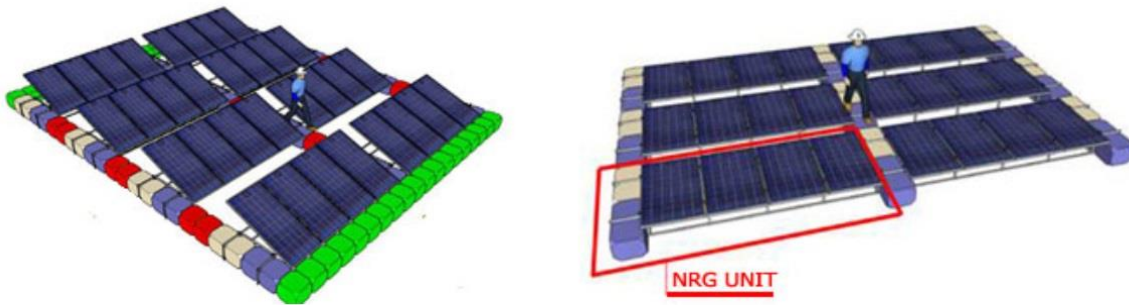

Figure 13: NRG Island Floating photovoltaic system and NRG unit, NRG Energia.

What entails success to the NRG Island is in part thanks to the innovative and functional floats. The distinctive cube shaped design allows to quickly and easily connect all the parts. Involving a small amount of time for the installation. The floats can be also merged into platforms of every customer desired shape providing a floatability of 350 kg/m^2. Thanks to the wide flat surface of the floats, a better stability is maintained even when people are walking on it. Furthermore, the compactness of the structure improves the general island's resistance. The elevated resistance is also provided by the anchoring and mooring systems which are each time specifically designed for every situation and which can be designed to resist also to extreme weather conditions [13] [14] [15].

Figures 14-15: On the left NRG Island deployed letting the pre-assembled system slip on the shore, on the right a NRG Island system assembled on site, NRG Energia.

5. Florida and relative photovoltaic applications

5.1. The state of Florida

The peninsula of Florida, often nominated panhandle due to its similar shape is the most tropical state of the 50 United States of America, it is situated at the south-east of the American coast, is wet by the Atlantic Ocean from the east side and the Gulf of Mexico on the west side and confines to the states of Georgia and Alabama on the north.

Figure 16: United States of America and highlighted the State of Florida, Encyclopedia Britannica Florida Image.

It is the 4° state per population, densely located at the coastal sides at the south and more distributed at the northern parts, and is the 22° state in terms of land surface presenting mostly a flat surface rich of lakes and the highest points are represented by hills of around a hundred meters.

The weather is strictly correlated to the Atlantic and Gulf currents and to the proximity of the tropic of cancer which results in sub-tropical climate mostly warm and humid. The seasons are alternated by dry winter seasons and warm and rainy summer seasons, the temperatures could vary from about 10 °C to 35 °C depending also on the regions of Florida: the northern part could also face a 0° while the southern part has a warmer weather but can reach temperatures over 40° in the summer season. The state of Florida is also very famous for storms and lightning being one of the

rainiest states and the major state struck by lightnings. From June 1st to the end of November the hurricane season hits the state providing tropical storms and strong hurricanes near or on the peninsula which generate fear and destruction along their path [17] [18].

5.2. Solar PV in Florida

Every state in the USA has one or more attributed name which represents the history, the philosophy, the weather or other important characteristics of such state, the most important attribute can be found on the backside of the dollar quarters, the car license plates and on everything that represents the state. Florida since 1970 is nicknamed "The Sunshine State" because of the huge amount of sunlight that hits the state all year long, in fact it is located on the world's sun belt, which is the stripe of surface near and between the tropics that guarantees a small difference in sun irradiance from summer to winter, providing a constant and persistent illumination during daytime all year long.

Thanks to its main attribute the Florida's region is one of the best places not just in the US but also in the world to install solar photovoltaic panels and not only has a lot of sunlight, but it is also densely populated and presents a high electric consumption, greatly related to air conditioning.

Even though Florida is one of the southest states of US, it is just the fifth state for solar PV cumulative installed capacity, with northern states such as California, North Carolina, Arizona and Texas above it. But this state is quickly moving towards solar since in 2019 the state of Florida has been the second solar PV installer in the US with almost 1 GWp installed (see *Fig. 17*). An abundant share of this installed renewable energy was from utility photovoltaic plants while the minor part from distributed plants [26], [27], [28], [29].
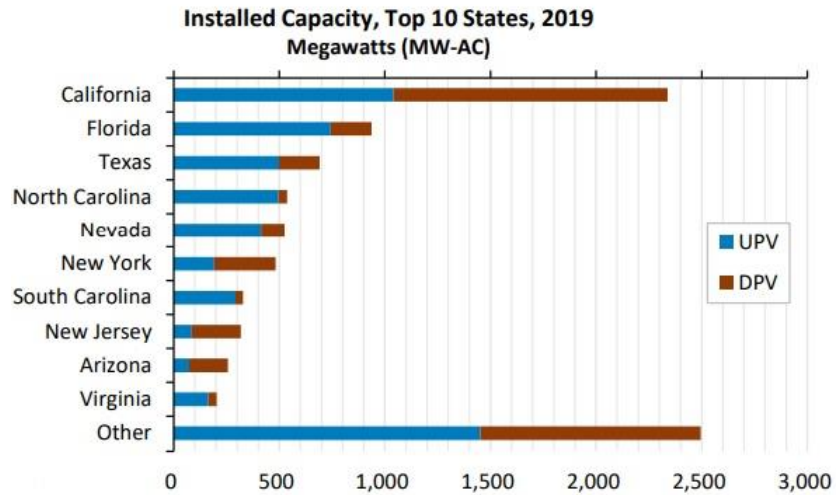
Figure 17: U.S. Installation breakdown by state, installed capacity in 2019, EIA monthly data, Q4 2019/Q1 2020 Solar industry update from NREL [27]
Note: UPV= utility scale photovoltaics, DPV= distributed photovoltaics

The *Figure 17* shows how the Floridian market is actually increasing, seeking more solar energy and mostly on a wide scale such as the utility one.

In Miami (FL) the final yield, defined as kWh/kWp, which describes the amount of hours a PV system is averagely providing its max power production, equals to 1550 kWh/kWp. This high value if compared to other cities let understand how a kWp installed in Miami produces 47% more energy than Paris, 21% more energy than Rome, and 19% more than New York City [19]. This higher production is translated into a lower levelized cost of electricity produced by the sun which could represent the PV technology as one possible major electricity producer in the state since the cost of a kWh produced by PV is lowering over time becoming cheaper than any other electricity generator. Thanks to this, PV is not only the future of Florida but also Florida is the future of PV. Despite not high incentives the amount of solar PV installed in the state is increasing exponentially lowering the cost and providing a highly competitive payback time of 6 to 7 years in the Miami region with tax credit [19].

Solar PV in Florida is not only a great renewable energy solution due to the cheapness of the energy produced but also due to the production curve which is similar to the statal electricity load curve. In other colder states and countries, the load curve is the typically shaped duck curve, which is a double peak daily curve presenting the first peak during the early morning (7.00-9.00 am) and the second big peak at the late afternoon (7.00-9.00 pm), both periods where the photovoltaic production is at the lowest rate. In Florida there is still a consumption with those two sunset and sunrise located peaks, but another high portion of consumption is located right during the midday since a very high consumption is associated to cooling activities for residential, commercial and industrial use (see *Fig. 18*) [20]. This period matches the solar PV production curve which is higher during most sunny and so warmer periods of time.
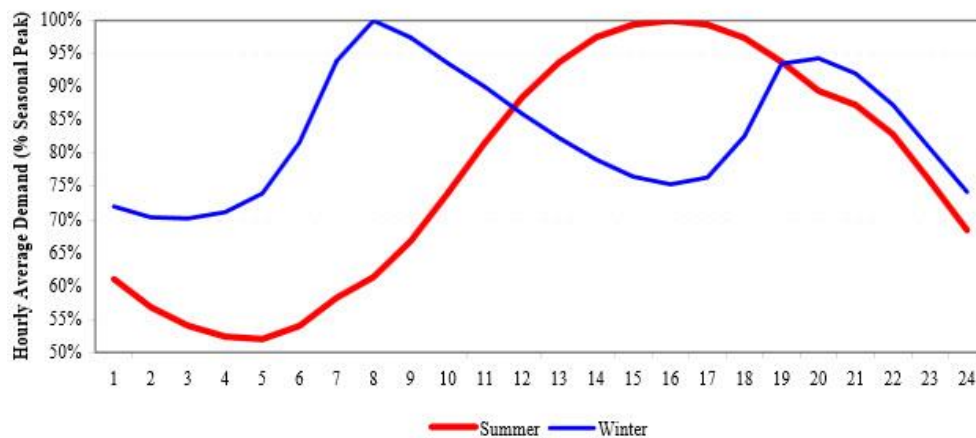

Figure 18: Daily electricity demand curve in Florida in summer and winter, Florida Public Utility Commission, energymag [20].

This match can be found in other states only during the summer period, but in Florida it is present for most of the year. Furthermore, the USA has a higher consumption of energy if compared to other countries, for example a residential house electricity contract in Italy could be 3 to 6 kWp while in Florida could exceed the 20 kWp. This amount of power is mostly provided by fossil sources, in 2020 77.4 % of electricity was produced by generators fed with gas, mostly gas turbines, the 11.7 % was produced by nuclear, 6.6 % was produced by coal and just 4.3 % was produced by renewable sources of which solar plays a major role [21]. This energy mix, if related to one of the highest consumer per capita state, shows the pollution and global warming potential that is produced. Here solar could make a big difference competing with fossil fuels generators

28

and old nuclear power plants, it could shift the electric energy production market providing a cheaper and cleaner energy that could also be produced in a decentralized way.

5.3. Land and lakes in south Florida for PV applications

Preamble:

A deeper focus of this work will be on the southern east part of the state which is one of the most densely inhabited and which has Miami as populated vertex.

The populated southern east part of Florida is crushed to the east banks of the peninsula since the protected natural area of the Everglades national park is taking all the south-central part of the region. The Everglades park covers more than 6000 km^2 and is recognized as a world heritage from UNESCO, it is a wild area of marshy land mostly under water and covered by tall grass and mangroves. Inaccessible if not from few roads the Everglades park is a zone of border to the densely populated metropolitan area of Miami and all the southern and northern parts of the region [22]. Therefore, this park on the west side and the ocean on the east side represent the two limits of anthropic growth, due to this problem the residential and industrial growth developed vertically towards north reaching over time a saturation. This peculiar situation, very different from the average USA free space available for buildings, brought over time to a dramatic growth of prices in the building sector. The growth is not only due to the low space but also because of a general market price growth, but the rate land price growth is distinguishable greater in the Miami zone compared to the Orlando or average state rate.
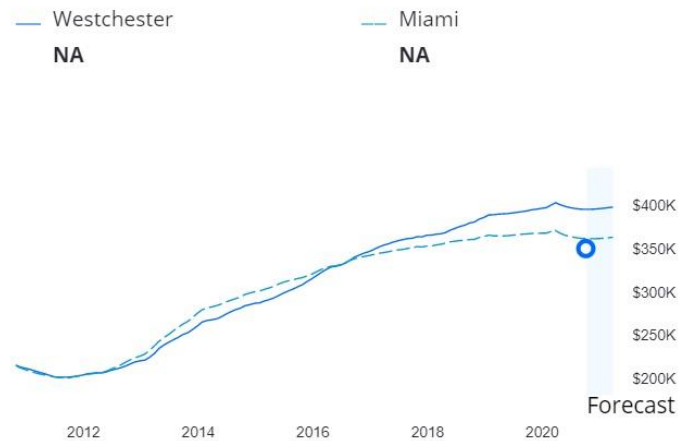
Figure 19: Rise of house prices in Miami and in the near Westchester, Zillow, https://www.zillow.com/homedetails/9633-SW-20th-Ter-0-Miami-FL-33165/2077541483_zpid/.

From the above *Figure 19* it possible to grasp how the market of a residential house is increasing both in Miami and in the more western zone of Westchester, the drop that could be seen before 2012 is associated to the global economic crisis that drastically reduced the house price values and the small drop at the beginning of 2020 is associated to the coronavirus pandemic but the trend is increasing. This increase in the residential, industrial and general building sector is related to the increasing value of the land. Since less land is available and the request is high the prices will continue to skyrocket. A higher land price can be extremely negative for the ground mounting PV market and due to the limited zones of the region it might be incentivized the activities that can yield a higher return such the residential market.

In addition to the sun light another asset Florida is very rich of are lakes, especially in the southern part of the state, the *Figure 20* below, captured from Google Earth, shows the view of a big part of the northern side of Miami, as it is possible to see the anthropized area is embedded between

the green Everglades at west and the blue Atlantic Ocean at east, also it is possible to denote the blueish spots from the smallest to the widest which are lakes.
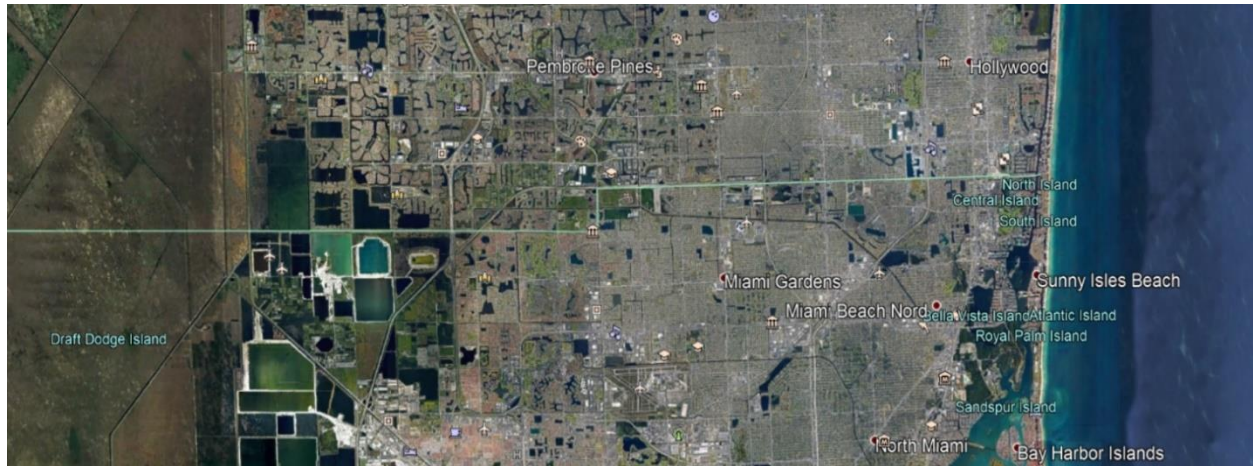
Figure 20: View of the north Miami metropolitan area, sight of numerous lakes, Google Earth Pro.

Lakes and ponds in Florida provide habitat opportunities for a wide variety of plants and animals, the state has thousands of lakes that provide drinking water, habitat to flora and fauna, and aesthetic and recreational values. Most of the lakes in the urban areas are artificial lakes and can be divided into two types: the big industrial lakes and the small residential lakes which could also be subdivided in branched lakes and ponds. In the industrial field, lakes are mostly used to provide water to the industry that could be used for a wide number of purposes such as cooling, washing, manufacturing, diluting, high pressure machines exc. Some lakes have been also created by digging the terrain in order to higher up the industrial infrastructure and guarantee a less harm in case of storm induced flooding [18]. Some of these lakes have wide areas, in the order of 1 to 5 km^2, so on a single industrial lake dozens or hundreds of MW of floating photovoltaic could be potentially installed.

Figure 21: View of the north Miami industrial area, sight of numerous lakes, Google Earth Pro

Some wide lakes are also reservoirs and salt flats on which FPV systems can also be installed. The residential use of lake is essentially aesthetic, the south Florida land was largely marshy so a reclamation of the swamp area has been actuated through time, in order to guarantee a solid resistance of the residential lands and to higher the basement to resist to flooding, the land has been digged and deposited creating large ground depressions which created lakes. In the urban areas these lakes can have a branched form, permitting the passage of kayaks in some residential neighborhoods and providing a pleasant view from the houses.

Figure 22: View of the north Miami residential area, sight of numerous branched lakes, Google Earth Pro

Other residential locations have the lake at the center of the resort, sometimes these lakes have fountains that can make it look cuter and oxygenate the water, but most of the times these lakes are not very inviting to swim or do recreational activities since they are mostly dark and full of algae.

Figure 23: View of the north Miami residential area, sight of numerous resort lakes, Google Earth Pro

The lakes are not always a safe place to swim also because of the pollutants they contain. Indeed, when it rains the water rushes over streets, highways, lawns, and industrial sites and collect sediments, litter, nutrients, toxins, metals, oils and other harmful pollutants, these streams of water can flow in the aquifers but also into lakes which will collect these elements, increasing over time their concentration. These lakes do not usually have a high variety and number of fish, some of them do not have fish at all, but they have a large multiplicity of algae and seaweeds. Algae grow everywhere they can reach the sunlight, from the littoral zones to the shallower parts. Since the ponds and lakes present in the urban areas are not deep, the algae can reach easily the light and spread. The high spread of algae is also induced by the invasive species coming from abroad and because of the excess of nutrients the lakes receive, such as phosphorus coming from detergents and fertilizers from human activities. The algae bloom is a common problem in Florida's lakes, they can create scum on the water surface and affect the water taste, color and odor. Moreover, since they are near living areas the unpleasant odor and the murky water color can transform the beautiful sight into a filthy and smelly environment. In order to avoid this problem different techniques are adopted:

- *Mechanical cutting*: it is inexpensive and provides immediate results but the roots will regrow and so numerous cuts might be needed
- *Manual methods*: inexpensive and nontoxic but are labor intensive and can agitate the sediments
- *Benthic barriers*: the bottom covers limit the light penetration and so are harmful to algae but can also be easily damaged over time and needs to be strongly anchored to resist to gasses formed from the bottom
- *Mechanical harvesting*: it is effective but also labor intensive and expensive and can also cut until 10 cm below the surface
- *Hydro racking*: removes the entire plant but increases the lake's turbidity lifting sediments
- *Biocontrols*: will have an effective slow response and can be expensive
- *Herbicides*: are very effective but can be toxic and can harness the aquatic life

All these methods can be adopted to limit or to solve the algae bloom problems, but a simpler way can be used: floating photovoltaic systems [23].

5.4. The weather in Florida and the relative implications

Since the Florida peninsula develops mainly from south to north passing from Key West at the latitude of 24° 30' to East with a latitude of almost 31°00' the weather is different all over the state. The optimal place to install floating solar panels is the southeast part due to the large quantity of lakes and the higher light exposure, for this reason the focus will be on the southern Florida weather with a specific focus on the neighboring area of Miami.

Miami, called also the "economical capital of south America", is the hub of the southern-east part of Florida, the metropolitan area of the city welcomes more than 6 million of Americans each of which averagely consumes more than three times the electric energy a European does. The high consumption is related to the American standards but also to the high utilization of air conditioning systems in the warm periods. The weather in Miami during the year is mostly sunny and cloudy, with a precipitation period starting at the end of May and ending in October. It is because of the cloudy environment that Florida has a lower potential solar PV production compared to the northern but arid Texas. The temperatures are mild in the winter period and become warm from April to the end of October, forcing people to use cooling systems to reduce the temperatures and moist (see *Figures 24,25)*. The precipitations and the winds are rarely strong, except in the hurricane season where strong wind gusts can reach over 200 km/h and water bombs can produce over 100 mm of water during the day (*Figures 26,27,28*). The wind is averagely blowing to the east direction, from the Gulf of Mexico to the Atlantic Ocean providing humidity and clouds (see *Fig. 29*) [33],[18].
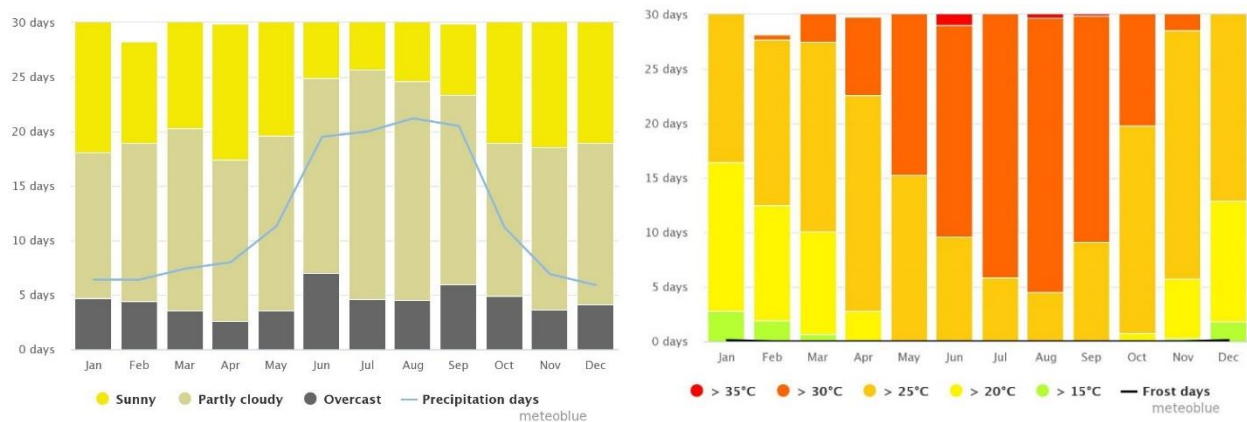
Figures 24-25: Miami monthly weather, on the left the mean monthly weather, on the right the mean monthly temperatures, meteoblue.

Figures 26-27: Miami monthly weather, on the left the mean monthly mm of rain, on the right the mean monthly wind speeds, meteoblue.
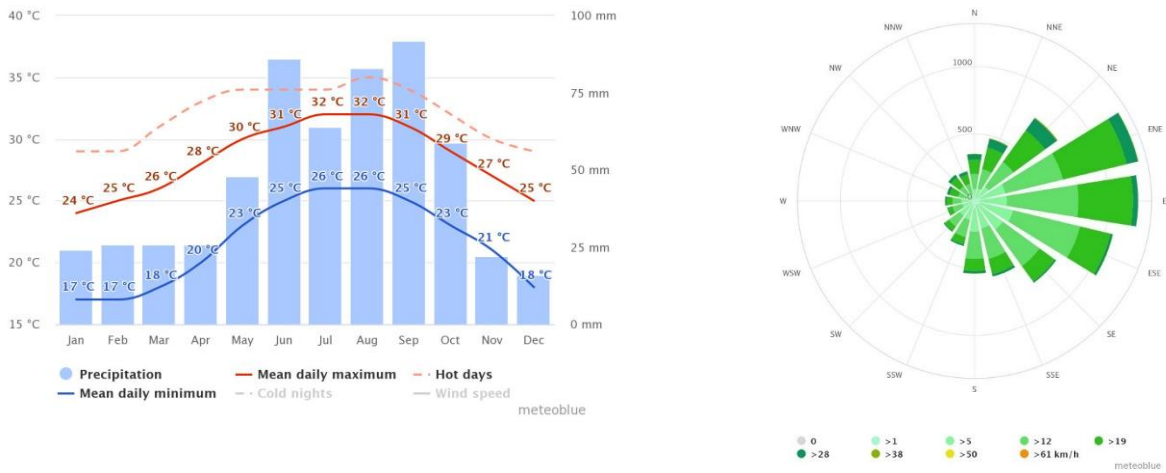
Figures 28-29: Miami monthly weather, on the left the mean monthly precipitation, on the right the rose of winds, meteoblue.

Conventional solar PV in Miami has a great potential due to the low latitude and high consumption of energy of the region, but it is limited by the cloudy environment and greatly by the high temperatures. The matching between the electricity consumption and the PV production is indeed shifted, the expected maximum solar productivity is in July but in reality it is in May. This is partly induced by the cloudy season but mostly induced by high temperatures of July that can lead the panel to reach temperatures over 80°C, which drastically lower the yield providing also possible damages to the cells and to the adjacent materials such as the ethylene vinyl acetate sealant. The following *figure 30* realized through an Helioscope analysis, shows the monthly solar energy production of a simulated plant over a bank building located on the north west side of the Miami metropolitan area[4].
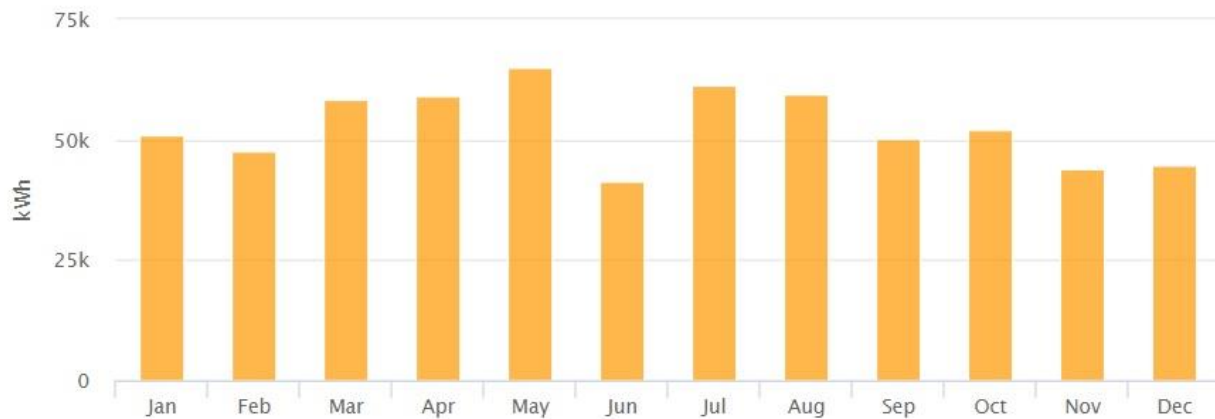

Figure 30: Simulated monthly energy production in Miami of a 403 kWp photovoltaic system roof mounted, HelioScope.

The installed power is 403 kWp DC and the yearly final yield is 1572,8 kWh/kWp, the month of maximum production is May while June, July and August perform a lower production compared to the one expected. As previously explained, a cause of this lowered production is the weather (which in this case is simulated using previously year data from near weather datasets), the rainy and storm season lowers the potential production of solar as well, but an abundant loss is related to the higher temperature of the summer season.

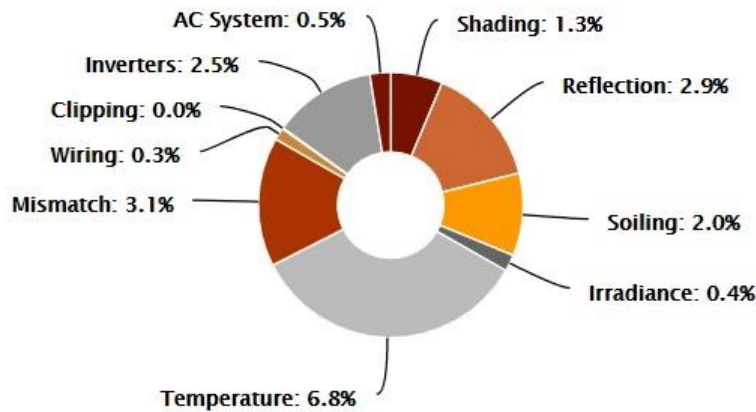[4] HelioScope: Advanced Solar Design Software. https://www.helioscope.com

Figure 31: Simulated losses of a photovoltaic system roof mounted in Miami, HelioScope.

A losses cake diagram of the aforementioned system is shown in the *Figure 31*; what can be instantly grasped is the higher share of the thermal losses which represents more than a third of the total losses.

This reduction in yield and so in energy production is also reached during the middle of the day when the higher electric consumption is achieved, making panels unable to produce the potential energy expected. This is a well-known problem in warm countries and brought to the study of different cooling techniques, the great majority of this techniques in order to cool the panels need external energy and in some cases the energy saved by the cooling effects is equal to the energy utilized to freshen the panels, producing a useless effort and making the system more expensive and with higher operational and maintenance costs. Another innovative way to cool panels is to install them on floating platforms over water bodies.

5.5. Floating photovoltaic systems in south Florida

The expansion of the human being on the world has eradicated the natural world passing from a 66% of natural wild land in 1937 to a 35% in 2020 [25], this expansion brought terrible global problems such as the effects of climate warm up. Further anthropic expansion could harness the wild ecosystems who were masters of those lands for millions of years, indeed a re-naturalization of lands needs to be adopted in order to keep future generations living in a pleasant world. A further expansion of the Miami metropolitan area is not allowed because of the Everglades national park, which however has been greatly reduced over time. The limits imposed will quickly saturate the already dense urban situation. This can be a big problem for the deployment of renewable energies and may lead to a forced use of densely energetic fossil and nuclear fuels that, as amply demonstrated, are harnessing the biosphere with the unavoidable production of pollutants. Since the price per m^2 of land is increasing over time on the south Florida region, the installation of ground mounted solar panels will have to face high land prices that can lead to a levelized cost of electricity higher than the one of the conventional energy producers, making this renewable technology unaffordable on the economic point of view. By contrast the region is abundant of unused and unprofitable artificial lakes. Due to their uselessness, the cost of the lake lease is low, then an installation of floating photovoltaic system is incentivized by the low rental cost. The FPV system is also very versatile and can be installed for just a period of time since it is very easy to place it and remove it, letting the lake's owner to decide whether to keep it or disconnect it. The use of floating platforms on lakes is not only used for photovoltaic systems. NRG Energia installed floating structures for recreational uses such as scenic walks, jogging, kayaking. Transforming unprofitable zones into touristic recreational centers. Becoming also pleasant for residential areas where the neighboring zones could higher their house value thanks to such attractive parks and could enjoy renewable energy locally produced.

From the point of view of algae bloom FPV is also an innovative solution. While producing energy and reducing the water evaporation the systems acts as a sunlight cover that permits oxygenation of the water but limits the algae growth. In lakes rich of fish, a small percentage of covered water does not provide harness, and is highly enjoyed by fish, that appreciate the shade during the day. While in polluted artificial fishless lakes the majority part the lake can be covered without produce

any environmental problems, but reducing odorous unpleasant algae increasing the quality of water. With this approach there would not be the need to apply the expensive and in some cases effortless techniques, mentioned in the previous chapter, that have been adopted so far. Besides exceeding the conventional ground mounted PV from the economic and environmental point of view FPV systems enjoy a natural cooling that increases their performance directly matching the peaks of demand. The cooling effect can increase the yield to over 10% and reduces the possible damages that high temperature can create in the panel. The produced energy would not be much higher than the conventional systems because the FPV modules tilt is usually lower than ground mounted systems but the shape of the production will be lower during morning and evening while higher during midday. In order to flatten the FPV production curve to guarantee also a higher production after sunrise and before sunset an east-west design can be utilized, this design will be explained in the *paragraph 8*.

6. The biggest concern

A reason why Florida is not in the top 3 cumulative solar installers is the biggest concern this part of the continent is affected by: Hurricanes. Tropical storms and hurricanes have always been an inner part of the Florida experience, and the threat posed by these immense storms cannot be overstated.

6.1. Hurricanes

The expression "hurricane", used in the northeast Pacific Ocean and the north Atlantic Ocean, derives from the word "hurakàn" used by the inhabitants of the Greater Antilles (The Arawak) meaning "god of the storm". Hurricanes are warm core regions of low pressure fed by tropical moisture and warm waters released by convection from the oceans. The necessary ingredients to form a tropical cyclone are listed below.

- Unstable humid atmosphere that can allow the air rise
- Warm oceanic waters with temperatures over 27 °C
- Adequate Coriolis force that provides the initial spin
- High relative vorticity

Prior to the hurricane formation an atmospheric disturbance is formed through the merging of air. This convergence usually arises in the intertropical convergence zone, where the airstreams from the southern hemisphere cross the equator meeting their northern hemisphere equivalents. The storms can be created from the moist and air that form near the west coast of the African continent. As air moves through these places the conjunction occurs causing the air to rise and creating a strong disturbance.

When this disturbance is large enough and is well structured with organized wind rotation, it forms what is called a "tropical depression". If the cyclonic circulation produces winds with speeds over 17 m/s (61.2 km/h) it becomes a "tropical storm" and from the 1950 a named is assigned to each of them. Once formed, the storm begins to trail westward to higher latitudes usually getting

stronger and bigger. When the wind speed increases and surpasses the 33 m/s (119 km/h) threshold, the storm mass becomes a hurricane. Hurricanes are then ranked by their strength using the Saffir-Simpson scale that can assign 5 different categories and attributes them to the destructive damage these hurricanes can cause.

The category 1 hurricane entails wind speeds from 119 km/h to 153 km/h, if the hurricane makes landfall on the peninsula of Florida it can produce minimal to moderate damages providing storm surge flooding, high waves and damaging winds. The approximated cost that this type of storm can generate in Florida could vary from some millions to half a billion of dollars. The Cat. 2 Hurricane has speeds from 154 km/h to 177 km/h and provides moderate damages that can cost up to 1.5 billion of American dollars. From category 3 on the event is called "major hurricane" and is usually responsible for extensive damages, the Cat. 3 is assigned to hurricanes with wind speeds over 178 km/h, the pressure from the standard 1,01325 bar is now lower than 0,964 bar and the damaging effects can lead to billionaires costs on the panhandle. The Cat. 4 event has winds with speeds greater than 211 km/h, the destruction of such a hurricane hitting land is extreme, most of the mobile homes will be destroyed, some frame homes can collapse and well-built concrete buildings may suffer from the damage of the roofs. The damage can cause also the uproot of trees, the blow out of windows and the shut of power lines; the damages estimated cost can reach 50 billion dollars. The most feared event in the region is a category 5 hurricane, near the eye the speeds are over 249 km/h, and the pressure has been dropped to less than 0,919 bar. The damaging effects are catastrophic and are difficult to estimate since few of these events have happened. Commercial buildings with wood roofs will encounter high damages, metal buildings may collapse and windows of highly rise buildings may completely blow out, power poles will be ruined shutting down the electricity distribution of vast areas for weeks or months. The expected damaging cost in this case is hard to be estimated but is over 50 billion of dollars. Luckily from 1924 the State has experienced only 3 hurricanes of this level, the famous hurricane Andrew in 1992 has been the last [18], [30], [31], [32].

Each year from June 1st the hurricane season begins and for the next five to six months the conditions in the tropical waters of the northern hemisphere are favorable to the formation of hurricanes. In the early season cyclones form in the Caribbean Sea or Gulf of Mexico where the temperature of water is higher and heats up faster than the Atlantic Ocean. With the passing of the months the warm waters produce hurricanes also from the ocean with a peak of births in September. These hurricanes often move toward north hitting the southeastern coast of the U.S.A. [18].
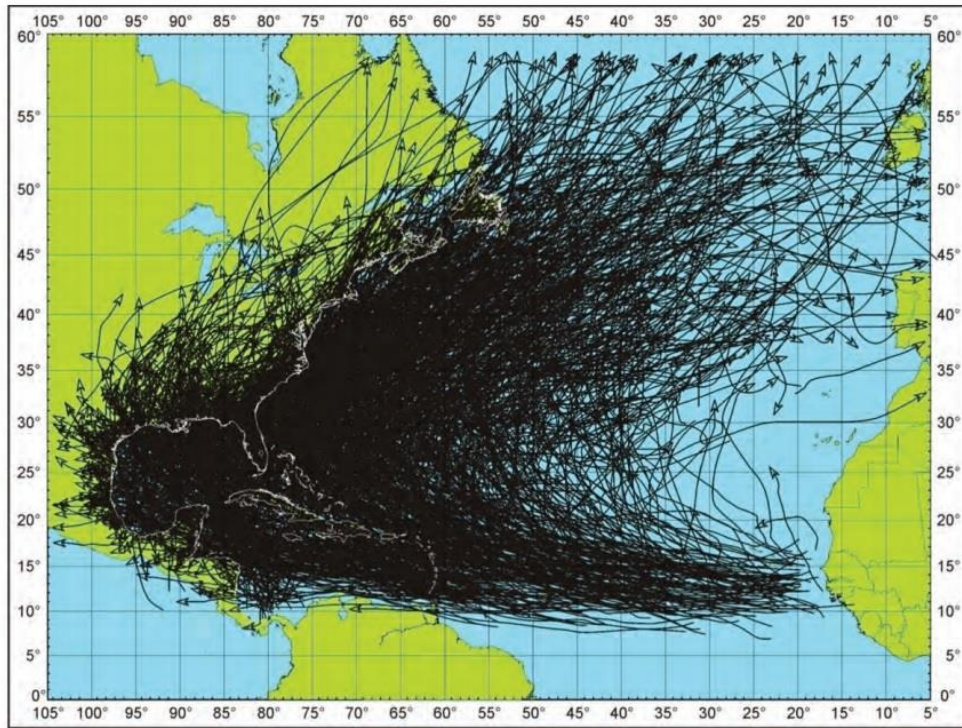
Figure 32: North Atlantic tropical storms and hurricanes, 1851-2006 (1370 occurrences) [32].

6.2. Hurricane probability and norms

Florida's residents suffer a double whammy since hurricanes can hit from both the coasts and can also cross the state from both the Gulf of Mexico and the Atlantic Ocean. This leads to a higher probability of being stroked from a hurricane. Since the state is right in the middle of the mean cyclonic path of hurricanes the probability is increased as well.

In the eastern coast of the United States the return period of a hurricane is shown in the *Figure 33* below.
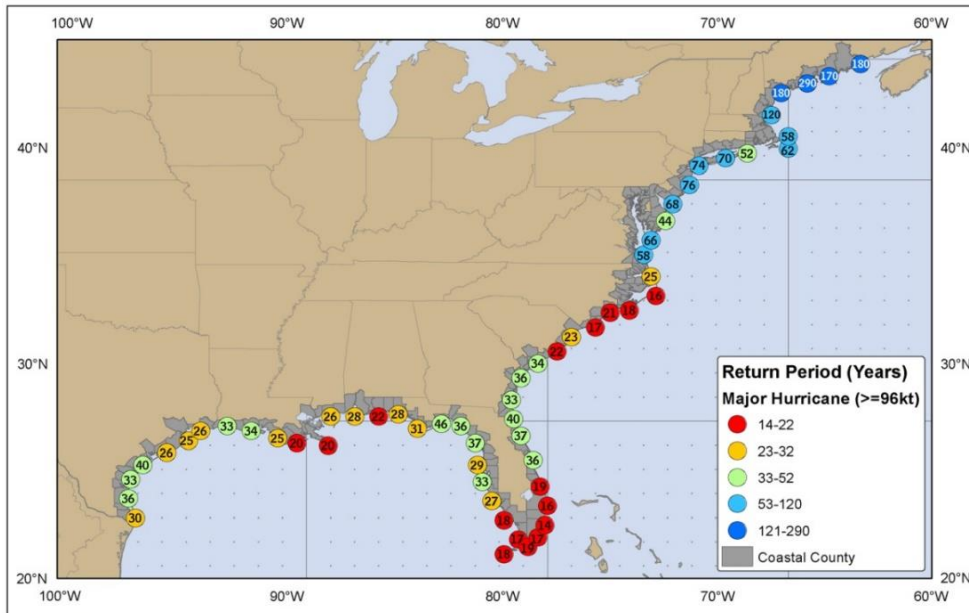
Figure 33: Estimated return period in years of major hurricanes in various locations on the U.S east coast, NOAA Technical Memorandum NWS NHC-6 [34].

These numbers are not a certain fact since there are not enough records available to precisely estimate the probability of such events, however a hurricane return period has been estimated. In the southern part of Florida, a major hurricane event (category 3 or over) is presumably to happen once every 14 to 19 years. These storms are then likely in the lifetime of an anthropic structure, and the occurrence of a great hurricane one year does not decrease the chance that a similar storm will strike the same or the next few years, maybe hitting the same region since these events are independent. The certain thing is that storms do not occur with a regular time spacing or in a regular pattern [18], [34]. What the climate change has brought and will continue to bring is a rise of probability of hurricane formation and an increase of their strength. The heating trend of the planet will warm up the ocean waters, warmer waters will often create hurricanes and such hurricanes will have a higher moisture and energetic content. Thus, with the current global warming tendency an increase of hurricane events and hurricane's strengths is expected.

Florida is indeed the most affected state, with more than 115 hurricanes that hit the state from 1851, followed by Texas and Louisiana. In southern east Florida, which is one of the most likely places in the US to encounter a big storm, the probability of facing a hurricane is 16% every year and the probability of facing a major destructive hurricane is 7% every year (see *Figures 33,34)*.

According to the National Oceanic and Atmospheric Administration (NOAA) records from 1900 to 2002, 59 hurricanes made landfall on the state of Florida and 35 of them did it on the east coast [34].
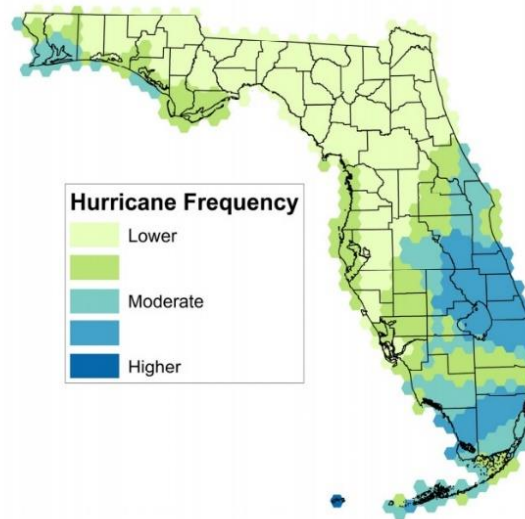
Figure 34: Historical hurricane wind frequency (1988-2014), Climate and weather extremes [30].

Thus, knowing the impacts and the probabilities of encountering a dangerous storm event the buildings of Florida should be hurricane proof. Unfortunately, only in the recent years effective laws from the American Society of Civil Engineers (ASCE) have been decreed. When the category 5 hurricane Andrew occurred with 285 km/h wind speed, it destroyed over 63,000.00 houses damaged 124,000.00 and killed 63 people on his entire path. From then an increased attention has been focused on the topic [35].

Solar panels are much affected by wind loads since their surface is large and on residential buildings can be placed on high buildings roofs. Floating systems can be badly affected too since they are on open lakes and are just anchored to the ground from few spots. In September 9th 2019 a strong typhoon hit the coast of Japan destroying 70% of the largest floatovoltaic plant of the state (13.7 MWp) on the Yamakura dam, producing also fire on some parts. The storm was not the top extreme level since the winds were averagely 148 km/h reaching top speeds of 207 km/h and the plant which has been inaugurated on march 2018 was well anchored and moored [36]. This event brought to a higher concern about the effects of strong winds on these floating systems.
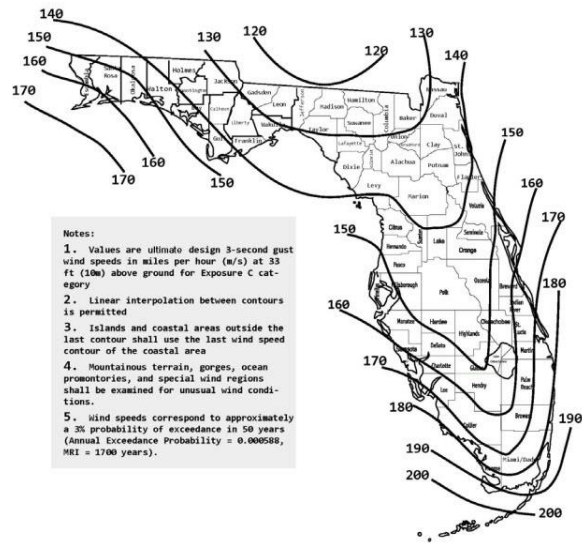
Figure 35: Ultimate design wind speeds for risk category 3 and 4 buildings and other structures, ASCE 7.

In the photovoltaic field there are not specific laws about the wind resistances so a major association to standard building codes is often used. In the U.S.A. the ASCE-7 is a code for the minimum design loads and associated criteria for buildings, it takes into account events such as earthquakes, hail, snow, rain, wind loads, floods and their combination. As possible to see in the *Figure 35* the ASCE-7-16 code defines the wind gust speed that a certain building needs to stand. In the Miami region this threshold speeds are 180 mph (289.68 km/h) which are the speeds of a strong category five hurricane. This velocity is the average 3 second wind gust speed at 10 m above the ground [37].

7. Computational fluid dynamic analysis

The major concern of solar floatovoltaic applications in South Florida is therefore the hurricanes threat, since floating structures and panels must resist to such high-speed humid winds and must observe the regional norms about wind resistance. In order to guarantee the system resistance under extreme conditions, the sizing of the mooring and anchorage arrangements need to be stated and a specific design layout needs to be adopted. Such interventions can be applied knowing the distributed wind induced loads on the floating structure and majorly on the panels, which are the most fragile and the exposed part. In order to calculate the loads acting on standard geometries such as spheres, cubes or cylinders with known fluid conditions, already existing mathematical methods can be adopted, and approximated drag and lift coefficients can be found on literature. For complex scenarios like air flow passing a floating solar system it is not possible to accurately describe the fluid behavior using simple equations, so to analyze the flow it becomes necessary to use either experimentation or numerical methods or combination of the two.

Experimental approaches can be very expensive and will need adequate wind rooms, in case of hurricane conditions they will need to produce high speed winds and moisture conditions very hard to create.

On the other side, numerical methods can be used to solve the Navier-Stokes equations, which is a system of partial differential equations that describes the behavior of fluids. These methods are generally called Computational Fluid Dynamics (CFD). To do this, it is necessary to define a model of the fluid domain around the geometry as a mesh of discrete elements, define boundary conditions and fluid properties and apply appropriate assessment techniques to find the solution [38]. Today, thanks to the advancements in computer processors, CFD is widely used in the automobile and aviation sectors since it provides very precise results with an extremely lower cost compared to experimental data acquisition tests.

For this reason, a CFD simulation will be used to simulate hurricanes flow.

7.1. The required analysis

As previously stated, this work aims at finding the best design for the panels and the floating system in order to resist to high hurricane induced wind gusts: the NRG island floating system has been considered for the analysis with the installation of commercial solar panels. The location chosen is a random lake in south Florida and the atmospheric conditions applied in the analysis are similar to the ones of the Cat 5 hurricane Dorian, which passed near the east coast of Florida at the beginning of September 2019 and produced wind of speeds over 295 km/h which created huge damages on the Bahamas islands.

Figure 36: Simulation of category 5 hurricane Dorian passing near the east coast of Florida on September 2019, The weather channel.

7.2. CFD Simulation

To simulate the flows acting on the panels and on the floating system the Ansys 2020 R1 Fluent software package has been used. Fluent is a simulation software used to predict fluid flow, heat and mass transfer and other phenomena delivering accurate solutions.

To create a simulation a certain sequence of steps needs to be tracked:

1) Geometry creation and relative fluid enclosure
2) Meshing of the whole geometry
3) Ansys Fluent physical and computational setups
4) Running the simulation
5) Analysis of the obtained results

7.3. Geometry creation

In a CFD simulation the creation of a geometry capable to simulate the real object is essential. Unfortunately, extremely precise geometries with all geometrical details of the panel may lead to very refined computational grid and, in turn, to high computational costs. Therefore, some degree of approximation is always needed.

The investigated geometry is the patented NRG Island unit with solar panels mounted on. The Island is an assembly of NRG units which are linked and repeated, therefore the single NRG unit can be firstly created and then multiplied to create the floatovoltaic farm.

The single unit shown in the previous *Chapter 3* is mainly composed by three parts: the floats, the supporting metal structure, and the solar panels. The floats are cube looking elements attached together, a float unit is composed by two cube looking elements, every NRG unit has 4 floating units, 2 on each lateral side. The floating elements have shapes which increase their floatability and stability; since these elements are patented and their shapes could increase a lot the computational effort by creating small peculiar zones, an approximation has been adopted. The union of the 2 linked blocks on each side of the unit has been approximated to a single parallelepiped block, still maintaining the same dimensions. The only modified dimension of the floating unit is the height, since part of the unit is under water in order to balance thanks to the Archimedes' force the weight of the system.

In the simulation the only fluid taken into account will be the wind air, the water surface will be approximated to a no slip wall with its own specific roughness. This is done as a reasonable first

approximation, however the aspect regarding the modeling of the water surface needs to be further investigated in the future. And then only the part coming out of the water will be analyzed.

To calculate the depth at which the floating element sinks into water, the weight of the whole unit and the floating elements volume is needed.

The volume of a floating element is (100 cm $\cdot$ 50 cm $\cdot$ 40 cm) 0.2 m^3. The volume of an element multiplied 4 times is equal to 0.8 m^3, it is the volume per NRG unit. The mass of the whole units corresponds to the sum of: 40 kg of the floating system, 10 kg each floating element, 28 kg the aluminum structure and 18 kg each solar panel. The total weight of a unit is therefore 140 kg. This weight represents 0.14 m^3 of water; the water volume divided by the base area of the floating unit will result the sink height: 0.14m^3/(1m $\cdot$ 0.5 m $\cdot$ 4 blocks) =0.07 m, so we would have 7 cm of sink. The height of the floating part will be 400 mm – 70 mm so 330 mm (see *Table 3*).

Floating unit	
Width (cm)	50
Length (cm)	100
Height (cm)	40
Volume (m^3)	0.2
Weight (kg)	10
NRG unit	
Floats (kg)	40
Aluminium structure (kg)	28
Solar panels (kg)	72
Total weight (kg)	140
Sinking of the unit (cm)	7

Table 3: Floating unit and NRG unit general properties and sinking of the unit into the water.

The aluminum supporting structure is also a critical part since it links the floating basement to the panels which are affected to loads. However, this structure has been simplified still using the same dimensions, since they are not much affected by the wind forces so a detail reduction will not produce results much different from the real case.

The panels are presumably the most affected part to wind. The 4 panels are usually set in the portrait design by NRG Energia, so the same setting has been used. Since the gaps between the panels could be a specific point that might create problems in the resolution and additional computational cost. In this work the choice has been to avoid the gaps between the panels. This

approach has also been used in numerous scientific articles which were analyzing similar simulation but on ground mounted systems [39], [40],[41], [44], [45], [46].

The panels have been approximated to parallelepiped elements, the frontal part remains the same but the back of the PV modules, which is usually distinguished by the frame and the back sheet of the panels, is approximated to a whole parallelepiped block, In this case a more homogeneous analysis is applied to the panels, still maintaining relevant results. The dimensions of the panels are the same of the original set and the thickness is the one of the panels adopted in the original NRG Island geometry.

Each panel has a width of 2000 mm, a length of 1000 mm and a thickness of 41 mm. The whole set composed by 4 panels presents 2000mm of width, 4000 mm of length and 41 mm of thickness.
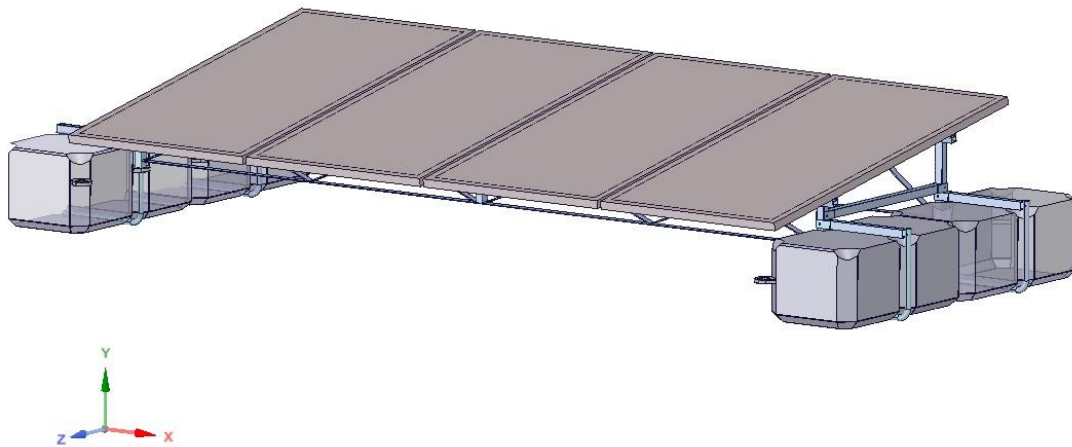
Figure 37: 3D geometry of NRG Island Unit patented by NRG Energia.
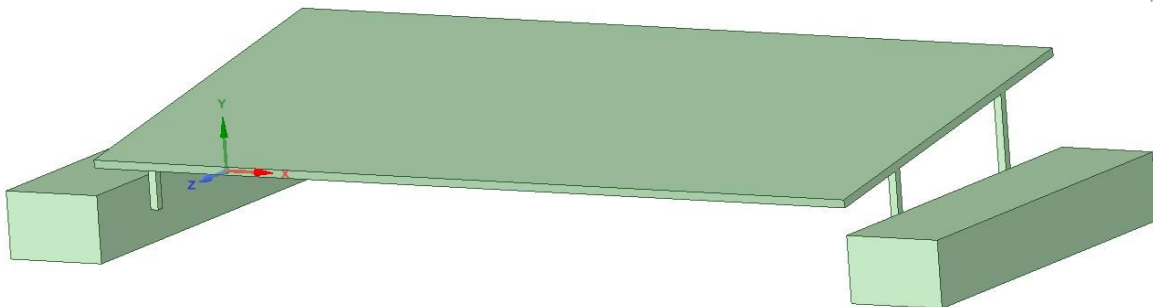
Figure 38: 3D approximated geometry of NRG Island Unit using Ansys SpaceClaim.

Since the panels can act like a sail and so produce high wind loads, a first CFD analysis will be made only on the panels in order to find the optimal design angle and configuration. Indeed, while the NRG unit can be strengthened adopting different solutions, the commercial solar panels have an average pressure resistance on the frontal face and on the back face. So, a more specific study will be carried out on the panels.

While developing the geometry, it has been set as a variable parameter the tilt of the panels in order to perform different simulations with various inclination angles. The tilt has been adopted from the lowest point of the panel since it is the point that usually does not change its height dimensions, while the back side can increase the height of the structure in order to increase the tilt. It is possible to see this configuration in *Figure 39*.
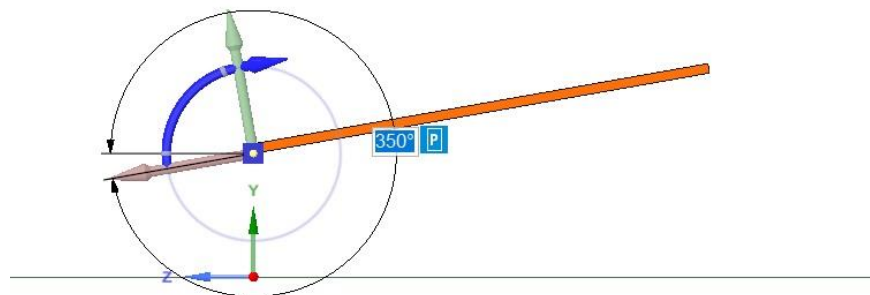
Figure 39: Tilt representation of the solar PV set of panels.

The software angle that leads the panels parallel to the ground is 0° or 360° and to increase the angle to 10° it needs to be set 350 or -10°.

The enclosure, which represents the fluid volume around the geometry, is defined using conventional methods for this type of applications. Knowing the height of the geometry (532.58 mm) from the water level to the top of the geometry, called H, the height of the enclosure needed to simulate the fluid is 6 H, the distance from the inlet should be 5 H, the distance from the object to the outlet of the flow needs to be 15 H and the lateral distance from the object to the boundary

fluid faces needs to be at least 2.3 H [39] [40]. In this way the enclosure could well represent the flow behavior and leads to a faster residual convergence.

For the whole geometry creation, the Ansys geometry creation software "Ansys SpaceClaim" has been used.

The analysis will be essentially on the fluid dynamics on the panels and surroundings. The effect of the wind load on the structural mechanics is not an object of this investigation, therefore a Boolean cut between the enclosure and the geometry has been applied. In this way the solid geometry of the NRG unit is accounted as an empty space in the fluid volume and still a fluid analysis can be applied.

7.4. Meshing

The discretization is a fundamental step for a fluid dynamic simulation. The process develops a set of algebraic equations that can be solved by the computer, to be used instead of the partial differential equations that describe the fluid flow.

There are numerous discretization techniques, the most used in fluid dynamic applications are: the *boundary element method*, the *finite difference method*, the *finite element method* and the *finite volume method*. Each method discretizes the continuous flow field in discrete values at specified locations.

The method used for this simulation is the finite volume method, since the flow is three dimensional. This approach divides the flow field into a series of small control volumetric elements, for each element the algebraic conservation equations (for mass and momentum) are set producing a volumetric average result.

By decreasing the volume element size and then increasing the number of elements, the simulation results will become more accurate since the error scales with the grid size, but the resolution will need more computational time since more equations will need to be solved.

A tradeoff between computational cost and mesh definition is necessary: a not well-defined grid resolution cannot capture relevant flow physics, producing a less accurate solution. The mesh

influences therefore the speed, the accuracy and the convergence of the simulation. It needs to be created in the best way to represent correctly the geometry and the flow physics.

The grid elements type is also an important setting that needs to be properly chosen, for 2D mesh the usual elements used are triangles or 2D prisms, while for 3D simulations there is a wider range to be chosen, the most frequent are: tetrahedrons, pyramids, prisms with triangular base, hexahedron prisms with quadrilateral base and arbitrary polyhedron.

The element geometry initially chosen was the hexahedron dominant with all quadrilateral base, since it would have produced a more homogeneous mesh size, but the "inflation" optimization was not possible in the Ansys meshing software with this configuration, therefore the tetrahedrons elements have been applied using the *patch conforming algorithm*, which enables a meshing process that starts from the edges, moves to the faces and then meshes the body.
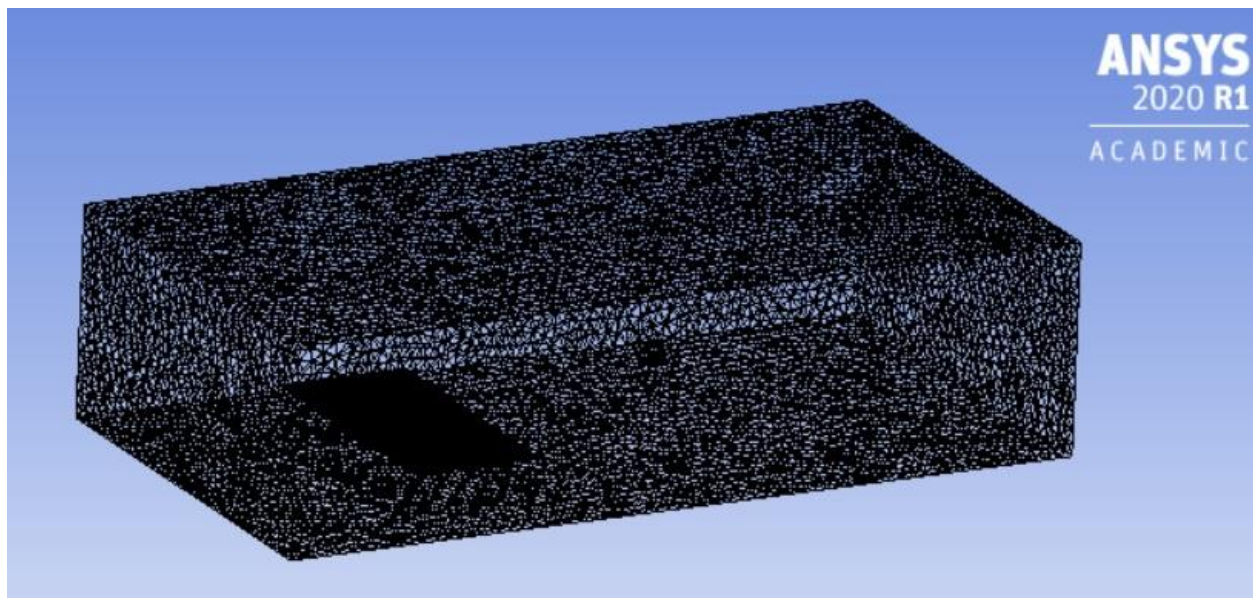
Figure 40: Mesh of the entire fluid domain, the darker part represents the solar panels set with a 0° tilt .

The mesh optimization, which is essential in order to obtain specific results in the most peculiar zones, has been applied on the whole solar panels (see *Fig. 40*).
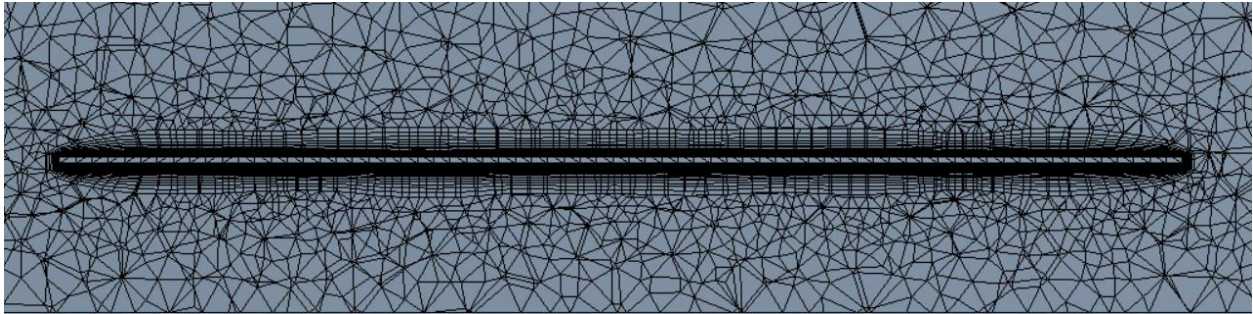
Figure 41: Section and zoom on the solar panels set, showing the dense mesh layers near the solar panels surface.

The inflation methodology enables to apply a certain number of this element's layers (20 for this case) on the geometry and lowers the size of the grid near the object, producing a smooth transition of element sized from the applied geometry to the far fluid flow. The effects of the inflation methodology can be seen in the *Figure 41*, where it is shown a part of the section of the fluid flow and the panel set geometry tilted 0° and so parallel to the ground. From the figure, it is possible to see the thickness of the panels and, around the modules, the dense element's layers. After the first 20 layers, the elements smoothly adapt to bigger ones while going far from the geometry. The element's size on the panels has been set as changeable parameter and is equal 0.06 m. The inflation has a particular importance on the evaluation of the forces acting on the panel. For this reason, in this work a reasonable amount of element layer has been used, as suggested in the literature [39], [41], [44].

In the *Figure 42* it is shown from the lateral side the section of the mesh when only a set of PV panels at 0° tilt is shown, it is possible to see the effects of the inflation methodology and its smooth transition. Moreover, there is also a denser elements discretization near the boundaries since are also peculiar points.

55
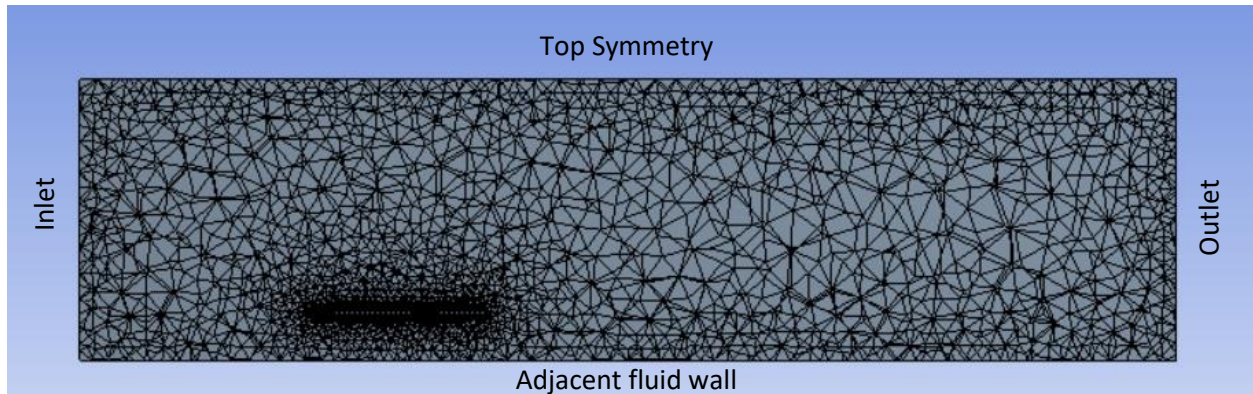
Figure 42: Fluid domain section showing the mesh, a denser mesh in near the solar panels set.

The boundaries have been properly chosen and set in the meshing software. Looking at the section in *Figure 42,* the left face of the fluid enclosure is the inlet of the fluid flow, the flow in this case enters with a normal direction to the inlet boundary face, while parallel to the inlet on the opposite side at the extreme right, there is the outlet of the fluid flow. The bottom boundary must simulate the water wall, so the name for the bottom boundary face has been imposed as "adjacent fluid wall" and furtherly adequate properties have been used to simulate the water. The other three faces of the 3D enclosure (the top face and the two lateral faces) have assumed the symmetry boundary layer in order to not affect the fluid flow inside the enclosure. The other boundary layers have been the ones of the solar panel, three boundaries have been adopted, all of them are walls which block the fluid flow. The frontal wall corresponds to the frontal face, which is the one that captures the light, a back wall simulates the rear of the panels and the adjacent panel wall which are positioned to the four thickness faces that represent the frame of the panels set.

For the mesh generation of the whole volumetric domain it produced 147,133.00 nodes and 440,357.00 elements.

7.5. Ansys Fluent simulation

A Fluid is a substance as gas or liquid, which is able to flow and which can change its shape, when forces are acting on it, or to match the container. The equations that describe the incompressible fluid behaviors are the Navier-Stokes equations:

$$\nabla u = 0$$

$$\rho \frac{Du}{Dt} = -\nabla p + \mu \nabla^2 u + \rho F$$

The first equation represents the conservation of mass, it is represented as the divergence of velocity on the three directions (x, y, z) which is set equal to zero in order to have a mass conservation. Nabla "∇" is the symbol that represents the gradient and u represents the velocity. The second equation represents the conservation of momentum described by the Newton second law; in fact, it defines the force equal to mass times acceleration. On the first member of the second equation it is represented the material derivative (considering variations in time and space) of velocity, which represents acceleration. Mass in fluids is better represented by density ρ, so on the first member of the equation mass times acceleration of a fluid is described. On the second member of the equation the forces are represented: $-\nabla p + \mu \nabla^2 u$ represents the internal forces and ρF the external forces. ∇p is the gradient of pressure on the three major directions (x, y, z), $\mu \nabla^2 u$ describes the friction concerned to viscosity. These equations can be used on anything that involves a fluid, but the problem is that not always a solution exist or can be reached. In order to solve these equations some assumptions and approximations are applied, averaging the behavior of the fluid on a predefined cell domain [38]. What creates uncertainty in the prediction of the fluid actions is turbulence.

The laminar and turbulent flow regimes behave in different ways; the laminar flow is smooth and even and does not produce an elevated mix of the fluid. As the velocity increases, initial random motions start to appear, beginning the transition to a turbulent regime. The turbulent flow is characterized by chaotic movements and contains swirling regions called *eddies*, the unpredictable motions and eddies produce a significant mixing which increases the chaos. By recording the velocity at a certain point over time, if the fluid is laminar, the velocity will remain still while, if

the fluid is turbulent the velocity will change and the fluctuations with respect to the mean velocity will be higher as greater is the turbulence. In order to predict which regime is likely to be produced, the Reynolds number, defined by Osborne Reynolds in 1883, is used. The Reynolds number is a non-dimensional quantity and is defined as:

$$Re = \frac{\rho \cdot u \cdot L}{\mu}$$

Where, ρ is the fluid density, u is the velocity, L is the characteristic length, which for a flow passing an airfoil or a low tilted solar panel is equal to the cord of the geometry, and μ is the dynamic viscosity. Reynolds number is used to predict whether the flow is laminar or turbulent; the fraction is composed by inertial forces which are related to the momentum of the fluid, at the numerator, and viscous forces at the denominator which are related to the frictional shear forces. If viscous forces dominate, the flow is likely to be laminar because the frictional forces avoid and shut off any initial turbulent disturbance. If instead inertial forces dominate, the flow is more likely to be turbulent. For this reason, large Re number represents turbulent flows while small Reynolds numbers represent laminar regime. For geometries such as flat plates on open flow the transitional Reynolds number from laminar to turbulent varies from $2 \cdot 10^5$ to $3 \cdot 10^6$, in the analyzed hurricane case the Re has a value of over $8.4 \cdot 10^6$ so a fully turbulent behavior is expected [38]. The effects of turbulence introduce a high mixing, with a momentum transfer that at big scale homogenizes the wind velocity, even at different heights while the laminar flow would have different velocities changing the height, from the null velocity at the border of the land surface to the fully developed velocity up high. This turbulence's induced effect increases the velocity near the land increasing consequently the pressures near the anthropic constructions.

Because of its chaotic nature, analysis and modelling of turbulent flow is very complex, this is also due to the turbulent eddies. Larger eddies contain a lot of kinetic energy: over time these swirls feed the creation of smaller eddies until, at the smallest scale, the turbulent energy is dissipated as heat due to the frictional forces associated to the fluid viscosity.

For complex scenarios like flow passing on a solar panel, it is not possible to accurately describe the fluid behavior applying simple equations. One of the main challenges to simulate turbulence is to capture the wide range length scales associated to the turbulent eddies, for the computational

fluid dynamic analysis three main techniques are utilized to simulate fluid flows and they differ primarily on how they consider turbulence at different scales.

- **Direct numerical simulation** (DNS): It solves the Navier Stokes equations explicitly until the smallest scales of eddies are fully resolved. This approach is enormously computational expensive and cannot be applied in a great range of fluid flow problems.
- **Large eddies simulation** (LES): This technique solves explicitly large scales eddies approximating or filtering out the smaller ones. This method is less computational expensive compared to the DNS, but still has a medium to high computational cost.
- **Reynolds averaged Navier Stokes** (RANS): It entails a lower computational cost; it is time averaged and does not resolve the eddies explicitly, but models the eddy's effects exploiting the concept of turbulent viscosity.

In this simulation of the present work the RANS method available on Ansys Fluent will be used. For this method, several turbulent models can be used, the most functional ones for hurricanes simulations are the k-ε and k-ω models. The last one is used in this simulation because it is the one that permits to reach low residual values with less iterations. The k value represents the *turbulence kinetic energy* measured in m^2/s^2 and represents the kinetic energy of the eddies in the turbulent flow while ω is the *specific dissipation rate*, which corresponds to the rate at which turbulence kinetic energy is converted into thermal energy and is measured in s^{-1}[39],[40],[41],[44], [45],[46].

7.6. Ansys Fluent numerical details

After updating the meshed geometry to Ansys Fluent, the software setup needs to be updated with physical and computational input data.

The turbulence model used is the viscous *shear stress transport k-ω* method which is one of the most used in open air wind simulations; other methods such as k-ε and *Spalart-Allmaras* have been tried but the k-ω was the one who showed better results and reached convergence faster [39], [41].

The analysis adopted is steady state.

After the setting of the turbulent model, the physical material properties needed to be set. The only material present is the fluid because the panels geometry has been cut from the enclosure as the

analysis will be only on the fluid dynamics.

The properties of a category 5 hurricane wind are different from the air standard conditions.

In order to calculate the density of the hurricane wind, the following equation has been used.

$$\rho_{humid\ air} = \frac{p_{dry\ air}}{R_{dry\ air} \cdot T} \cdot (1 - x) + \frac{p_{vapor}}{R_{vapor} \cdot T}$$

The symbol $\rho_{humid\ air}$ is the density of the humid air, $p_{dry\ air}$ is the pressure of the dry air in the hurricane, which for standard conditions is around 101325 Pa, while in a hurricane of category five is lower since the upward air fluxed lowers the pressure. The pressure could vary from around 90000 Pa to 93000 Pa. For the current simulation the pressure of hurricane Dorian has been used, which is also very similar to the category five hurricane Andrew, namely 92200 Pa [51]. $R_{dry\ air}$ is the specific gas constant and is equal to 287.05 J/kg/K. T is the fluid temperature, in order to guarantee a conservative density value, the lowest temperature value of Florida hurricanes has been used and is about 20 °C which in the equation is represented as 293.15 K. The vapor fraction x, defined as $kg_{h20}/kg_{dry\ air}$ has been obtained from the psychrometric chart Carrier, knowing the fluid temperature and the relative humidity. The relative humidity (Φ) of a hurricane can vary from 80% to 94%, an 85% value of relative humidity has been adopted. From the Carrier chart the resultant vapor fraction was equal to 0.015. The vapor pressure p_{vapor} has been obtained from psychrometric tables at the temperature value of 20 °C and is equal to 2339 Pa [57]. R_{vapor} is the specific gas constant of water vapor, its value is 461.495 J/kg/K. The resulting value of the density of humid air is then 1.0795 kg/m^3. Hurricanes are often rich of rain, the air-rain mixture has been treated as a homogeneous fluid with a higher density than just humid air. A violent rain can produce over 80 mm/h of water dropping to the ground. For the analysis 100 mm/h of water has been taken for the sake of conservativeness; on a m^2 of surface the volumetric water flowrate is then 2.778 · 10^{-5} m^3/s which considering the density of water equal to 1000 kg/m^3 can be written as a mass flowrate of 0.02778 kg/s. Rain drop velocity can vary from 2 m/s to 11.11 m/s, the 11.11 m/s rain speed has been adopted [52] . So, a raindrop will remain 0.09 s inside a m^3 of air. By multiplying the mass flowrate at the seconds, a raindrop remains inside a m^3 of air, it is possible to obtain the density apported by the rain (σ). In this case the value is

$$\sigma = 2.778 \cdot 10^{-5} \frac{kg}{s} \cdot 0.09 \frac{s}{m^3} = 2.5 \cdot 10^{-3} \frac{kg}{m^3}$$

This raindrop density contribution, added to the already calculated humid air density, leads to a final hurricane wind density of *1.082* kg/m³.

The dynamic viscosity has been calculated using a similar approach, the relative humidity does not affect as much the dynamic viscosity so its value is the one found on psychrometric tables at 20°C: μ_{air}=1.82 · 10⁻⁵ Pa·s. The mass fraction between raindrop mass and air mass is the weight of rain in a m³ of air divided by the density of air: $x_\mu = \dfrac{2.5 \cdot 10^{-3} \frac{kg_{h2o}}{m_{air}^3}}{1.225 \frac{kg_{air}}{m_{air}^3}} = 2.315 \cdot 10^{-3} \frac{kg}{m^3}$. The dynamic viscosity of water at the same temperature is 1.002 mPa·s, the total dynamic viscosity of hurricane wind is calculated using the formula below [53].

$$\mu_{hurricane} = \mu_{air} \cdot (1 - x_\mu) + \mu_{water} \cdot x_\mu$$

$$\mu_{hurricane} = 1.82 \cdot 10^{-5} \, Pa \cdot s \, (1 - 2.315 \cdot 10^{-3}) + 1.002 \cdot 10^{-3} Pa \cdot s \cdot 2.315 \cdot 10^{-3}$$
$$= 2.0477 \, Pa \cdot s$$

The material has then been set as a fluid denominated *air-moisture*, with the density and dynamic viscosity calculated above.

After checking the cell zone conditions, the boundary conditions need to be accurately defined. The inlet face of the enclosure is defined as a *velocity-inlet* boundary condition, the direction of the velocity is normal to the face, the initial gauge pressure is set to zero but the velocity magnitude changes as function of the height following the below mentioned power law.

$$u = u_{ref} \cdot \left(\frac{y}{y_{ref}}\right)^\alpha$$

This power law describes how the wind speed increases by increasing the height, u_{ref} represents the reference velocity defined at a reference height y_{ref}, y is the height variable and α is the power parameter. By changing the value of α the variation of velocity over the height will increase or decrease. Since hurricanes have a turbulent regime, they will produce a more homogenized velocity profile and so the value of α will be low. For hurricane conditions α can be set equal to 0.1 on land, and on open ocean equal to 0.06. Since the type of flow analyzed is a wind gust it will be more turbulent and so higher speeds can reach low heights, therefore the α value has been set to 0.08 [49]. The reference speed should be defined as the threshold in the ASCE-7 norm, for the Miami zone it is equal to 180 mph at 10 m above ground which is equal to 289.68 km/s. In order to perform simulations with the most conservative conditions, the reference speed has been set to 300 km/h at 10 m as reference height. The wind will then averagely impact the panel at a speed of 240 km/h. A precise analysis would have also considered the value of the turbulence kinetic energy k and the specific dissipation rate ω as function of height at the inlet, but, since their simultaneously application increases the complexity of the simulation problem leading to high residuals and higher computational cost, they have been assumed constant at the inlet and outlet. The turbulence specification method used for the inlet is the intensity and length scale, the turbulent intensity has been set to 20 % and its length scale to 1 m. The outlet boundary condition is the *pressure-outlet* type with a zero-gauge pressure, the turbulence specification method and its parameters are the same as the inlet. Both the lateral enclosure faces and the top one are set as *symmetry* conditions, the bottom enclosure face is a stationary wall with no slip condition, it simulates the water roughness, the roughness height of water can be approximated as 0.01 m and the roughness constant is 0.9. The solar panels faces have been set as *stationary wall* with no slip and the roughness height of glass which is 300 nm for rough glass [53].

The Ansys Fluent settings referred as "Reference values" are essential to determine the exact coefficients of drag and lift of the geometry. Usually the reference area is the frontal area the wind is facing, but for airfoils and low tilted solar panels it is used the area of the top surface which in this case is 4.14m $\cdot$ 2 m = 8.28 m^2. The reference length is the length of the solar panels in the wind direction also called the cord, which is 2 m. The temperature is 293.15 K and the other reference parameters have been set by computing from the inlet.

The solution method describes the algebraic equation solving methodology, for the pressure and velocity a *coupled scheme* is used since it solves the pressure and velocity equations contemporarily. This method usually needs more calculation time but provides better quality results. For the gradient spatial discretization, the *least squares cell-based* method has been used while, the pressure, momentum, turbulent kinetic energy and specific dissipation rate spatial discretization are set as *second order upwind solution*, as in this way the solution will be more accurate than the first order one.

A standard initialization computed from the inlet prepares the volume geometry with the predefined fluid properties, the initialized turbulent kinetic energy k is equal to 299.72 m^2/s^2 and the specific dissipation rate ω is 191.88 s^{-1}.

The principal physical values and the boundary conditions are respectively summarized in *Table 4* and *Table 5*.

Physical input property	Value
$p_{dry\ air}$ (Pa)	92200
p_{vapor} (Pa)	2339
$R_{dry\ air}$ (J/kg/K)	287.05
R_{vapor} (J/kg/K)	461.495
T (K)	293.15
x (-)	0.015
$\rho_{humid\ air}$ (kg/m^3)	1.0795
Φ (%)	85
σ (kg/m^3)	$2.5 \cdot 10^{-3}$
$\rho_{hurricane}$ (kg/m^3)	1.082
x_μ	$2.315 \cdot 10^{-3}$
μ_{air} (Pa ·s)	$1.82 \cdot 10^{-5}$
μ_{water} (Pa ·s)	$1.002 \cdot 10^{-3}$
$\mu_{hurricane}$ (Pa ·s)	2.0477

Table 4: Physical hurricane properties set as input in Ansys Fluent

Boundary conditions	Value
Inlet	
Velocity Magnitude (m/s)	$83.33 \cdot (y/10)^{0.08}$
Turbulent Intensity (%)	20
Turbulent Length Scale (m)	1
Outlet	
Gauge Pressure (Pa)	0
Backflow Turbulent Intensity (%)	20
Backflow Turbulent Length Scale (m)	1
Adjacent fluid wall	
Wall motion	Stationary Wall
Shear condition	No Slip
Roughness height (m)	0.01
Roughness Constant	0.9
Top and lateral enclosure surfaces	
Boundary	Symmetry
Front and back panel walls	
Wall motion	Stationary Wall
Shear condition	No Slip
Roughness height (m)	3e-7
Roughness constant	0.5
Adjacent panel walls	
Wall motion	Stationary Wall
Shear condition	No Slip
Roughness height (m)	0
Roughness constant	0.5

Table 5: Boundary conditions set in Ansys Fluent

7.7. Simulation of a hurricane hitting a set of solar panels

After performing the initialization, it is possible to run the calculation. The residuals measure the local difference of the conserved variables, residuals will never be equal to zero but the lower the residuals are the more accurate the solution is. In the 0° tilted panel scenario with wind in the z direction the residuals have been the following.
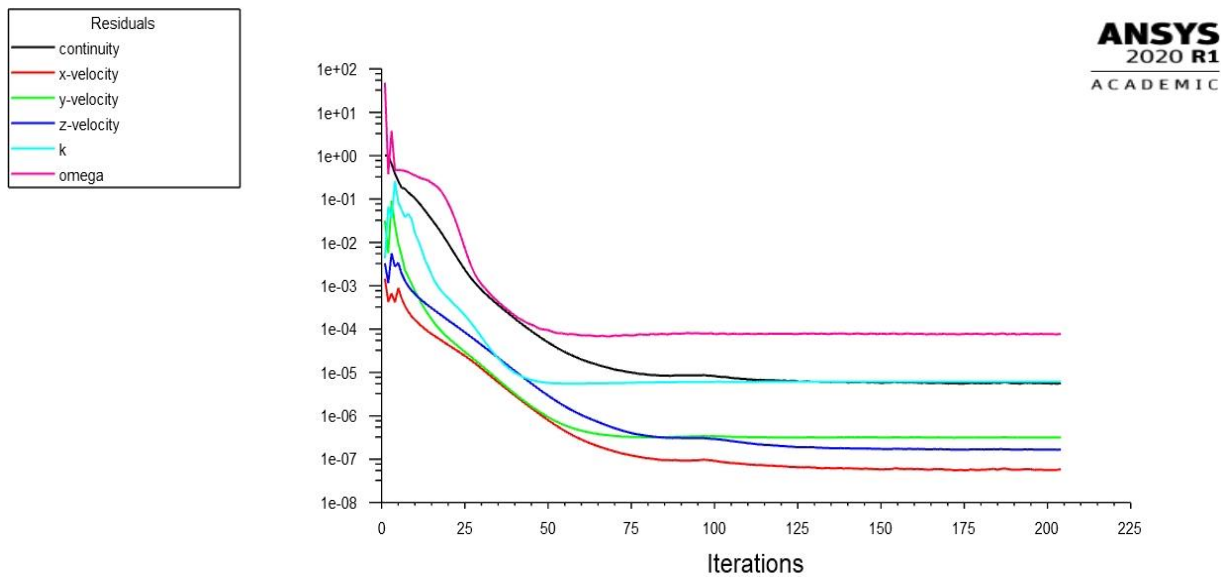
Figure 43: Residuals for the 0° tilted solar panels.

The velocities reach residuals in the order of 10^{-8} to 10^{-7}, the continuity which is one of the most important parameters reaches residuals of 10^{-6} like the turbulence kinetic energy, omega is in the 10^{-5} range. The residuals reach the convergence after computing more than 150 iterations so a fast convergence is reached; at the beginning their value oscillates since the preliminary iterations are far from the solution. By increasing the iterations the software finds the regular path lowering the residuals. By changing the tilt, the residual convergence will change, the more complex the fluid behavior is the higher the residuals will be. For further residual reduction a more refined mesh with a higher number of elements would be needed, but at the price of higher computational costs. However, for the aim of the simulation the residuals reached are adequate.

The analysis has been performed to obtain reliable results that describe the forces, the pressures and the drag and lift coefficients on the geometry in the hurricane flow condition.

The force in the z direction which produces drag is defined as:

$$F_D = \frac{1}{2} \cdot \rho \cdot U^2 \cdot C_D \cdot A$$

The drag force depends on the density ρ, the velocity U elevated at the power of two, the reference area A and the drag coefficient C_D.

The drag coefficient is a non-dimensional parameter which depends primarily on the shape of the geometry but also on the Reynolds number (see *Fig. 44*).
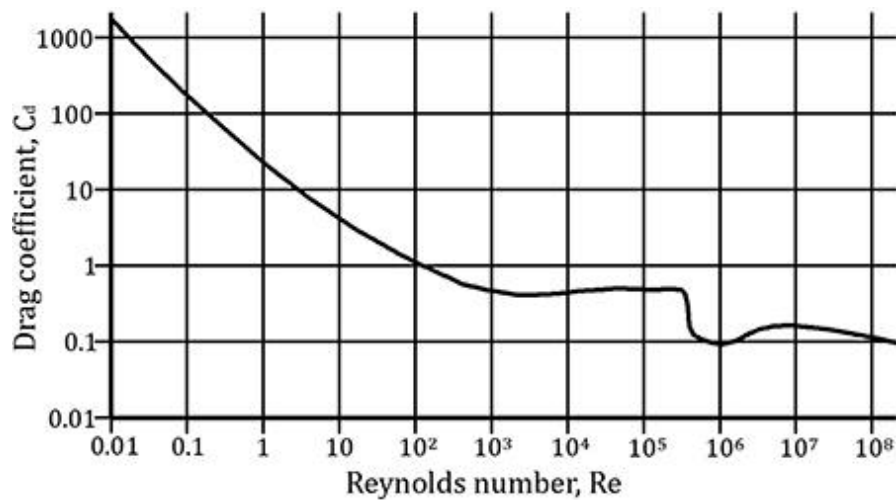
Figure 44: Drag coefficient of a sphere as function of the Reynolds number,[54]

Since the turbulence on the geometry is not homogeneous a specific calculation of the drag coefficient would have been almost impossible analytically. The coefficient of drag depends also on the relative roughness of the surfaces. And by increasing the roughness the coefficient will increase as well.

The lift force is the corresponding of the drag but in the y direction

$$F_L = \frac{1}{2} \cdot \rho \cdot U^2 \cdot C_L \cdot A$$

and the coefficient of lift C_L presents the same dependences as the drag one.

Both coefficients have been calculated for the set of solar panels in the case of frontal wind for every tilt angle from 3° to 15° which are the most applied angles for floating photovoltaic applications, also the 0° tilt angle has been analyzed (see *Fig. 45*).
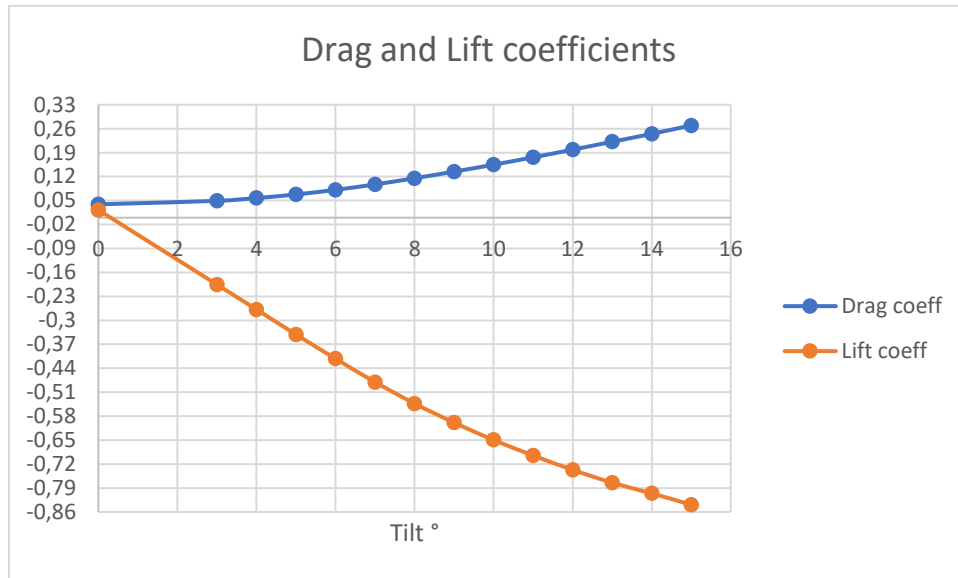

Figure 45: Drag and Lift coefficients of the solar panels as function of the inclination angle when wind is impacting from the front.

By increasing the tilt, the drag coefficient increases since more panel area is impacted by the wind. This increment for each angle of inclination shows a nonlinear function with a concavity facing upwards, meaning that by increasing the tilt the coefficient will not increase linearly but following a power law. The lift coefficient is negative since in this case the force is pushing down the panels: the absolute value is much larger than the drag one, so a further attention will be kept on the lift force. The curve that describes the lift coefficients when changing the tilt has a slight concavity downwards related to the tilt axis, so by increasing the tilt the lift coefficient will increase its absolute value in a lower way compared to a linear correlation.

These coefficients are very similar to the ones calculated in different papers that describe similar problems [39],[41],[45].

The drag and lift forces are then described in the following graph and have a behavior like their relative coefficient (see *Fig. 46*).
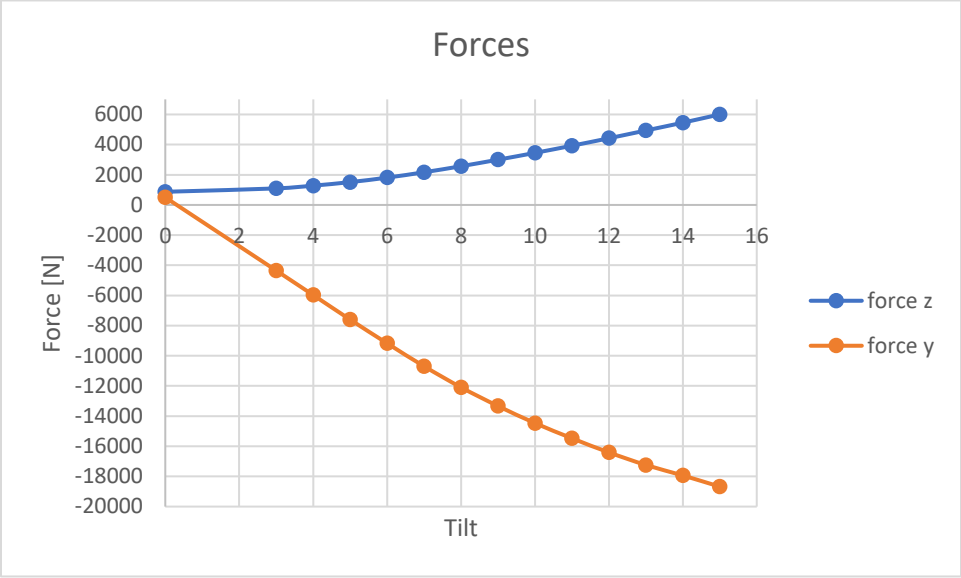
Figure 46: Drag and Lift forces of the solar panels as function of the inclination angle when wind is impacting from the front.

These forces have high values since the speed is high, but they do not mean as much if not related to an area, for this reason pressure calculations have been adopted.

Both the pressures on the frontal and rear side of the panels have a downward concavity, the frontal pressures increase as the tilt increases and the back-side pressure is negative due to the depressions induced by turbulence. And the depression increases following the tilt trend (see *Fig. 47*).
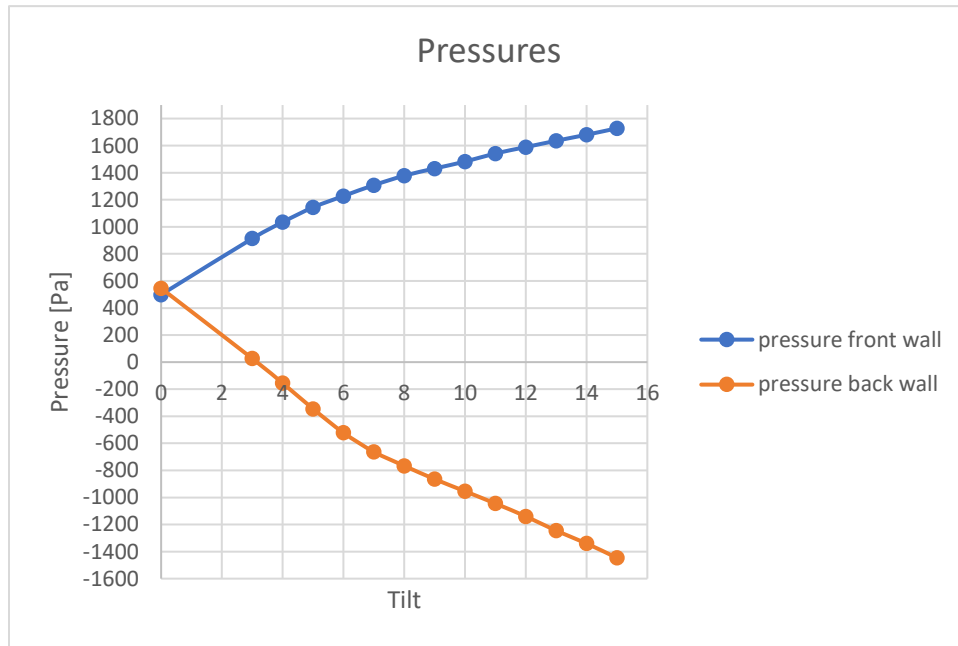
Figure 47: Pressures on the frontal and back wall of the panels as function of the inclination angle when wind is impacting from the front.

The worst-case scenario for a set of panels facing south is when the wind is impacting from the rear side. Both drag and lift coefficients are greater than in the frontal wind simulation, but their dependence on the tilt angle is very similar. The lift coefficient in this case is positive since the panels are lifted by the wind (see *Figure 48*).
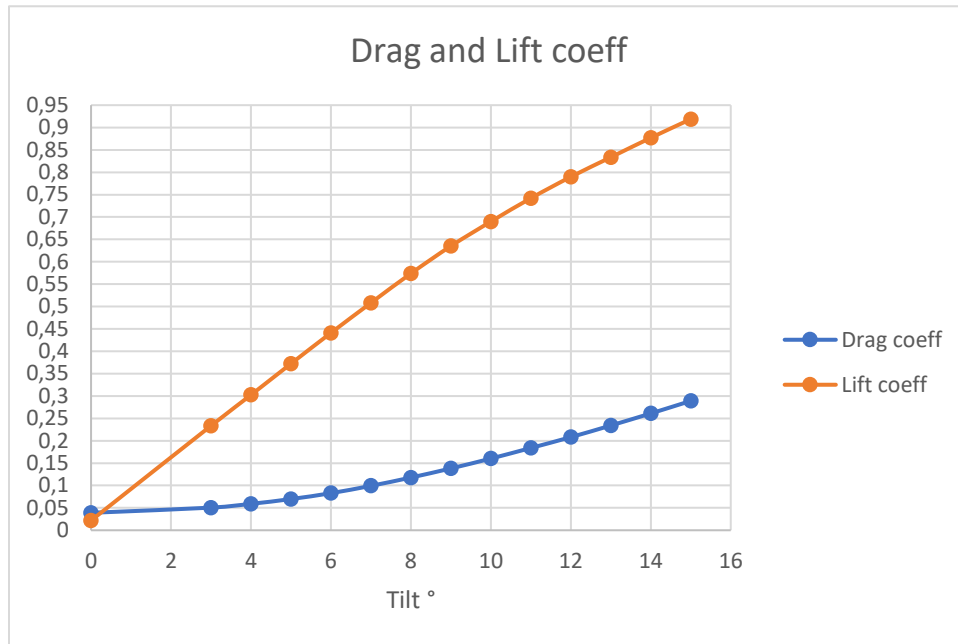
Figure 48: Drag and Lift coefficients of the solar panels as function of the inclination angle when wind is impacting from the back.

The forces are also higher than the front wind simulation, the reason is that while in the first simulation the wind impacting on the panels is reflected upwards to the open flux volume, in this case the wind is instead canalized in the space between the ground and the panel (see *Fig. 49*). By doing so the velocity increases since it is affected by the venturi effect, and a higher velocity can produce stronger forces and elevated pressures.
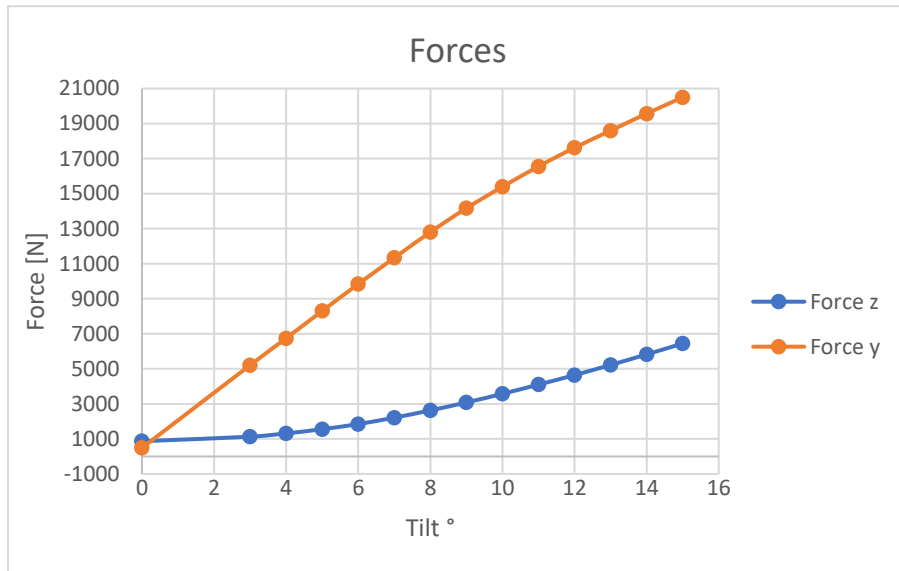
Figure 49: Drag and Lift forces of the solar panels as function of the inclination angle when wind is impacting from the back.

The pressures on both frontal and rear sides are higher so this will be the case limit through which the optimal PV tilt will be chosen (see *Fig. 50*).
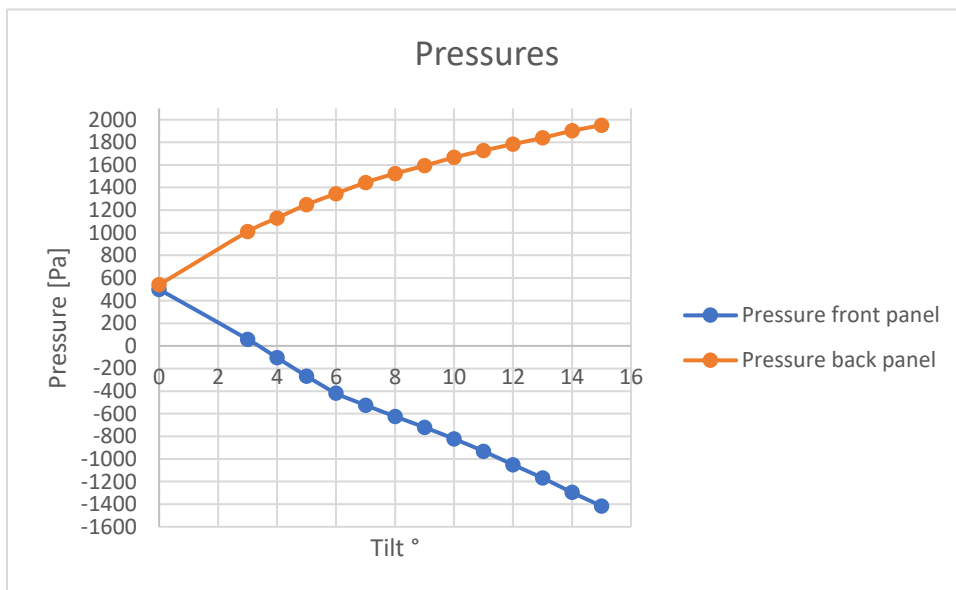
Figure 50: Pressures on the frontal and back wall of the panels as function of the inclination angle when wind is impacting from the back.

Most of the commercial solar panels can resist to frontal pressures from 3000 Pa to 5400 Pa while from back pressures have a resistance from 2000 Pa to 4000 Pa. One of the most resistant commercial solar panel is the LG NeON-R, it can resist to 5400 Pa of frontal pressure and 4000 Pa of rear pressure. Most of the commercial panels in Florida however have a frontal resistance of 5000 Pa and a rear resistance of 2400 Pa, like the Trina solar, Canadian solar, Qcell, and Jasolar panels; the threshold is then set respecting these values.

As it is possible to grasp, the frontal pressure is not a big threat since in the frontal wind condition the maximum total pressure is reached at 15° tilt and is equal to the difference between the frontal pressure and the back pressure, in the case of 15° tilt angle the total pressure is equal to 3174.4 Pa which is lower than the average panel resistance. The problems appear when analyzing the backward wind direction simulation, in this case the limit is 2400 Pa and can be reached only for the tilt of 9°. In this case the pressure is calculated as the back module pressure minus the frontal side depression. The maximum value is still reached at 15 ° and is equal to 3366.8 Pa, at 10° the total pressure is 2488.9 Pa and at 9° is equal to 2313.4 Pa so the last angle has been chosen as highest angle that can let the panels resist to a Cat. 5 hurricane even though the optimal tilt for energy production is 25°. Since the greater the angle the higher the energy production, this will be the angle that guarantees the maximum production still resisting to major hurricanes wind gusts.

The simulation results are reported in *Table 6* and *Table 7* for respectively front and back wind:

Front wind simulation							
Tilt	Drag-coeff	Lift-coeff	Force-z	Force-y	Pressure-front-modules	Pressure-back-modules	Total frontal pressure
degree			N	N	Pa	Pa	Pa
0	0.039124643	0.022509166	871.1778	501.1893	498.85667	545.9727	-47.11603
3	0.049230823	-0.19544855	1096.216	-4351.859	913.57602	26.702258	886.873762
4	0.05743152	-0.26823043	1278.741	-5972.421	1035.0151	-155.36861	1190.38371
5	0.067973465	-0.34135096	1513.551	-7600.523	1143.8402	-345.16513	1489.00533
6	0.081323938	-0.41199168	1810.929	-9173.41	1227.6608	-521.46027	1749.12107
7	0.0973347	-0.48043759	2167.582	-10697.43	1307.9724	-662.44986	1970.42226
8	0.11525466	-0.54314033	2567.928	-12093.57	1377.8474	-766.05945	2143.90685
9	0.1347149	-0.59880937	3001.244	-13333.09	1431.0594	-864.42741	2295.48681
10	0.15493391	-0.6496295	3451.388	-14464.66	1482.0011	-954.17333	2436.17443
11	0.17644452	-0.69485971	3927.134	-15471.75	1542.0637	-1044.728	2586.7917
12	0.19883408	-0.73686679	4421.185	-16407.08	1589.1205	-1139.8343	2728.9548
13	0.22196588	-0.77441603	4937.311	-17243.15	1636.0202	-1245.2966	2881.3168
14	0.24501776	-0.80554074	5454.817	-17936.18	1680.3382	-1340.1084	3020.4466
15	0.26960262	-0.83887243	6003.391	-18678.34	1728.0237	-1446.4214	3174.4451

Table 6: Data from the front wind simulation.

Back wind simulation							
Tilt	Drag-coeff	Lift-coeff	Force-z	Force-y	Pressure-front-modules	Pressure-back-modules	Total rear side pressure
degree			N	N	Pa	Pa	Pa
0	0.038996802	0.021757301	870.1196	485.4617	499.12057	540.6382	41.51763
3	0.05059679	0.23349769	1128.945	5209.938	58.50777	1009.5091	951.00133
4	0.0590134	0.30243737	1316.742	6748.161	-104.78184	1130.225	1235.00684
5	0.06975423	0.37228207	1556.398	8306.577	-267.41835	1248.9266	1516.34495
6	0.082883434	0.44109699	1849.344	9842.016	-418.91019	1345.7637	1764.67389
7	0.099293472	0.50815376	2215.495	11338.23	-524.82381	1445.0595	1969.88331
8	0.11781073	0.57389757	2628.663	12805.14	-624.14815	1523.7021	2147.85025
9	0.13820821	0.63514459	3083.783	14171.72	-720.60512	1592.7835	2313.38862
10	0.16023219	0.68986781	3575.195	15392.74	-822.51311	1666.355	2488.86811
11	0.18386898	0.74207044	4102.593	16557.51	-931.85022	1727.0921	2658.94232
12	0.20809189	0.78984022	4643.069	17623.38	-1051.8567	1783.9642	2835.8209
13	0.23411229	0.83360301	5223.652	18599.84	-1167.9633	1839.0833	3007.0466
14	0.26107522	0.87712708	5825.264	19570.98	-1296.4228	1901.8251	3198.2479
15	0.28901137	0.91879288	6448.592	20500.65	-1416.344	1950.4411	3366.7851

Table 7: Data from the back wind simulation.

The highlighted colors have been adopted to show whether the modules will suffer or not the effects of high speed wind gusts, the 0° tilt is white since this application is usually avoided due to the dust that may form on the panels if are not tilted. The green zone is the safe zone, the yellow zone is the not guaranteed zone and the orange zone is the dangerous zone for standard PV panels. For high resistive solar panels higher angles can be set, these panels are more expensive and have a higher efficiency in most cases but the high tilted panel will produce greater lift and drag forces which are already quite high. For the 9° case a lifting force of 14,171.72 N is difficult to handle, it represents a counterbalanced anchoring weight of more than 1.4 ton just for an NRG unit. With forces of a similar magnitude, it would be very hard to keep still an entire floating farm, but these values are only true for the first wind affected row. From the second row on the sheltering effect will take place, the first row will act as a shield, resisting and deviating the strong wind gusts and leaving a less fast wind behind them.

The simulation with two panels has been performed using less elements on the first-row panel and focusing the analysis on the second one with more elements. The panels have been spaced apart 0.3 m to limit the shading effects especially in the winter season. Greater distances might increase

too much the cost of the floating farm while too close panels will highly decrease the energy production. In this configuration the following results (see *Tab.* 8) came out of the simulation:

	Drag-coeff	Lift-coeff	Force-z	Force-y	Pressure-front-modules	Pressure-back-modules	Total pressure
Wind impacting on the second row simulation							
			N	N	Pa	Pa	Pa
Front wind	0.05877878	-0.2231817	1308.769	-4969.365	392.678	-193.310	585.988
Back wind	0.05734163	0.2097077	1258.648	4603.079	124.760	181.368	-56.608

Table 8: Data from the second row simulation when wind is impacting front the front and back.

All the values have dropped, the drag coefficient lowered almost 60 % compared to the first row, nearly 70 % is the lowering factor for the lift coefficient and same percentages are similar for the relative forces. This means that the first row needs to be tightened and secured to resist to the first impact while the following rows will need less than half the resistance applied to the first line.

7.8. Visual results and considerations

The visual results help to understand how wind behaves when an obstacle is fixed on the path. The velocity contour for the frontal wind simulation is shown in *Figure* 51
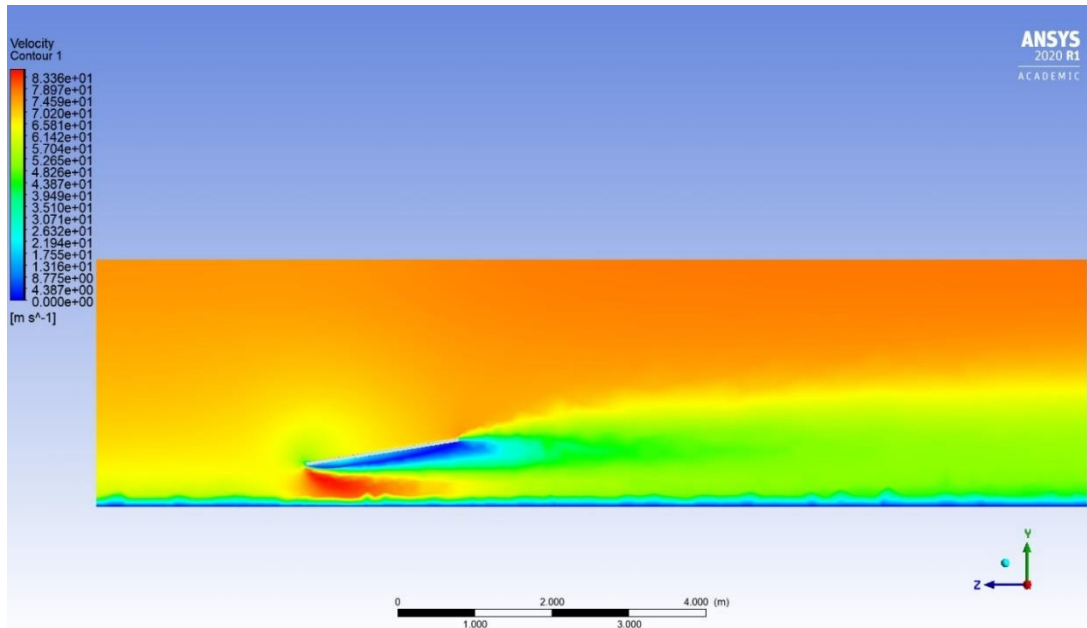
Figure 51: Velocity contour when wind is impacting the 9° tilted panels from the front, plane zy.

The velocity values are shown in the labels on the top left of the figure and are represented by colors, from the low speed represented in blue to the highest speed indicated in red. The velocity profile at the inlet follows the power law profile that reaches a velocity of 300 km/h (83.33 m/s) at 10 m above the ground. The roughness of the lake lowers the speed as well and is well seen in the figure at the bottom. The solar panels 9° tilted endure the wind, the effect is a high speed under and over the panels and a very low speed on the back of the modules, where the turbulent induced depressions take place. The wind speed is reduced behind the panels producing a sheltering effect on the set of panels that could have been installed behind. The first row of panels will be indeed the most impacted by wind loads.

The velocity in the y direction is shown in the *Figure 52*.
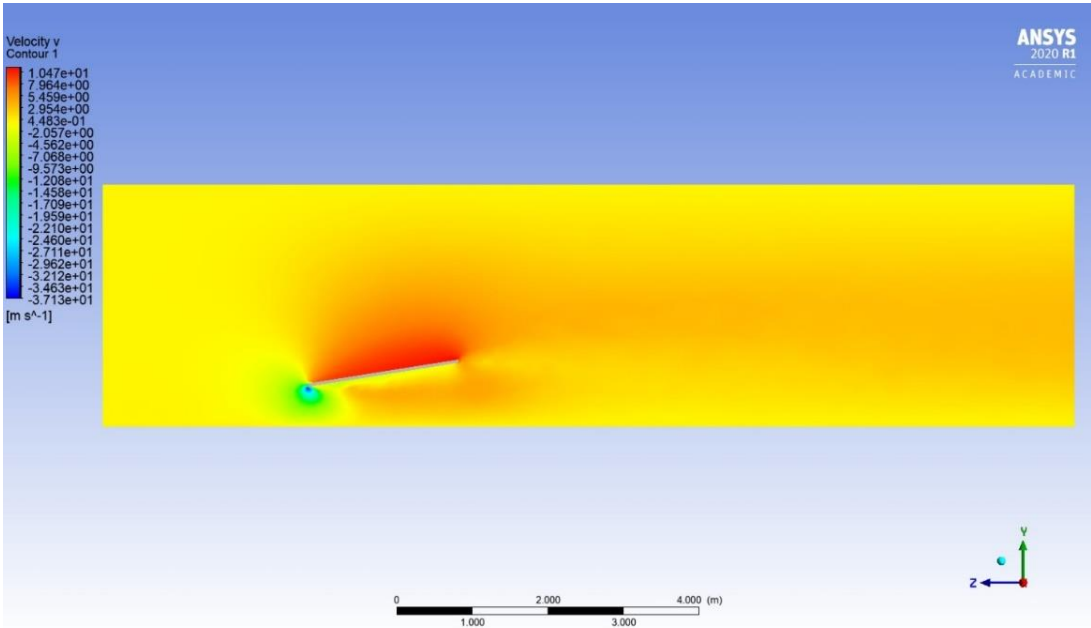
Figure 52: Velocity contour in the y direction when wind is impacting the 9° tilted panels from the front, plane zy.

The high velocities on the front part of the panels show how the lift force in the y direction is acting. And in the first point the wind encounters the panels on the bottom left side a high downward velocity can create momentum on the set of panels since the force will not be homogeneous.

The velocity streamline contour is shown below in *Figure 53*.
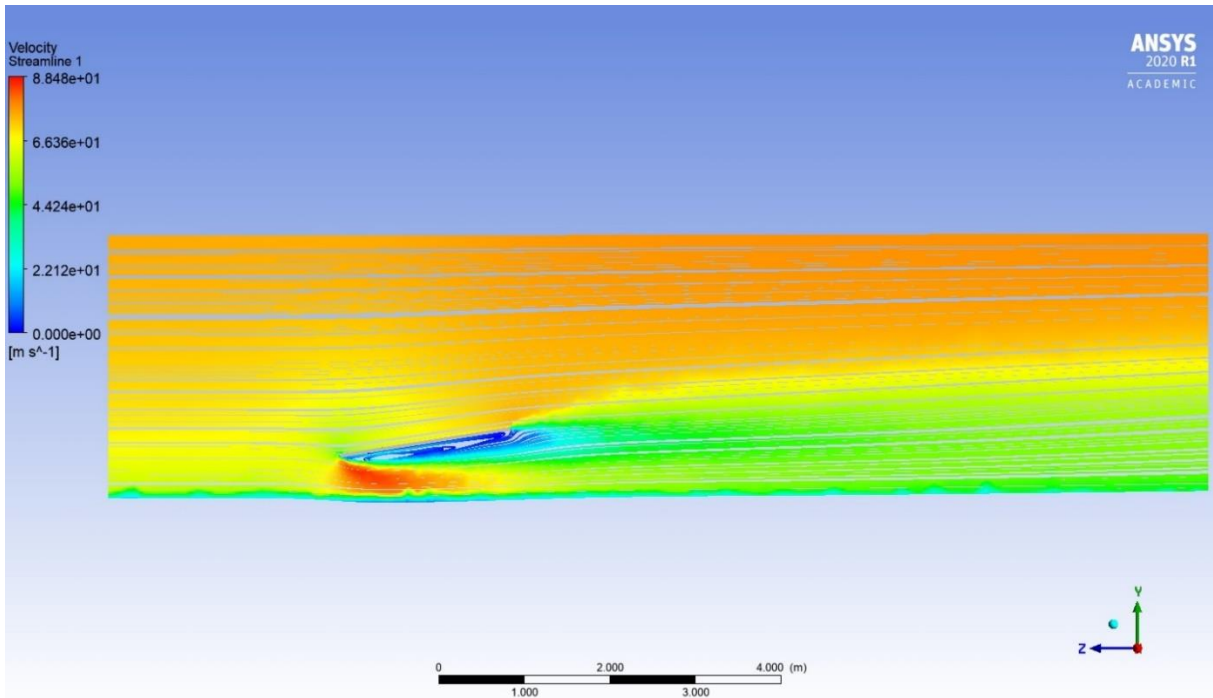
Figure 53: Velocity streamline when wind is impacting the 9° tilted panels from the front, plane zy.

From the streamline profile it is possible to see the turbulences behind the panels and the relative macroscopic turbulent structures, A further zoom has been taken on the wind area behind the panels.
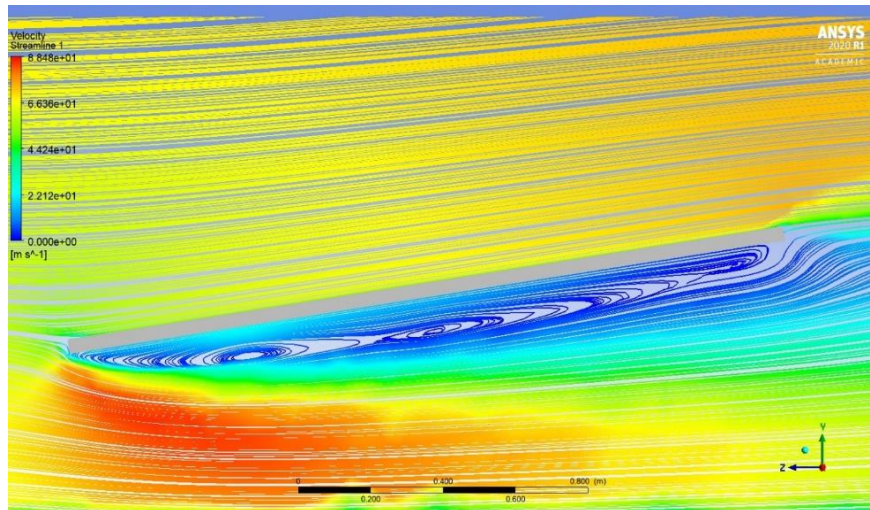
Figure 54: Velocity streamline showing swirls under the solar panels, plane zy.

From the *Figure 54* it is possible to observe the largest scales vortices and their respective lengths. A medium sized swirl is positioned on the left side, where the velocities are the highest and a high kinetic energy feeds the swirls. A small recirculation is placed at the top right where the flows going upwards confine the vortices area, and a center positioned recirculation is also established with a medium size. These swirls are problematic since they create high and difficult to predict depressions on the rear side of the modules, increasing the overall pressure on the whole panels.

The turbulent kinetic energy shown in the *Figure 55* is high under the solar modules but seems to be well dissipated in a small amount of space. The value k is also high at the inlet since it has a 20 % turbulent intensity, which is a reasonable value for a category 5 hurricane.
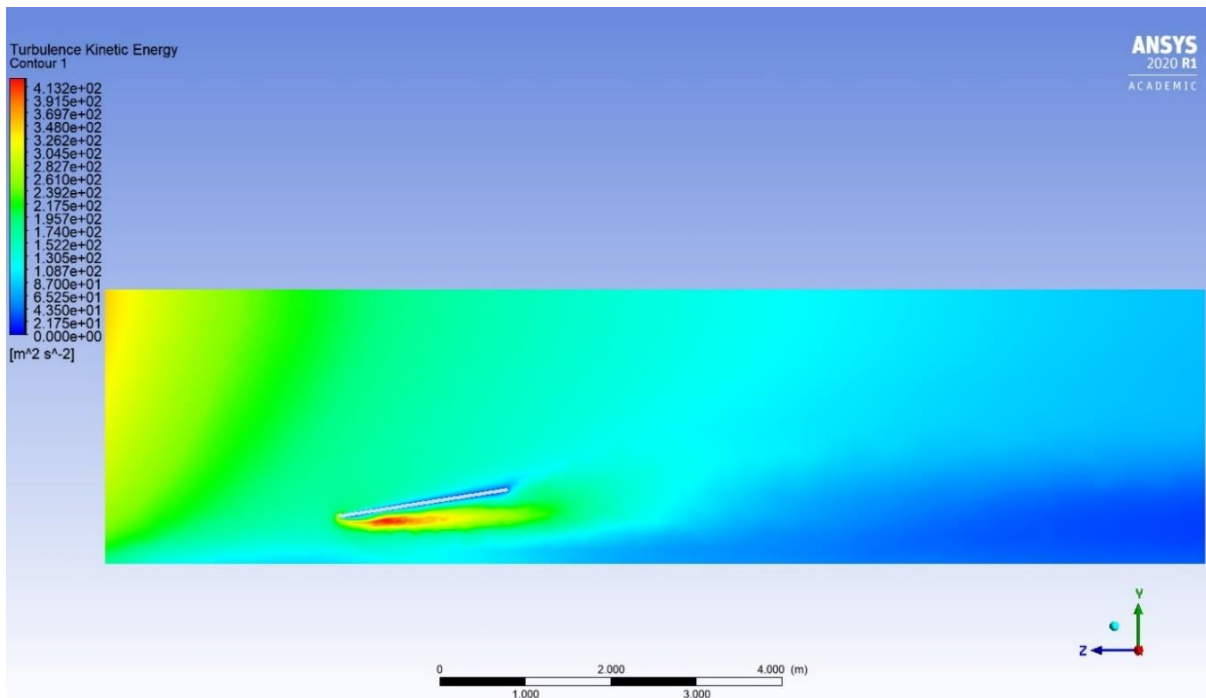
Figure 55: Turbulent kinetic energy contour when wind is impacting the 9° tilted panels from the front, plane zy.

What can show how well is the turbulence dissipated is the turbulence viscosity. The higher the viscosity the higher the turbulence energy transfer that can give rise to tangential stresses. the eddy viscosity already present in the turbulent wind is lowered by the presence of the solar panels, the first row will then face lower wind loads and turbulences if well-spaced from panels behind the first row (see *Fig. 56*).
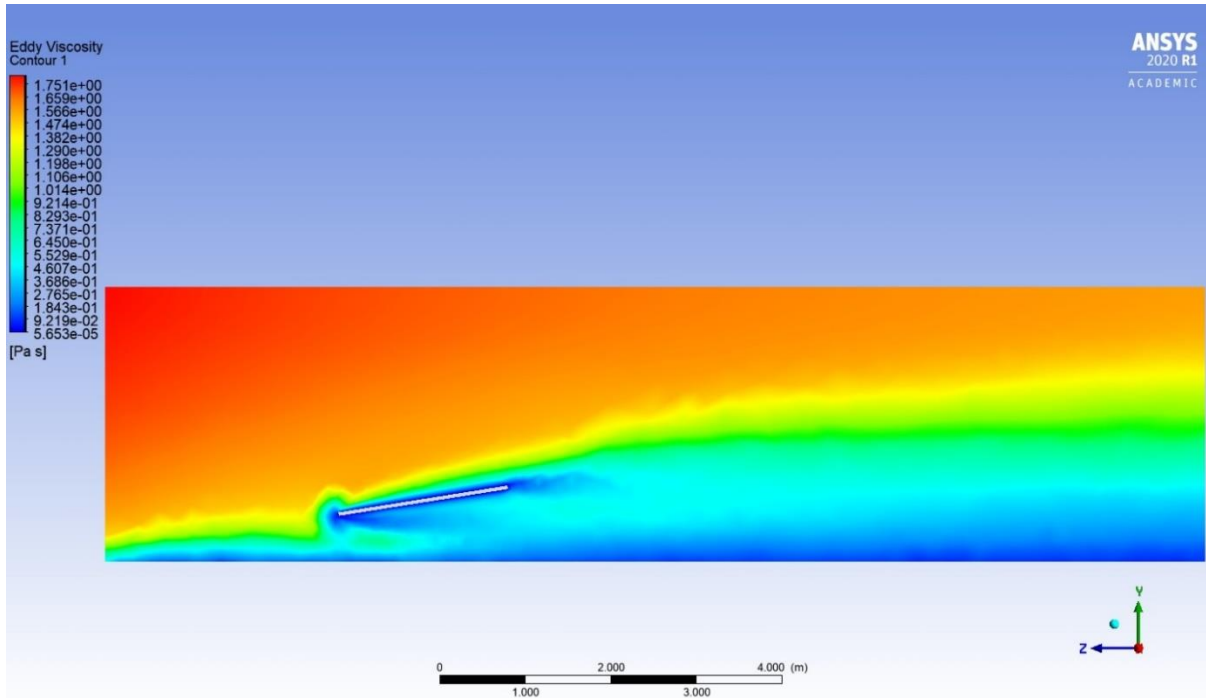
Figure 56: Eddy viscosity contour when wind is impacting the 9° tilted panels from the front, plane zy.

The wind from a plane impacting the panels and producing pressures is shown in the *Figure 57*.
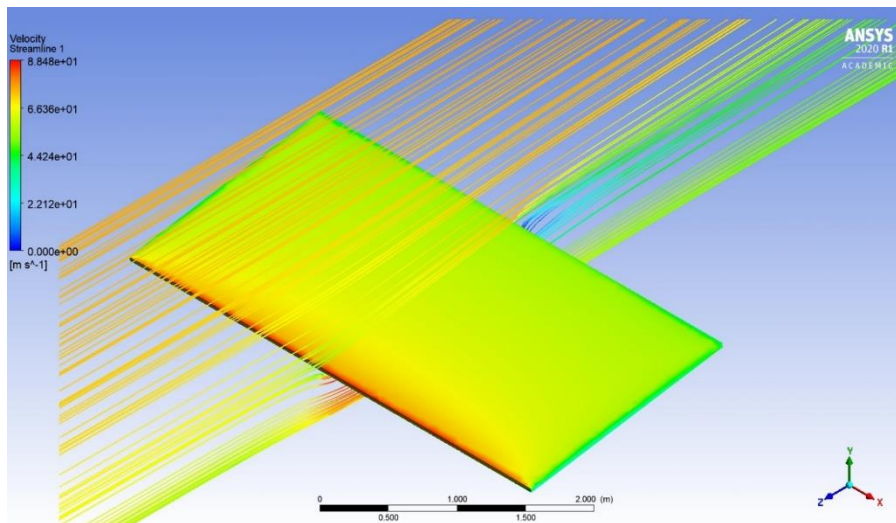
Figure 57: Wind path on plane zy and solar panels facing pressures.

On the frontal face of the panels a high pressure is formed at the bottom tilting side. The frontal part of the frame is the most affected part, since it is almost normal to the wind direction, and at the edges there is a lowering pressure. The mean pressure on the frontal face of the panels is 1431 Pa but on the most affected spots this pressure is over 2000 Pa. These concentrated forces can lead

to momentums that might break the panels so a reinforcement might be needed on the frontal impacting part (see *Fig. 58*).
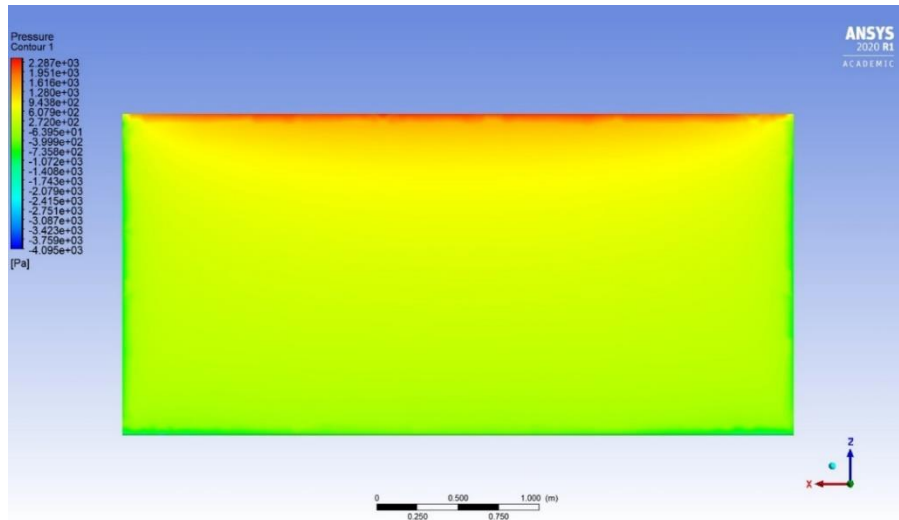
Figure 58: Pressure contour when wind is impacting the 9° tilted panels from the front, frontal panel face.

On the rear side of the panels shown in *Figure 59* high depressions are formed especially on the lower part of the panels where a strong medium sized vortex is placed. Combining the high pressures located on the lower part of the module's frontal faces and a very low pressure on the same spots but on the back side, an overall high pressure is formed at the beginning of the panels, producing mechanical stresses that needs to be handled by the aluminum supporting structures of the floating unit.
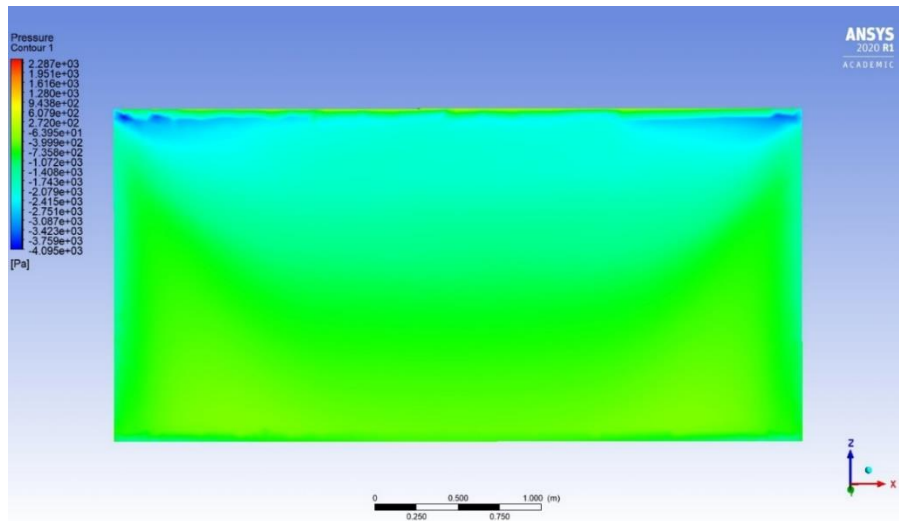
Figure 59: Pressure contour when wind is impacting the 9° tilted panels from the front, back panel face.

On the rear side the averaged pressure is -864 Pa but peaks that reach -4000 Pa are locally present.

For the wind impacting the panels from the back simulations similar visual results are shown (see *Figures 60,61,62,63*).
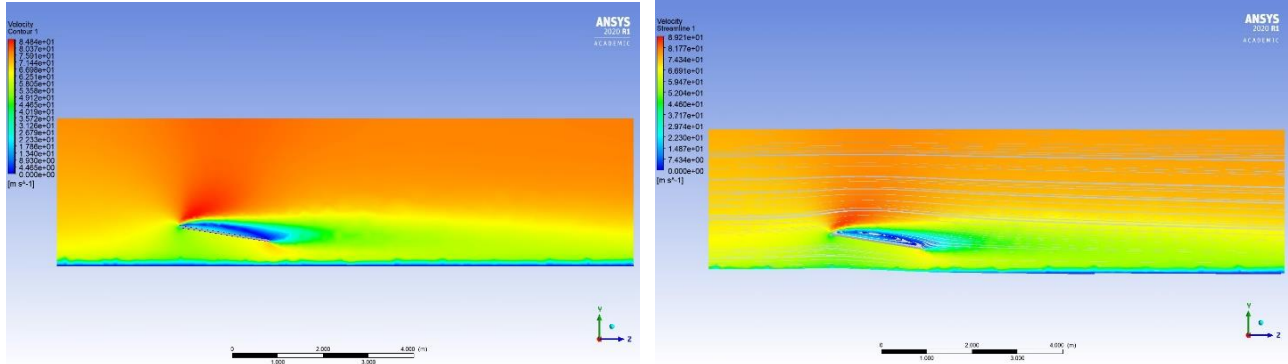
Figures 60-61: Velocity contour and streamlines when wind is impacting the 9° tilted panels from the back, plane zy.
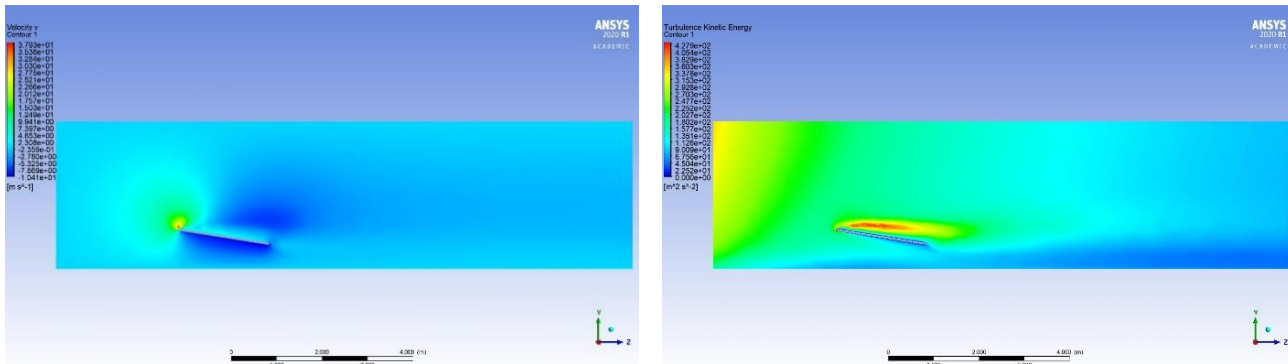
Figures 62-63: Velocity contour in y direction when wind is impacting the 9° tilted panels from the back, turbulent kinetic energy, plane zy.

Apart from the higher pressures related to this setting, what also changes is the sheltering effect. In fact, the eddy viscosity has a different profile compared to the frontal wind simulation, high velocity wind is reduced by the obstacle but the speeds and turbulences are higher on the wind area behind the first row (see *Fig. 64*).
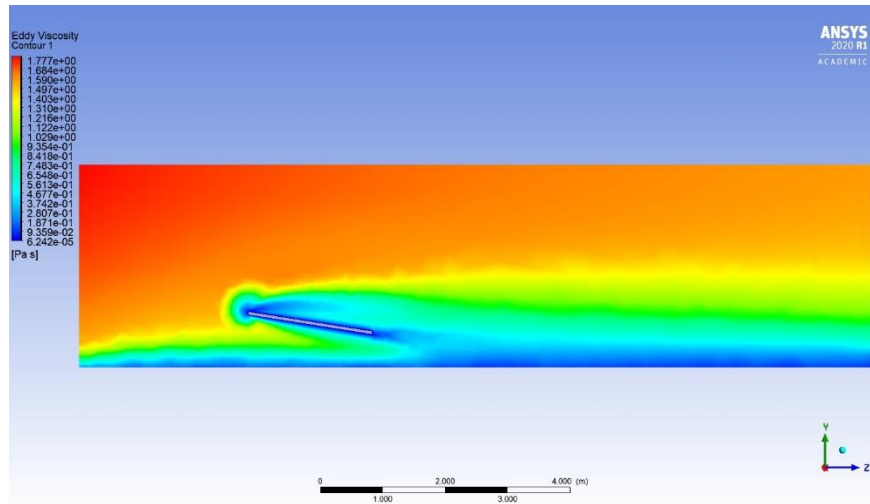
Figure 64: Eddy viscosity when wind is impacting the 9° tilted panels from the back, plane zy.

The panels pressures are slightly higher but follow the same behaviors as the first front wind simulation (see *Figures 65,66*).
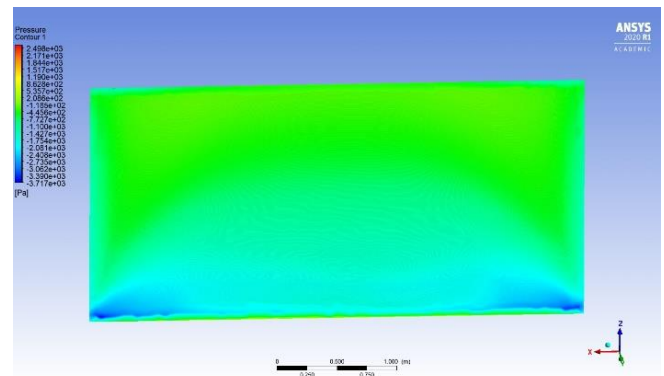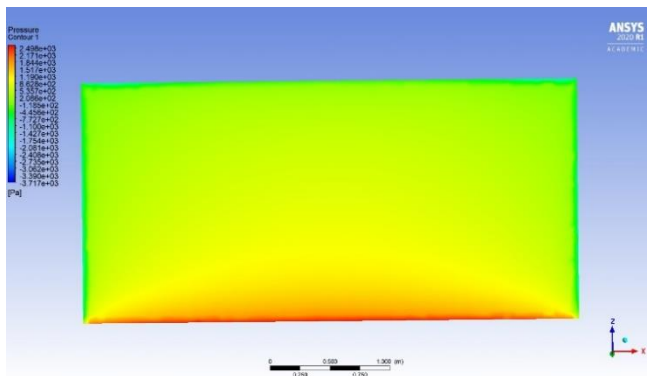
Figures 65-66: Pressure contour when wind is impacting the 9° tilted panels from the back, back and front panels face.

In the two rows case the sheltering effect is more visible, between the two panel's set a high turbulent depression is formed lowering considerably the pressures on the second row (see *Fig.67*).
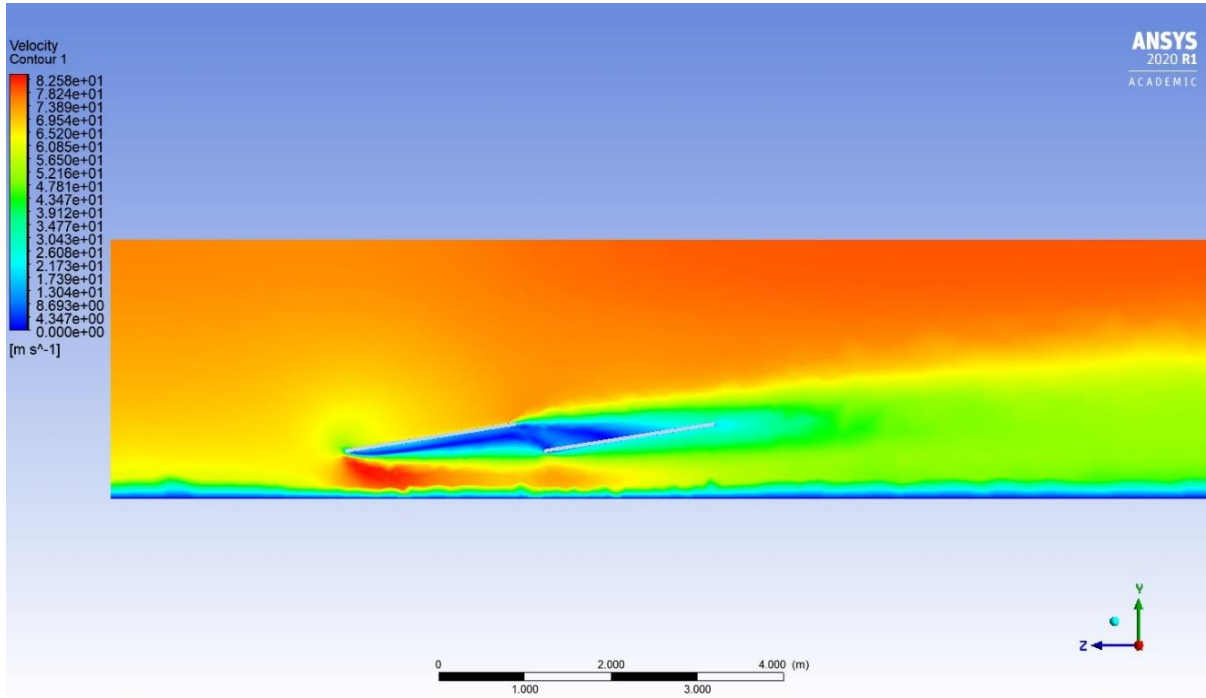
Figure 67: Velocity contour when wind is impacting the 9° tilted panels from the front with two panel's rows, plane zy.
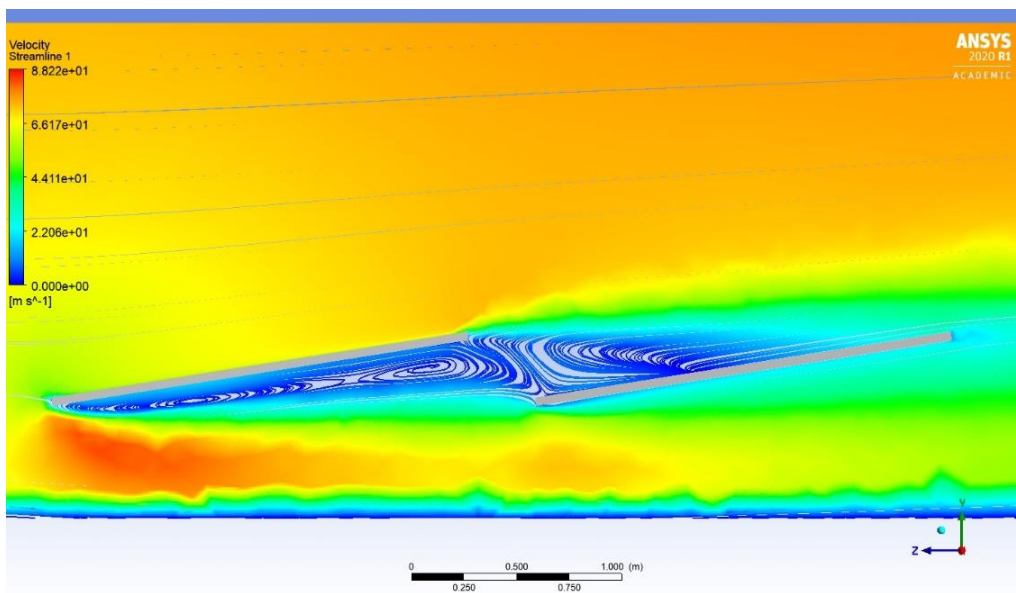
Figure 68: Velocity streamlines when wind is impacting the 9° tilted panels from the front with two panel's rows, zoom on the swirls, plane zy.

The turbulences formed between the rows are highly diffused under the back face of the first row and over the front face on the second one, which reduces drastically the frontal pressure on the second row and the overall drag and lift effects. Not well-established vortices can be denoted on the second row since the fast wind might break the swirls from the top side, nevertheless turbulent streamline curvatures can be seen and so small swirls can still occur and affect the panels (see *Fig. 68*).

8. NRG Unit simulation

A simulation similar to the one developed for the panels set has been performed for the NRG unit, using similar setup and boundary conditions.

Once defined the limit tilt as 9° for the modules, the geometry of the NRG island unit has been created. The difference in the analysis can be found in the meshing, since the NRG unit is wider and a bigger enclosure is needed for an accurate simulation. While the elements length on the geometry surface has been set the same as the previous simulations (0.06 m). The inflation method has been used on the unit geometry as well (see *Fig. 69*).
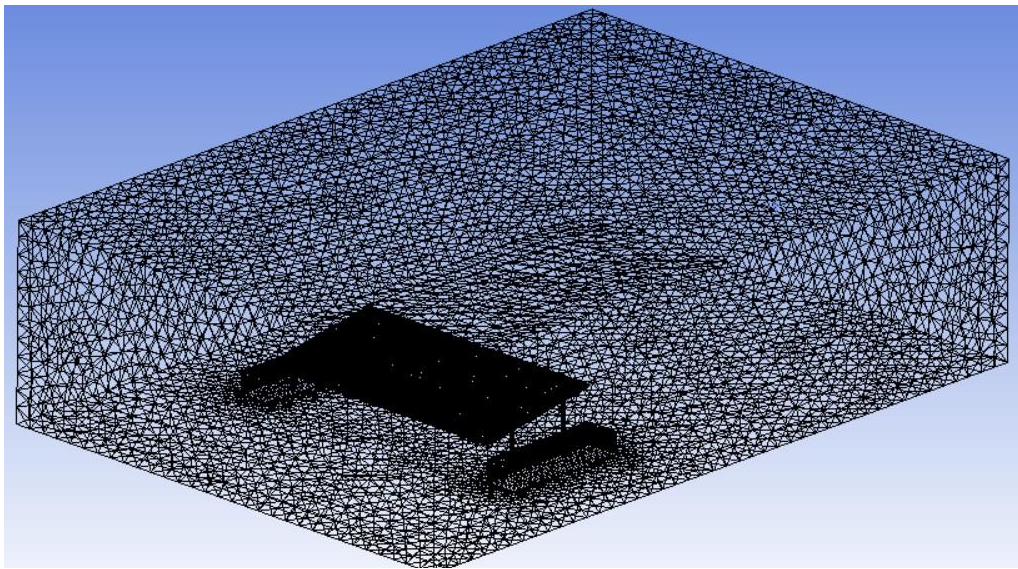
Figure 69: Mesh of the entire fluid domain, the darker part represents the NRG island unit with 9° tilt panels.

For this simulation the residuals reached higher values, especially in the back-wind flow setup, the more complex geometry creates peculiar spots the software struggles to solve. The residuals reached values vary between 10^{-5} to 10^{-4} leading to a less accurate solution. The residuals however assure values reliable for the final sake of the thesis.

For this simulation the drag and lift coefficients of the whole NRG island unit has been calculated as well as the relative drag and lift forces.

When comparing the NRG unit data to the panels 9° tilted scenario some differences can be observed. The drag coefficient of the unit is greater since the added float and structure geometries

obstacle the wind path creating more resistance. The lift coefficient as absolute value is lower than the simulation with only the panels. This happens because the unit geometry added impacts the wind path, creating additional turbulences that alter the lift coefficients. The lift force is greater instead, this means that the effect of the lift coefficient is lower than the local speeds influence. Therefore, even if the lift coefficients are lower both for frontal and back wind effects, the lift forces are higher in the case of NRG unit instead of just panels. This behavior does not happen for the drag force since in this case the higher C_D corresponds to a higher drag force (see *Tab. 9*).

NRG Island unit simulation				
Front wind	**Drag-coeff**	**Lift-coeff**	**Drag-force**	**Lift-force**
Unit			*N*	*N*
NRG unit	0.1499161	-0.4889035	4168.670	-13594.79
Panels only	0.1347149	-0.5988093	3001.244	-13333.09
Back wind	**Drag-coeff**	**Lift-coeff**	**Drag-force**	**Lift-force**
Unit			*N*	*N*
NRG unit	0.1591800	0.6230272	4368.854	17099.61
Panels only	0.1382082	0.6351445	3083.783	14171.72

Table 9: Fluid domain section showing the mesh, a denser mesh in near the solar panels set.

The front and back-wind configurations have some differences, since both the coefficients and forces are greater in the back-wind configurations. This event was expected since in the panels configuration the back flow created more drag compared to the frontal one, but a higher delta can be found for this simulation. The wind that converged beneath the panels is also limited on the sideways by the floats, therefore more wind is conveyed under the structure, creating higher force effects. For the frontal simulation, the wind under the panels is diverged thanks to the upwards inclination on the modules, while in the back flow the wind faces a convergence effect that increases the forces and pressures on the structures around.

These forces shall be handled by the unit and at large scale by the anchoring and mooring systems that needs to be well designed and engineered in order to resist to extreme events.

Moreover, a detailed analysis on the momentum induced stresses is needed since these pressures are not homogeneous on the panel.

8.1. Visual results and considerations for the floating unit simulation

On the plane secant the panels on the yz plane the velocity profile is shown in the *Figure 70* when the wind is hitting in the frontal way.
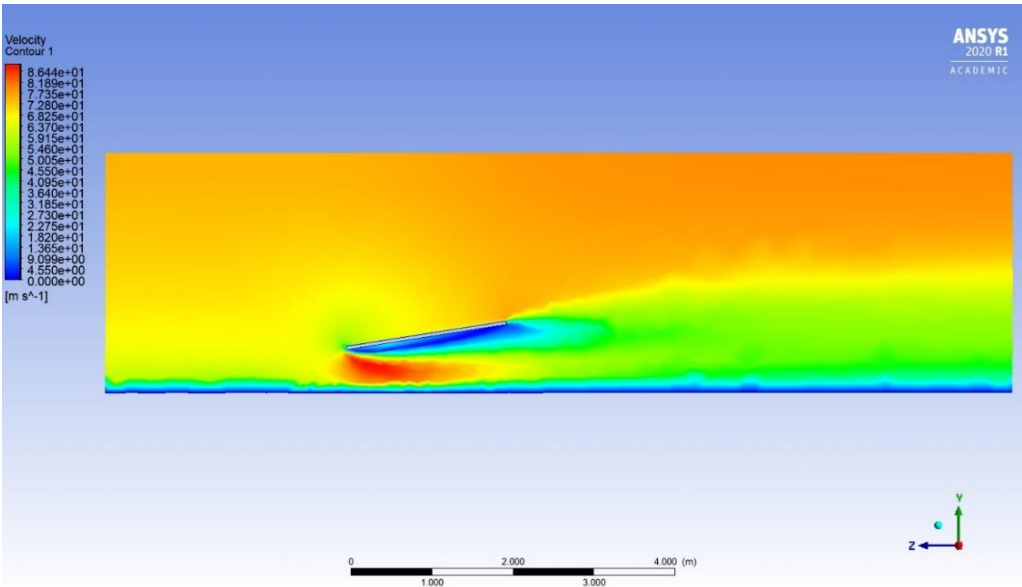

Figure 70: Velocity contour when wind is impacting the NRG island 9° tilted panels from the front, plane zy.

The wind profile is similar to the one of the previous simulations showing the sheltering effect. On the floats the effects shown in the *Figure 71* are limited by the lower speed near the ground, but is possible to see the turbulences behind the floating blocks.
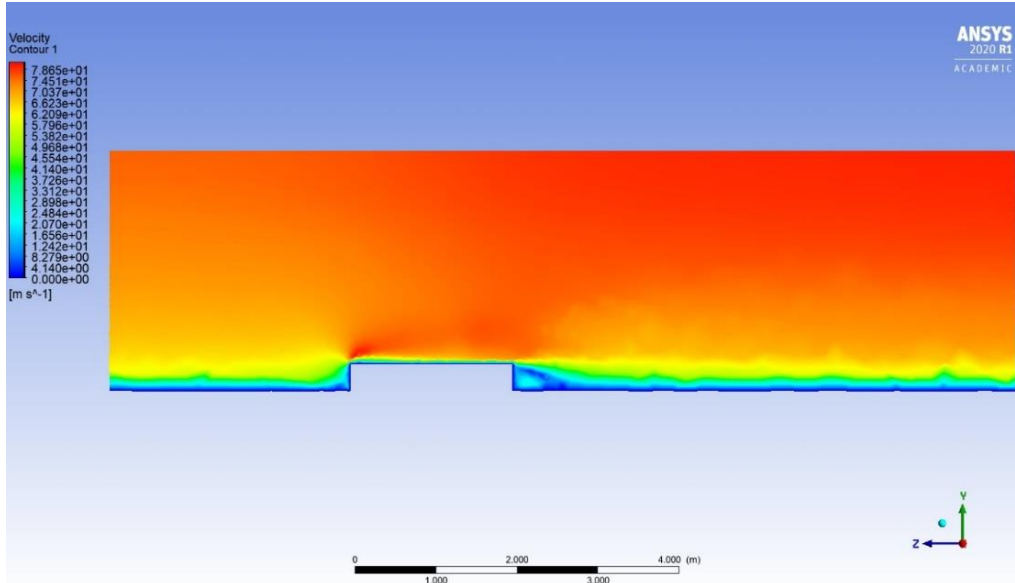
Figure 71: Velocity contour when wind is impacting the floats from the front, plane zy.

Better visual results of the float effects are shown in the *Figure 72*: the secant plane xz cuts the floats in half. From the figure it is possible to see the turbulences behind the floats colored in blue, the higher speed at the center is due to the blocking effect of the panels and the floats which convey and increase the speed and the lowering speed colored in green shows the sheltering effect induced by the blocking panels.
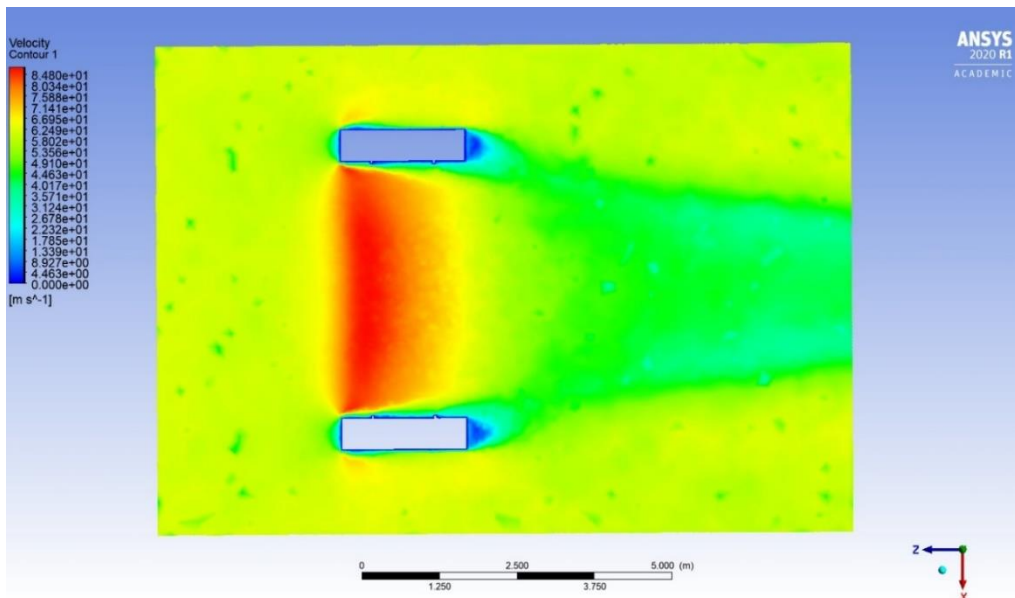
Figure 72: Velocity contour when wind is impacting the floats from the front, plane zx.

The following figure represents the secant plane yz that cuts the metal structures and shows how the wind is lowered by such structures and near the floats.
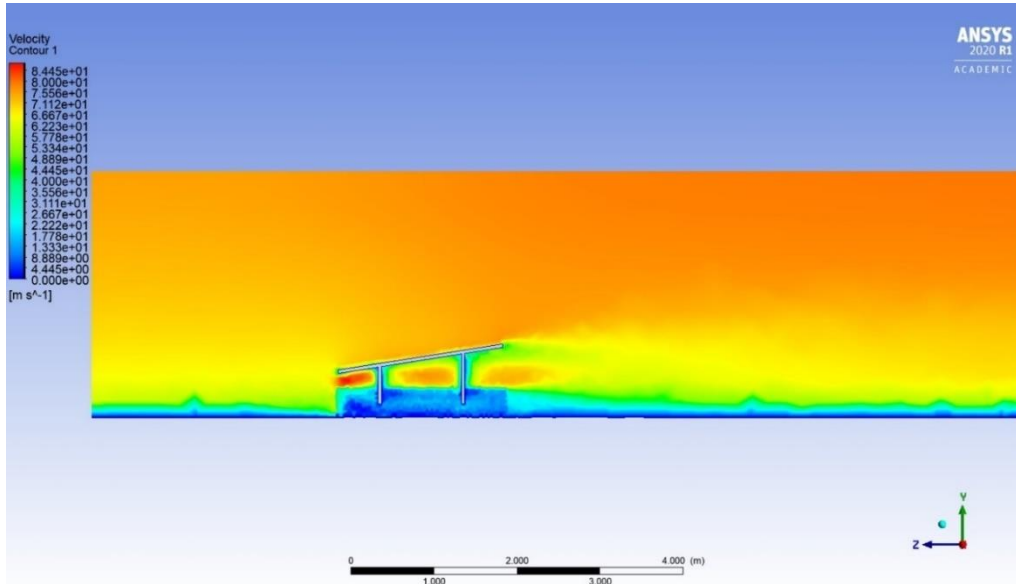
Figure 73: Velocity contour when wind is impacting the structures and panels from the front, plane zy.

A yx plane positioned in the middle of the unit is shown in the *Figure 74*, under the modules a wide depression produced by the turbulences is shown in the color blue. Right under the turbulences the speed is increased because of the convergence effect.
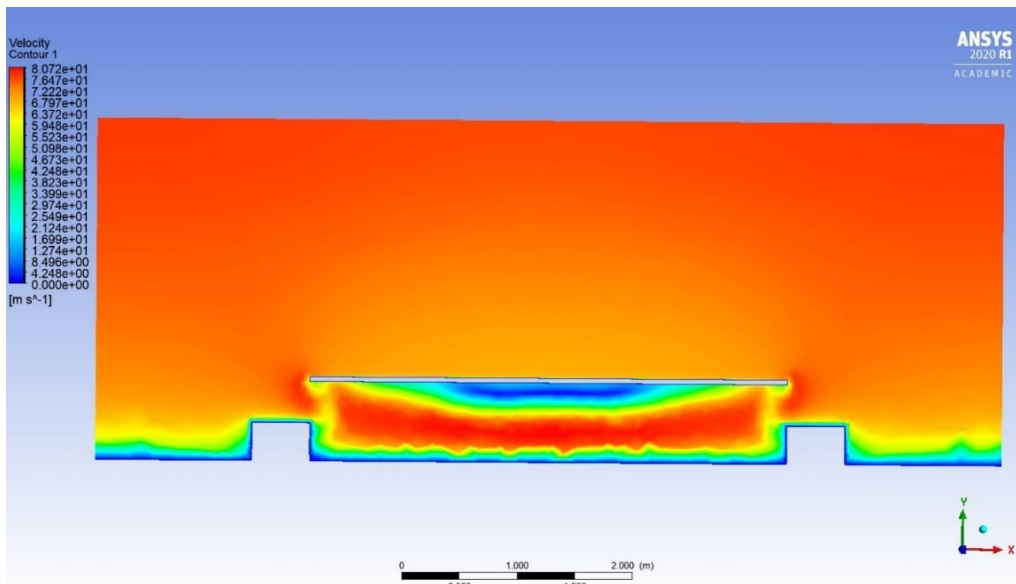
Figure 74: Velocity contour when wind is impacting the panels from the front, plane in the middle of NRG unit, plane yx.

What better shows the turbulences beneath the panels is the 3D streamline flow positioned on the zx plane under the modules (see *Fig. 75*). Big vortices are formed at the center of the figure which represents the position under the PV panels, these whirls are wider at the center and become smaller near the edges. This zone will create high depressions that can have significant impacts on the overall resistance on the floatovoltaic unit.
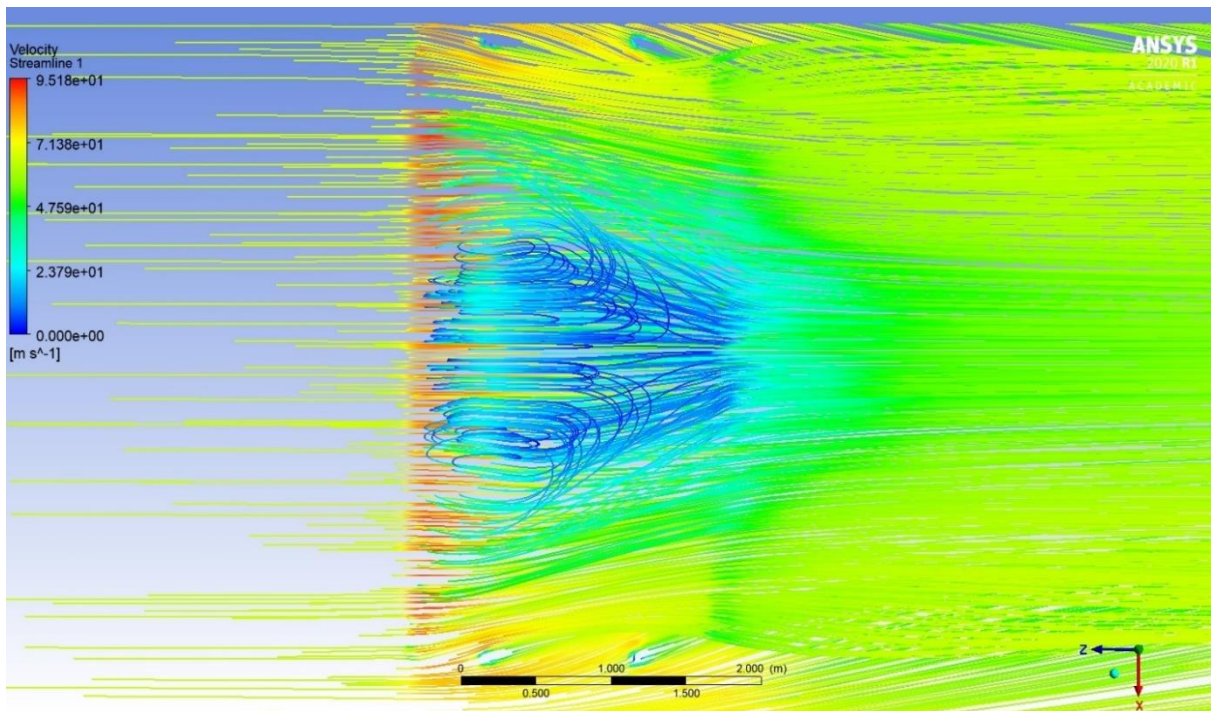
Figure 75: Velocity 3D streamline when wind is impacting the panels from the front plane under the panels, plane zx.

The impacts mentioned can be seen from the pressure contour of the whole unit. In the frontal wind configuration, the panels are affected by high pressures especially on the initial frontal edge colored in red in the *Figure 76*, and the floats are also impacted since they have a face perpendicular to the flow direction. But the great pressure effect that can create issues on the panels and on the unit is the turbulence induced depression that reaches locally -4000 Pa on the rear side of the panels (see *Fig. 77*). This effect can lead to overall localized pressure in the order of 6000 Pa on the panels which might be difficult to be handled by the panels and by the structures and create momentums that can generate high localized stresses.
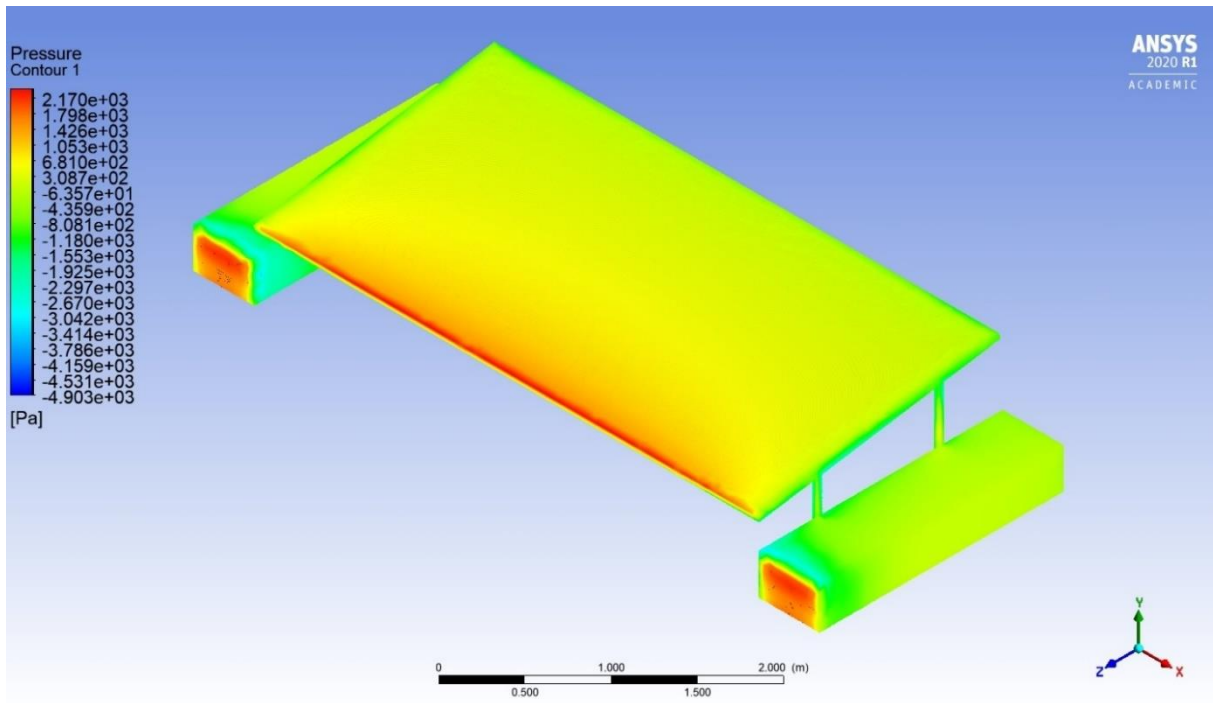
Figure 76: Pressure contour when wind is impacting the NRG island unit from the front.
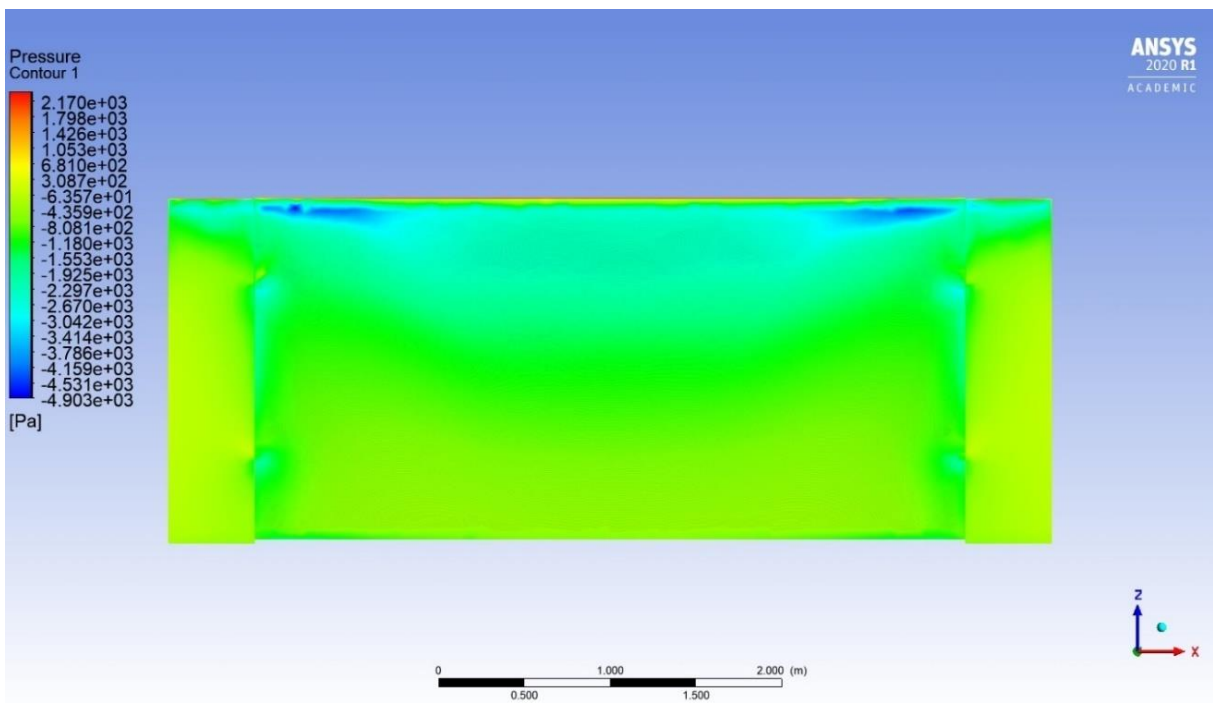

Figure 77: Pressure contour when wind is impacting the panels from the front, view from below.

For the back wind the viewings are similar to the front flow for the floats and structures, for the panels it is analogous to the back-wind simulation of the panels previously analyzed. In this case the depressions are slightly less effective and the impacting pressures in the rear of the panels have a greater role compared to the front wind configuration (see *Fig. 78*).
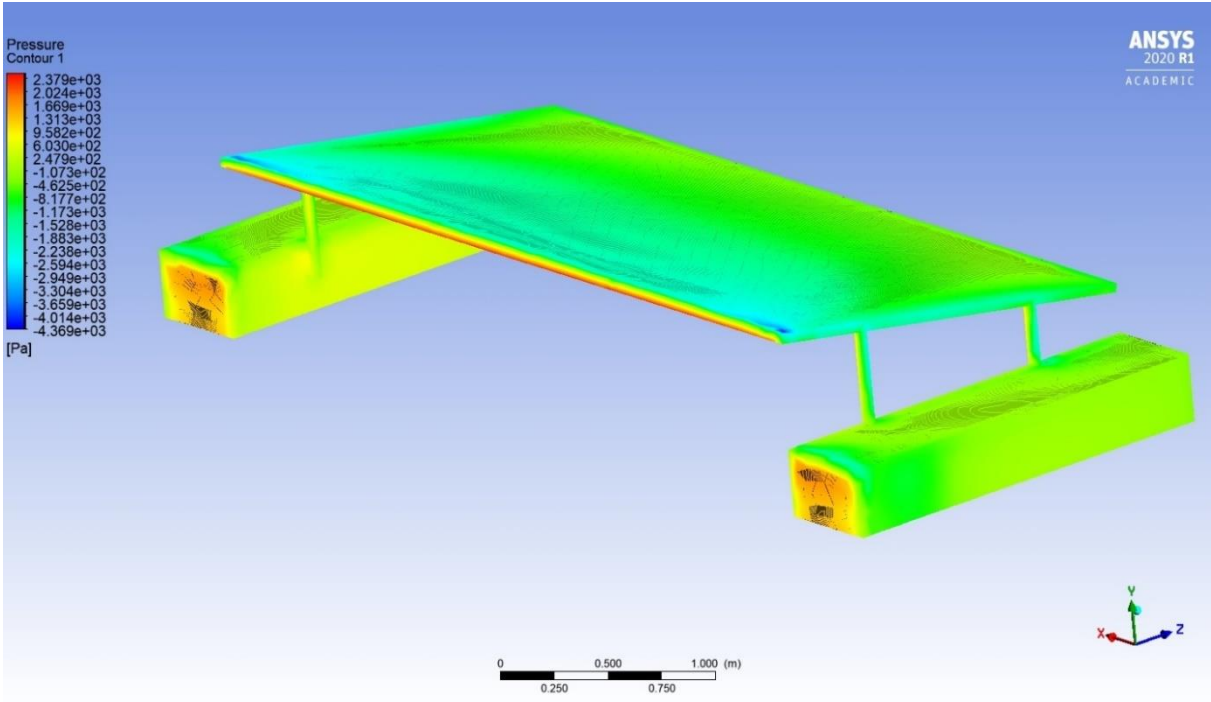
Figure 78: Pressure contour when wind is impacting the NRG island unit from the back.

9. Dome configuration

It is well known that modules do best when facing towards the equator, but the south facing solar panel configuration is not the only possible design for photovoltaic systems in Florida. If modules instead of facing true south will create a roof or dome shape facing one towards east and the other to west, they will still produce a high amount of power (see *Fig. 79*).

Figure 79: Representation of the dome configuration for landscape positioned solar panels, Landpower solar.

The east-west design also known as *dome configuration* is largely used and entails numerous advantages. The most evident benefits are briefly listed below:

✓ Since this configuration compacts the panels with the effect of squeezing the rows, this design can perform a greater generation capacity on the same employed land.

✓ The best dome configuration comes up with a low tilt, thanks to the roof looking configuration and the small slopes fewer shading losses will occur and the more compact the solar farm can be.

✓ The east-west configuration may reduce the output compared to the south facing design, but the value of the produced electricity is intrinsically higher since the generation is in part shifted during the morning and evening when the demand is high and so the price, and is less produced during midday when the electricity price is cheaper.

The University of Sheffield conducted a comparison on the kWh produced during the day from 1 kWp solar PV installation in England, one system facing south, and the other configuration designed east-west (see *Fig. 80*). The south facing configuration presents a sharp curvature with the peak during midday while the dome configuration represented in the blue color is more flatten, still presents the peak during 12.00 but it has a high production also in the first and last daylight hours [58].
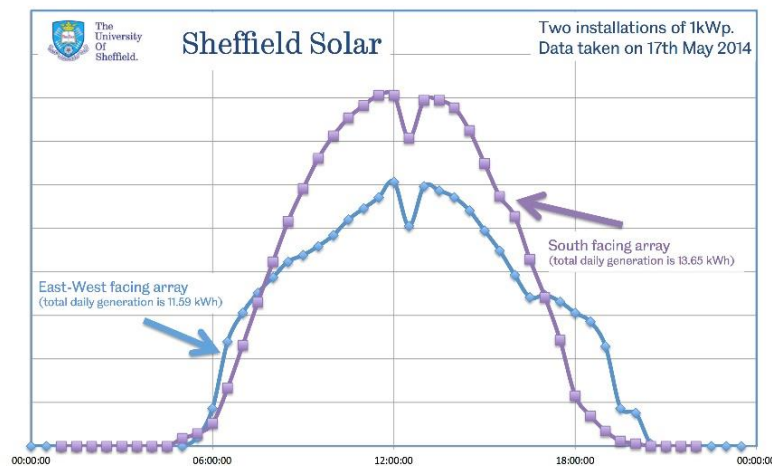

Figure 80: Hourly productivity comparison of 1 kWp facing south and 1kWp facing east-west, University of Sheffield.

✓ The energy production for the dome configuration is not as function of the azimuth as much as the south facing one, so it can match the space available more easily. If the dome configuration is not well placed east and west the total energy produced will remain the same since the panel that will be positioned more toward north will produce less but the other symmetric panel facing further in the direction of south will produce more. The same thing does not happen for the south facing configuration. For this reason, the dome configuration is more versatile and can fit into different lakes and land shapes.

✓ In regions highly affected by strong winds the dome configuration guarantees a higher resistance since the tilt is very low and the sheltering effect is superior thanks to the design. A better resistance and safety can be translated in less cost related to the fastening systems.

Some consequences act on this configuration too

X Less production with the same number of solar panels compared to the south facing configuration. In order to reach the same power production in some cases more panels need to be installed and a higher cost is related to this.

X More soiling losses due to the low tilt utilized which reduces the falling of dust. Additional cost related to the cleaning of modules since they need to be wiped more often.

X The east-west configuration can work well in low latitude places but performs a very low output energy production compared to the south facing layout for high latitude locations.

The dome design can resist to stronger winds compared to the conventional south facing design. Due to this advantage the optimal angle for such design in Florida is chosen in order to match the optimal energy production. An analysis has been carried out simulating the installation of 1.03 MWp of solar PV on a lake situated north to Miami called Chaves lake. In order to simulate the weather conditions and the energy production of the panels the software Helioscope has been adopted. The modules used are the Canadian Solar CS6U 345M each representing a peak power of 345 W, they are designed in the portrait mode and the settings used are showed in the *Figure 81*.
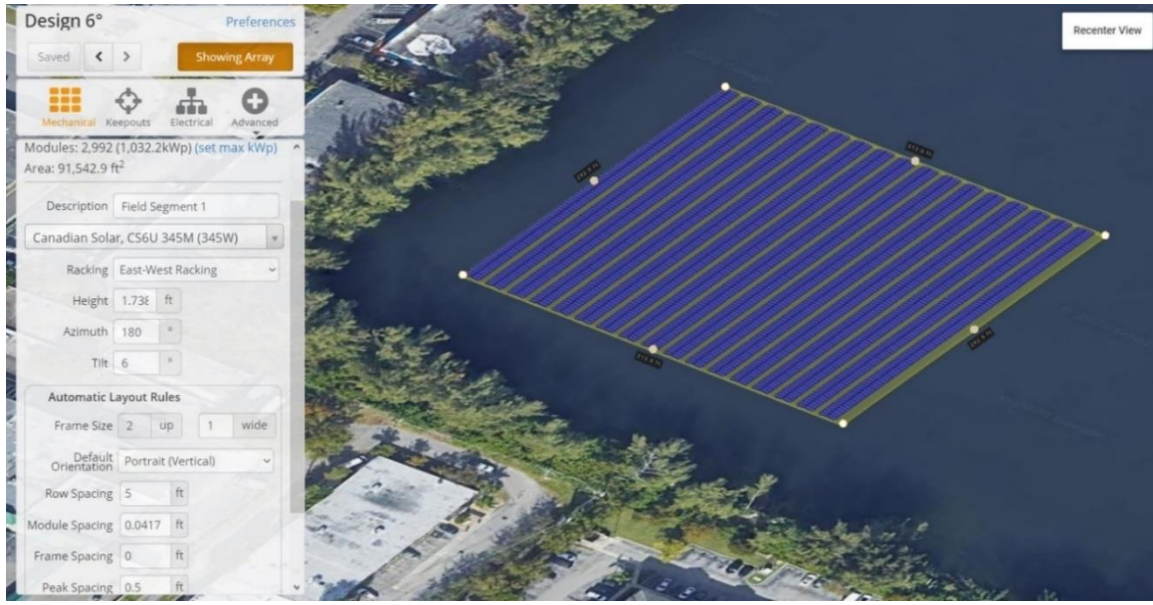
Figure 81: Floating solar farm in east west configuration 2992 panels used and 1,032.2 kWp installed, Helioscope.

For this configuration and this location, the optimal tilt angle is 1°, but a small inclination can lead to deposition losses that overtime decrease the productivity and the software cannot simulate this incremental deposition. If the module is not sloped enough the dust that naturally deposits on the panels will have a high probability to remain on the modules, covering the glass and limiting the solar beams to hit the doped silicon cells. This loss can reach 3%-4% of the total producible output. In order to decrease these percentages and let the dust slip off the modules an incremented slope must be configured or a surface cleaning should be adopted more often increasing the O&M costs. By increasing the panel's tilt to over 1° the final yield decreases but the soiling losses become less relevant. In order to guarantee a final yield loss below 1% and permit a steepness that could increase the soiling slip the angles from 4° to 7° should be set (*Figures 82,83*).
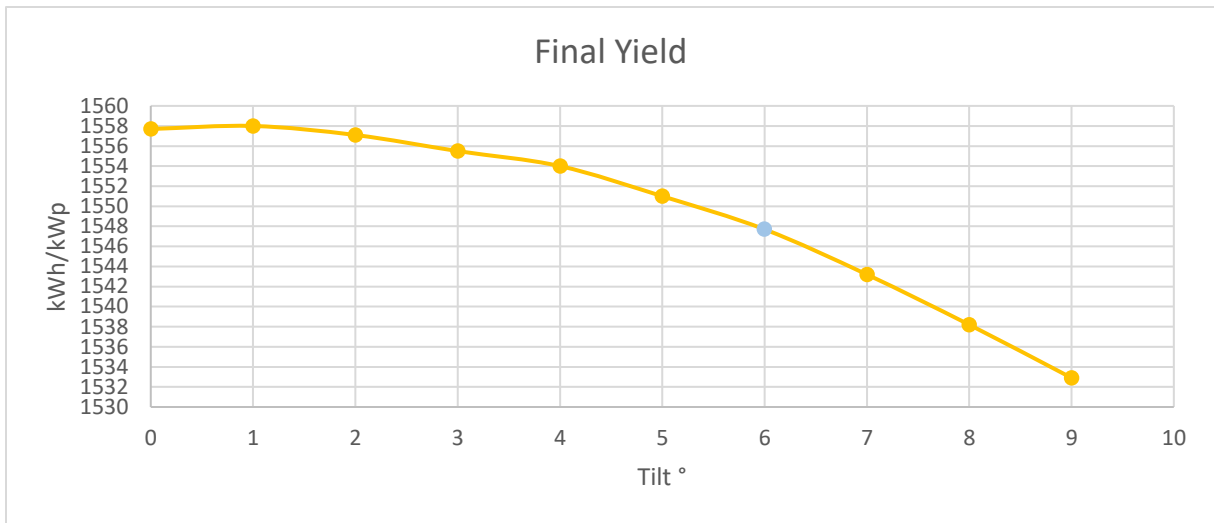
Figure 82: Final Yield as function of the tilt angle in the east-west configuration.
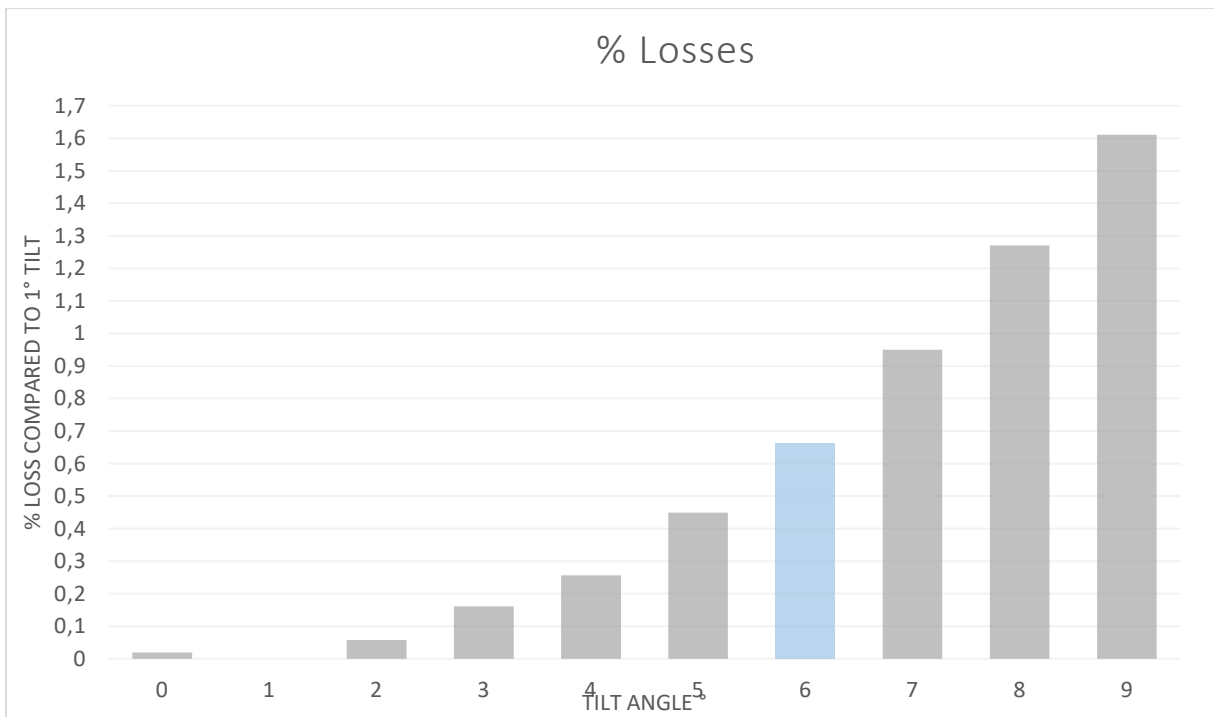
Figure 83: Histogram of the percentual losses compared to the optimal tilt which is 1°.

For the CFD simulation, a 6° angle has been adopted since it leads to 0.6611% of energy loss compared to the 1° angle and is sloped enough to guarantee a significant soiling slip. The panel's sets are spaced apart 100mm and are designed in the portrait mode.

A simulation with the wind acting frontally on one set of panels would have brought similar results to the previous analysis, so the wind direction has been chosen in order to face one of the worst cases, which is when the wind hits the panels with a lateral 45° from the frontal configuration. In this way the wind impacts the back of the second panels set, the configuration is showed in the *Figure 84.* If the wind was acting with an angle lower than 45° the rear panel would have been hit by a more orthogonal flux producing locally more pressure, but the frontal panel would have covered a lot the flow, so the high pressures on the rear panels would have been just local, and the overall pressure would have been small. By increasing the direction angle to more than 45°, the rear panel area of the back panel's set will be more affected by the wind, but the flow will hit the back panel in a more tangential way thus the pressure would not be as much high. The resultant 45 ° would be therefore one of the worst conditions of wind impacting the panels (see *Fig. 85*).
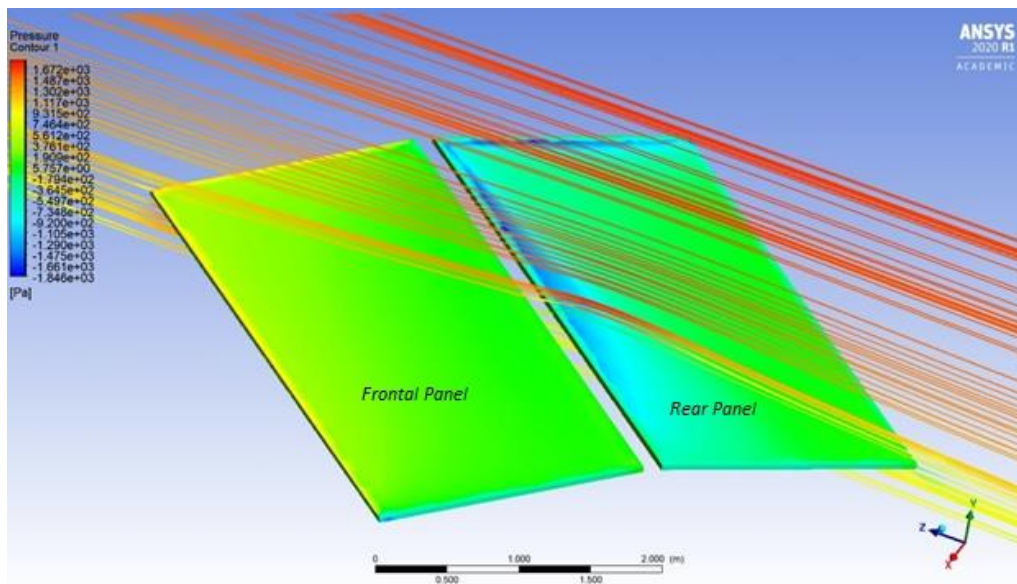
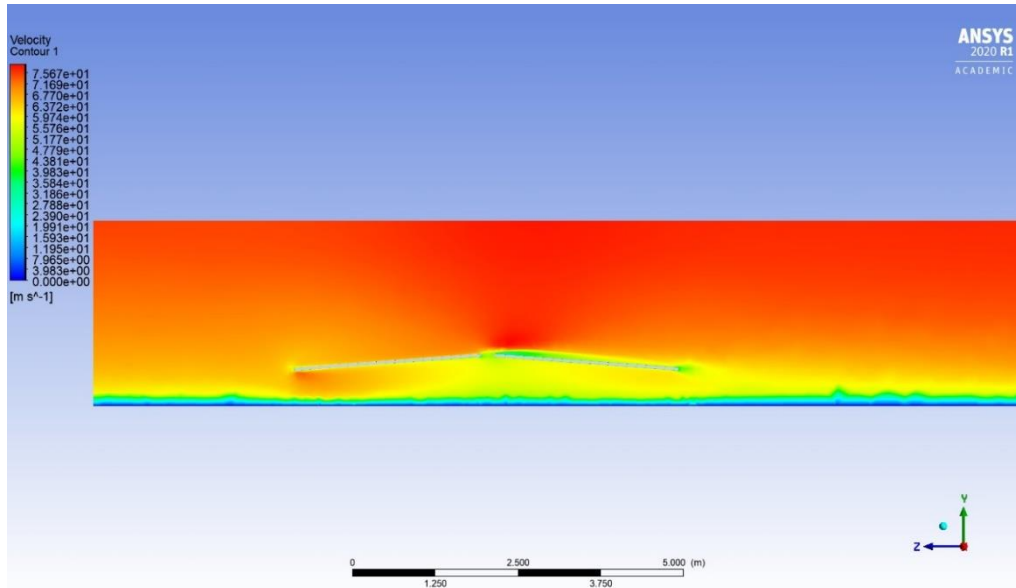*Figure 84: Velocity streamlines on the plane zy hitting the panels and pressure contour on the panels.*

Figure 85: Velocity contour of wind is impacting east-west panels from a 45° angle, plane zy.

When a category 5 hurricane with 300 km/h wind gusts at 10 m above ground hits the solar panels with a 45° direction from the frontal face the panels endure the following effects (see *Tables 10,11,12*).

East-West configuration Drag and Lift coefficients results				
	Drag coeff rear panels	Drag coeff front panels	Lift coeff rear panels	Lift coeff front panels
Unit				
	0.041783313	0.033140701	0.25692676	-0.096198605

Table 10: Drag and lift coefficients for the frontal and rear panels.

East-West configuration Drag and Lift forces results				
	Drag force rear panels	Drag force front panels	Lift force rear panels	Lift force front panels
Unit	N	N	N	N
	911.05285	722.60738	5602.0894	-2097.5362

Table 11: Drag and lift forces for the frontal and rear panels.

East-West configuration pressures results				
	Pressure back wall rear panels	Pressure back wall front panels	Pressure front wall rear panels	Pressure front wall front panels
Unit	Pa	Pa	Pa	Pa
	977.2334	523.02356	233.06854	1074.6727

Table 12: Pressures on the frontal and back faces of the panels for the frontal and rear sets.

The pressure acting on the panels is inside the range of feasible pressures for standard panels.

The other results need to be compared to the conventional south facing 9° case with back-wind. In the dome layout the drag and lift coefficients are lower, the drag coefficient decreased by almost 70% and the lift coefficient decreased by nearly 60%. The same reduction can be observed for the drag and lift forces. And a reduction of 60% takes place on the total pressure for the worst conditioned panel.

From the energetic point of view the dome configuration with a 6° tilt has a Final Yield of 1547.7 kWh/kWp while in the south facing configuration with the maximum possible tilt of 9° the final yield is 1572.1 kWh/kWp. The east-west application in this case exhibits therefore a loss of 1.552 % compared to the south facing layout.

The optimal configuration for designing floating solar systems in south Florida is then the dome configuration, which despite losing 1.552 % of energy, it grants a bit more than one third of the lift and drag forces. The low forces translate in less efforts and so costs related to the fastening systems.

A final comparison between the south facing designs for both the first two rows and the east west configuration, using the best tilt angle in terms of energy production subject to the panel's structural limits during category 5 hurricane, is shown in the following tables. The values relative to the panel's pressures are shown in *Table 13,* and the lift and drag forces and coefficients, shown in *Table 14*.

Pressure results				
	Tilt	Pressure-front-modules	pressure-back-modules	Total frontal pressure
Unit	*Degree*	*Pa*	*Pa*	*Pa*
First row south facing design				
front wind	9	1431.0594	-864.42741	2295.4868
back wind	9	-720.6051	1592.7835	2313.3886
Second row south facing design				
Front wind	9	392.678	-193.310	585.988
Back wind	9	124.760	181.368	-56.608
East-West configuration worst condition				
Front panels	6	523.0236	1074.6727	-551.6491
Rear panels	6	977.2334	233.0685	744.1649

Table 13: Pressures on the panels for the first row south facing design, the second row south facing configuration and the dome configuration.

Drag and Lift results					
	Tilt	Drag-coeff	Lift-coeff	Force-z	Force-y
Unit	*Degree*			*N*	*N*
First row south facing design					
front wind	9	0.1347149	-0.5988094	3001.244	-13333.09
back wind	9	0.1382082	0.6351446	3083.783	14171.72
Second row south facing design					
Front wind	9	0.05877878	-0.22318168	1308.769	-4969.37
Back wind	9	0.05734164	0.20970767	1258.648	4603.08
East-West configuration worst condition					
Front panels	6	0.033140701	-0.09619861	722.60738	-2097.54
Rear panels	6	0.041783313	0.25692676	911.05285	5602.09

Table 14: Drag and Lift coefficients and forces on the panels for the first row south facing design, the second row south facing configuration and the dome configuration.

10. Conclusions

The floating version of photovoltaic systems boasts numerous advantages and demonstrates performance that leads this technology to be preferred to the ground mounted PV systems in a huge part of the State of Florida (hence in many areas included in the Northern Sun Belt).
The benefits of this technology are both of energetic and environmental nature and best fit the characteristics of the Sunshine State of Florida, rich of lakes and ponds. What limits this technology is the lack of technical maturity, which implicates a higher price compared with the ground mounted, and in some places, like the tropical regions, the threaten of hurricanes.

A first concern is on the resistance of the solar panels, which are the most critical and affected parts of the system. The CFD analysis carried out in this work shows that, on the standard south facing configuration the threshold tilt angle that guarantees a resistance of regular commercial solar panels under 300 km/h wind gusts is 9°. By exceeding this inclination, when the wind is coming from the back of the panels, the pressure on the rear face of the panels, overcomes the 2400 Pa, which is over the standard panel's structural capacity. Yet, the first row creates a sheltering effect on the following ones, so the second line of panels suffers much less the impacting pressures, but the tilt should not be increased, otherwise the shielding effect might fail.

The CFD analysis also confirmed that the dome configuration represents an excellent solution because this design works best for low tilts and the configuration produces low pressures and forces on the panels and on the structures. Yet the low tilt angle configuration suffers from soiling losses, the 6° tilt has been chosen in order to create a self-washing effect during the rainy days, balancing the energy losses related to the low tilt with the possible energy losses associated to the dust that covers the panels. Furthermore, the dome configuration shows lower values both lift and drag force compared to the traditional south facing panels.

In fact, the highest values in terms of drag and lift are mostly regarding the conventional south facing modules, especially for the lift force. These forces create stresses on the metallic floating structures of the system and on the anchors and moorings, nevertheless the second row of panels requires to withstand one third of the forces acting on the first one, thus, a more specific concern needs to be taken into account for the external rows of the floating field.

Therefore, the CFD analysis showed that the dome configuration results in the optimal solution for floating photovoltaic applications in Florida due to its low pressures, lift and drag forces, inducted by hurricane category 5 strong winds, and the negligible difference in energy production compared to the south configuration.

It is also highlighted that, with the dome configuration, the lift and drag efforts induced by this exceptional wind, are in compliance with the NRG Island's structural, floating and mooring features and do not require special anchoring and mooring criteria.

Further steps for this analysis will be required in the simulation of the lake's water and the floatability of the plants in order to take into consideration the stresses produced on the anchors and moorings by waves induced by strong winds.

11. Bibliography

[1] World Bank Group, ESMAP and SERIS. 2019. "Where Sun Meets Water: Floating Solar Handbook for Practitioners". Washington, DC: World Bank. 1-145.

[2] [Online] "Thesolarnerd.com". Available: https://www.thesolarnerd.com/blog/will-solar-get-cheaper/ .

[3] [Online] "Solar - Fuels & Technologies". IEA. Retrieved 18 June 2020 https://www.iea.org/fuels-and-technologies/solar.

[4] World Bank Group, ESMAP and SERIS. 2019. Where Sun Meets Water: Floating Solar Market Report. Washington, DC: World Bank. 1-122.

[5] Haugwitz F., "Floating solar PV gains global momentum" pv magazine. 2020 september 22.

[6] Tampa Bay Water - C.W. Bill Young Regional Reservoir Solar Options Study "C.W. Bill Young Regional Reservoir Solar Options Study", Project Report - 9/7/2018, 1-51.

[7] Carpignano A. , Uggenti A. "evaporating pool" localizzazione e impatto ambientale dei sistemi energetici, Politecnico di Torino, 2020.

[8] Pausini S., NRG Energia, "Evolution & Future of Floating Photovoltaic Systems", 2018

[9] Spertino F. ,"The current-voltage (I-U) characteristic curve: the effect of irradiance and temperature", Politecnico di Torino.

[10] Trinasolar, "allmax TSM-DE05A(II)" solar panel datasheet.

[11] [Online] iea.org, "IEA monthly electricity statistics" statistic report October 2020, https://www.iea.org/reports/monthly-electricity-statistics.

[12] pv-tech, floating solar special report, "at the heart of floating solar: Singapore", February 2018, 18-30.

[13] NRG Island, "document about floating pv plants- anchorage systems-cement blocks" , 2018, 1-8.

[14] NRG Energia "NRG ISLAND Advantages".

[15] [Online] https://www.nrgisland.com/index.html, "NRG Island",2020.

[16] Zhao L.,Liu H. Reindl T. "Floating PV Technologies and Singapore's Testbed Esperiences" Solar Energy Research Institute of Singapore (SERIS), May 31 2017, 1-28.

[17] McPherson B. Halley R, "The South Florida Environment", U.S. Geological Survey Circular 1134 National Water-Quality Assessment Program, 1996.

[18] Bush D. , Congleton J., Esteves L., Lindeman K., Longo N., Neal W. Pilkey O., Pilkey D. "Living with florida's atlantic beaches ",2004, 1-118.

[19] Burke Energy Solutions, "solar PV system solution presentation", 2020.

[20] [Online] energymag.net, "Daily energy demand curve", https://energymag.net/daily-energy-demand-curve/,2020.

[21] [Online] Energy Information Administration, "Florida net electricity generation by source, Jul. 2020", https://www.eia.gov/state/?sid=FL#tabs-4, Electric power monthly,2020.

[22] Kumar A., "The everglades national park of florida: its geological history and spectacular environments.", Carleton University, July 2013.

[23] Bachmann, M., Hoyer, M., and Canfield, D.E. "Living at the Lake-A Handbook for Florida Lakefront Owners". University of Florida, Institute of Food and Agricultural Sciences (IFAS) and Florida Cooperative Extension, 1999.

[24] [Online] statista.com, "Population of the Miami-forthlauderdale-west palm beach metro area in the united states from 2010 to 2019", https://www.statista.com/statistics/815202/miami-metro-area-population/, 2020.

[25] [Documentary] Sir. Attenborough D, "a life on our planet", 23 September 2020.

[26] EIA, "Electric Power Monthly," forms EIA-023, EIA-826, and EIA-861 (February 2020).

[27] Feldman D., Margolis R., NREL (National Renewable Energy Laboratory), "Q4 2019/Q1 2020 Solar Industry Update", May 28 2020.

[28] Ebers A., Feldman D., Margolis R., NREL (National Renewable Energy Laboratory),"Q3/Q4 2018 Solar Industry Update",January 2019.

[29] Fu R., Feldman D., Margolis R., NREL (National Renewable Energy Laboratory),"U.S. Solar Photovoltaic System Cost Benchmark:Q1 2018", November 2018.

[30] Collins J., Emrich C., Paxton C., Wahl T., "Climate and Weather Extremes", School of Geosciences, University of South Florida, Tampa, FL; Channelside Weather LLC, Tampa, FL; Department of Civil, Environmental, and Construction Engineering, University of Central Florida, Orlando, FL; National Center for Integrated Coastal Research, University of Central Florida, Orlando, FL , Chapter 20, 578-607.

[31] Elsner J., Malmstadt J., Scheitlin K., "Florida Hurricanes and Damage Costs", Florida statal university, 2009, 108-131.

[32] Blake E., David J., Landsea C., McAdie C., Neumann C., "tropical cyclones of the north Atlantic Ocean, 1851-2006" NOAA (National Oceanic and Atmospheric Administration), July 2009, 1-36.

[33][Online]   Meteoblue,   "Weather   Miami,   history   &   climate", https://www.meteoblue.com/en/weather/week/miami_united-states-of-america_4164138, 2020.

[34] Blake E., Landsea C. Gibney E. "The deadliest, costliest, and most intense united states tropical cyclones from1851 to 2010 (and other frequently requested hurricane facts)",NOAA Technical Memorandum NWS NHC-6, August 2011, 1-47.

[35] Black P.G., Willoughby H. E., "Hurricane Andrew in Florida: Dynamics of a Disaster", Hurricane reseach dicision, AOML/NOAA, Miami, Florida, 01 march 1996, 543-550.

[36] Bellini E., "Japan's largest floating PV plant catches fire after Typhoon Faxai impact" pv magazine, September 9 2019.

[37] ASCE 7-16 "minimum design loads and associated criteria for building and other structures", international building code (IBC), 2016, Section 26.5.3.

[38] Munson B., Huebsch W., Okiishi T., Rothmayer A., "Fluid Mechanics seventh edition", wiley, 2013, 478-542, 723-735.

[39] Sheikh I. "numerical investigation of drag and lift coefficient on a fixed tilt ground mounted photovoltaic module system over inclined terrain", Department of Mechanical Engineering, Sardar Patel College of engineering Mumbai University, India, 2019, 37-49.

[40] Carissimo B., Franke J., Hellesten A., Schlunzen H. "COST, best practice guideline for the cfd simunation of flows in the urban environment", Cost action 732, 1 May 2007.

[41] Saritas A.,Uslu V., Uzol O. "wind load acting on solar panels in a row by CFD Analysis", advances in civil, environmental and material research, 01 September 2016.

[42] Burgess C., Goodman J., "Solar under storm", Rocky mountain institute, June 2018

[43] Burges C. Detweiler S., Needham C., Oudheusden F.," Solar under storm part 2",Rocky mountain institute, Clinton foundation, February 2020.

[44] Kumar P., Sankar K., "CFD analysys of wind loading in solar panels", march 2019, 29-34.

[45] De Stefano G., Reina G., "computational evaluation of wind loads on sun-tracking ground-mounted photovoltaic panel arrays", Journal of wind engineering & industrial aerodynamics, 2017, 283-293.

[46] Hangan H., Jubayer C., "numerical simulation of wind effects on a stand-alone ground mounted photovoltaic (PV) system", Journal of wind engineering & industrial aerodynamics, 2014, 56-64.

[47] Berg R., Cangialosi J., Latto A., "Hurricane Irma" National hurricane center tropical cyclone report, 30 june 2018, 1-22.

[48] Bourke P.,Rohr C., "catching the sun", 2019, 42-45.

[49] DesAutels C., Schluman L., "computational fluid dynamics simulations to predict wind induced damage to a steel building during hurricane katrina", forensic engineering , 2013, 793-800.

[50] Heckert N., Simiu E., "ultimate wind loads and direction effects in non hurricane and hurricane prone regions",1988, 433-444.

[51] Hsu S. "verifying wind profile equations under hurricane conditions", the open ocean engineering journal, 2011, 60-64.

[52] Banks D., O'Brien C., "wind load", solarpro, July 2012, 72-92.

[53] [Online] National hurricane center and national pacific hurricane center https://www.nhc.noaa.gov/archive/2019/al05/al052019.public.037.shtml? NOAA, 2019.

[54] Aoki M., Ishii S., Iwai H., Mizutani K., Nakagawa K. [Measurements of rainfall velocity and raindrop size distribution using coherent doppler lidar", 13 september 2016.

[55] Brinkmann M., Fouckhardt H., Hagemann M., Steingoetter I., "nm and μm scale surface roughness on glass with specific optical scattering characteristics on demand", June 2007, 1-7.

[56] Fors S., Nord C., "Determination of aerodynamic drag coefficients using a drop test with a wireless accelerometer and its application to model rockets", 2019, 714-715.

[57] Torchio M F Tabelle di Termodinamica e Trasmissione del Calore - Proprietà delle sostanze di uso frequente. CLUT Ed., Torino 2012.

[58] [Online] Comparison of east-west arrays, https://www.solar.sheffield.ac.uk/panel-data/comparison-of-east-west-arrays/, Sheffield solar.